Slurry Deposition of High Quality Layers for 3D Printing

by

Bjørn N. DeBear

B.S. Mechanical Engineering
State University of New York at Buffalo, 1997

B.A. Political Science
University of North Carolina at Chapel Hill, 1993

Submitted to the Department of Mechanical Engineering in Partial Fulfillment of the Requirements for the Degree of

Master of Science in Mechanical Engineering

at the

Massachusetts Institute of Technology
June 1999

Signature of Author_____
Department of Mechanical Engineering
May 24, 1999

Certified by _____
Emanuel M. Sachs
Professor of Mechanical Engineering
Laboratory for Manufacturing and Productivity
Thesis Supervisor

Accepted by_____
Ain A. Sonin
Chairman of Graduate Committee

Slurry Deposition of High Quality Layers for 3D Printing

By

Bjørn N. DeBear

Submitted to the Department of Mechanical Engineering
On May 24, 1999 in Partial Fulfillment of the
Requirements for the Degree of Master of Science in
Mechanical Engineering

Abstract

Slurry-based three dimensional printing is being used to create ceramic parts directly from CAD files. Layers of slurry are deposited by using an x-y positioning system to raster a slurry nozzle over a powder bed. A binder material is selectively printed into each layer to define a slice of the part. This process is repeated until the last slice of the powder bed is defined. Afterwards, the powder bed is redispersed in water, leaving behind the printed green part. The green part is then sintered to full density. This thesis focuses on new ways to make slurry layers to minimize defects and improve surface quality.

A technique called line merging has been shown to rapidly create slurry layers containing minimal defects. This technique produces layers with better surface finish than other proven techniques. Line merging occurs when adjacent lines of slurry are deposited in rapid succession such that they merge together prior to slip casting. Line merging differs from nozzle rastering in two ways: the cycle time between deposited lines is reduced from approximately 1 second to as little as 0.1 second, and lines are deposited in one direction only. The very short cycle times are achieved by using springs rather than electromechanical means to reverse the direction of the nozzle assembly.

Initial line merging exploration was conducted with a rotary device that rapidly deposited arcs of slurry onto a moving substrate. Subsequently, an apparatus consisting of an oscillating wheel with a nozzle at the bottom was constructed to examine the operating space for successful line merging. Three boundaries to this operating space were discovered: bubbling, stitching, and perpendicular migration. Experimental results and physical equations were combined to produce a mathematical model predicting the behavior of the system. This model was useful in predicting the occurrence of bubbling and stitching, but was not helpful in predicting the occurrence of perpendicular migration. Using this model, a five layer powderbed was made that was free of line stitching defects and interlayer defects. Future machines will adapt the line merging technique to a linear system.

Thesis Supervisor: Emanuel M. Sachs
Title: Professor of Mechanical Engineering

Acknowledgments

This thesis is dedicated to my parents, who have always provided me with the encouragement and support to help me attain my professional and personal goals. Thank you both for everything.

Thanks also to TDK, for funding this project and for fostering the excellent partnership that will make this technology take off.

Although there is one name listed as the author of this work, this document would not have been possible without the help of many people. Although it would be impossible to list everyone who contributed to this work, several people deserve special thanks:

Thanks to Pat for being a pal and a trouper. I don't think my experience at MIT would have been as positive had I not been teamed up with you. Remember to keep in touch...especially if you get stationed in Hawaii...

Thanks to Ely, for encouraging me to think with my right brain. I learned a lot working with you, and wish you great success in the years to come.

Thanks to Mike Cima, for your great spirit and your wealth of knowledge.

Thanks to Helen, for being supportive and understanding; I don't know what I would have done without you.

Thanks to Jim Serdy for always helping out in a pinch, and for asking people to turn off the water. Good for you Jim! You are an inspiration. Everybody listen to Jim and do what he says.

Thanks to Adam, Peter and James for being great roomies. Let me know when you visit New York!!!

Thanks to Mark Belanger, for all the good times. Remember to check your butt before leaving the shop. Thanks also to Fred Cote, for teaching me not to drop end mills.

Thanks also to Scott and Richard, for all their help and encouragement. It's good to know that Pat and I aren't the only ones who squabble while jetting slurry.

Thanks to Diane for helping me with SolidWorks; thanks to Dave, for taking great pictures of my tape casting experiments before they went haywire; thanks to John Centorino for keeping things ticking in building 12.

Thanks to Julie, Barbara and Laura for taking care of business.

Thanks to Dave the Rave, Costas with the mostas, and Diana (BATTLE ON XENA!).

Thanks to everybody else who helped me get this far. I'll miss you all!

Table of Contents

Table of Figures

1. Introduction

1.1 Background

Reducing time-to-market has become very important to businesses around the world. The sooner a business can turn a new idea into a product, the sooner that business can start making money off that idea. The impetus to speed up the development cycle of a product and the desire to improve product quality by testing more prototypes prior to committing to a final design have encouraged the development of technologies allowing physical models to be created quickly and accurately (Myklegard).

"Rapid prototyping" is a technology that causes parts designed on a computer to be automatically fabricated in layers. As the name indicates, it is used in the production of prototypes, but in recent years the technology has gained wide acceptance as a means to create small numbers of end-use parts. Since this fact is obscured by the term "rapid prototyping," people who use the technology for the latter purpose often prefer to call their art "solid freeform manufacturing."

"3D printing" is a form of solid freeform manufacturing developed at MIT. MIT has associated its particular technique of solid freeform manufacturing with the trademark 3DP™. In the 3DP™ process the layers of the part are created by selectively printing binder into layers of powder (see Figure 1.1). The body of powder that is deposited layer-by-layer is called the "powderbed," and the unprinted regions of the powderbed serve as supports for regions that are printed above them. Thus it is possible to use the 3DP™ process to create parts with undercuts, overhangs, and internal passages. The 3DP™ process is fairly versatile, in that it has the capability of creating parts out of any material that can be obtained in powder form. One area in which 3DP™ technology shows great promise is in the fabrication of ceramic parts. 3D printing makes it possible to create complex ceramic green parts without a green-pressing die or mold. By eliminating the need for green-pressing dies, the 3DP™ process enables designers to

consider using structural ceramics in applications where only a few parts will be needed and where a complex geometry is necessary (Caradonna, p13).

Figure 1.1: Three Dimensional Printing

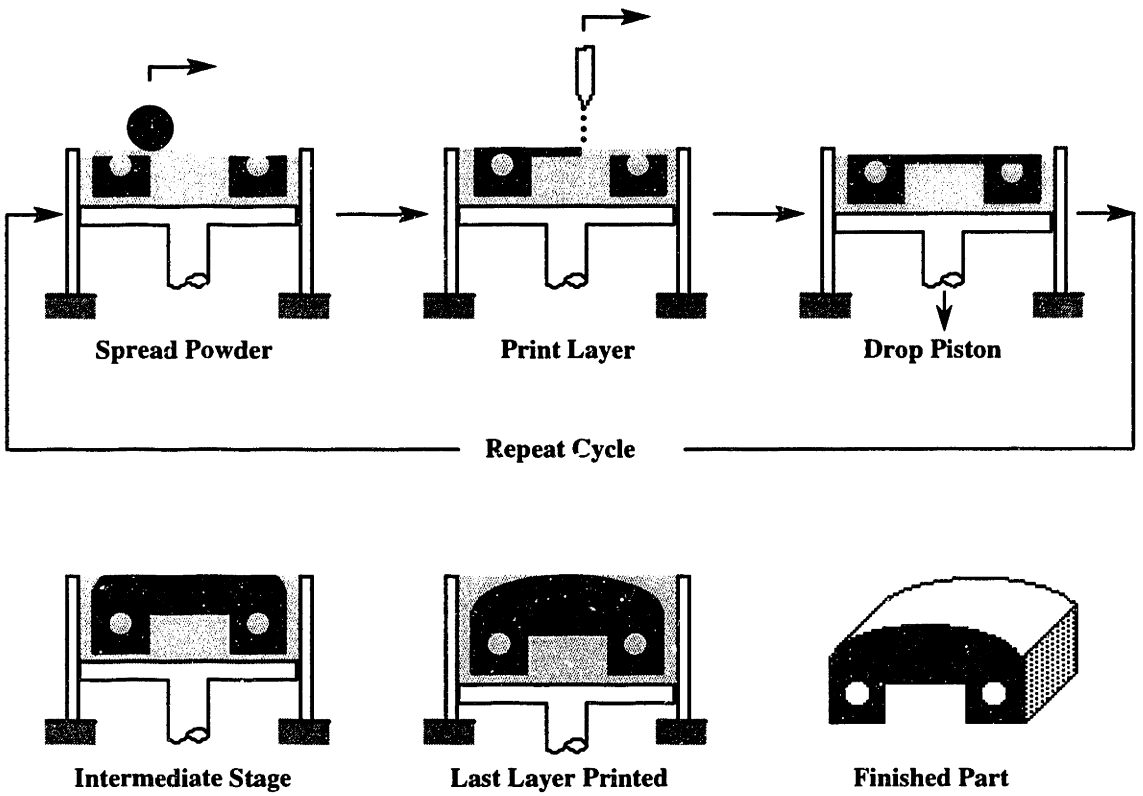

1.2 Motivation

There are many reasons why work should be done to determine how to apply 3D printing to the production of ceramic parts. There are many ceramic parts that could be made by 3D printing that are very difficult and expensive to make with traditional ceramics processing techniques. Turbine blades and investment casting shells, for example, often require complex geometries and very small batch sizes. 3D printing has the potential to quickly create turbine blades with internal cooling channels and investment casting shells complete with sprues, runners, gates, and internal cores.

Another application for ceramic 3DP™ which is being explored aggressively is the production of RF filters for use in cell phones and global positioning systems. These

devices are currently made using dry pressing techniques. 3D printing has three important advantages over these techniques. Firstly, 3D printing offers the ability to create internal geometries within the filters. Secondly, RF filters need metal channels to work, and 3D printing offers the ability to create these channels *during the printing process*, thereby eliminating an expensive and complicated metalization step. Finally, dry pressing techniques create parts with non-uniform densities. Filters with non-uniform densities pick up a wider range of frequencies than is desirable. 3D printing has the potential to improve the quality of these devices since every region of a 3D printed part is deposited in the same manner and experiences the same conditions, and therefore has the same density.

In addition to the above applications, there are opportunities for 3D printing to be used in the production of novel electronic devices, including smart structures containing embedded electronics. This possibility requires the development of metal slurry deposition techniques, and will not be explored in this paper.

In conclusion, there are several areas in which 3D printing might prove a viable alternative to traditional ceramic processing techniques. This thesis will explore different ways to make ceramic layers for 3D printing.

2. Slurry-Based 3DP™

2.1 Overview

Ceramic parts that are intended to bear loads must be fabricated from fine powders (1.0 μm and smaller) and be as dense as possible (Caradonna, p. 20). It is difficult to make dense parts out of fine ceramic powder using the standard 3DP™ procedure (spreading loose powder) for the following three reasons:

#1 Loose powders are nearly impossible to spread evenly when the constituent particles are smaller than 10 microns in diameter. Van der Waals forces cause them to clump together (Caradonna, p .20).

#2 Ballistic ejection of powder particles by binder droplets is a pervasive problem when printing on fine powders (Caradonna, p.20).

#3 It is impossible to achieve high packing ratios (greater than 40%) when spreading loose powders (Caradonna, p.20)

It is much more practical to make ceramic powder bed layers by depositing a *liquid dispersion* of the powder called a "slurry." Once the slurry is deposited, the solvent infiltrates the pores of the layer below in a process called "slip casting." When this happens, the slurry ceases to be fluid, the particles compact, and the new layer sticks firmly to the previous layer. If multiple layers are to be deposited, or if binder is to be printed into the powder bed, it is necessary to dry each layer thoroughly after it is deposited. If it is not dried, successive layers of slurry will not slip cast evenly, and binder printed on the powder bed will bleed.

By making layers in this manner instead of by spreading loose powder, it is possible to consistently achieve packing densities of 55% of theoretical.

2.2 Raster Scanning

The current layer fabrication technique is simple nozzle rastering using x-y positioning slides, as shown in Figure 2.1. The current approach uses a nozzle mounted

on a linear slide which travels along the x-axis. The entire linear slide is mounted on a carriage that moves along the y-axis. The substrate is mounted to a stage which controls z-axis positioning. Rastering a nozzle deposits a series of adjacent parallel lines of slurry, comprising a layer.

Figure 2.1 Raster scanning using x-y positioning system

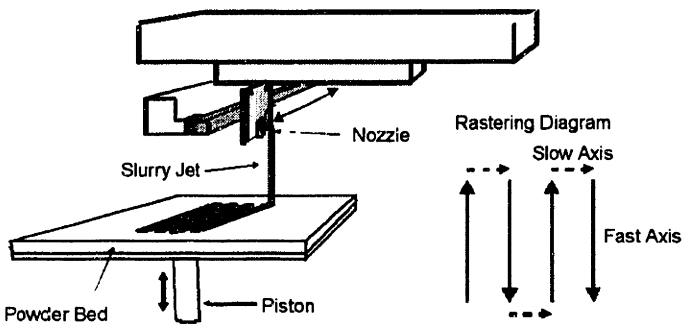

2.2.1 Observations

Powder beds created in this manner have ridged top surfaces which reflect the step-wise manner in which the slurry was deposited. Specifically, ridges occur wherever lines of slurry are deposited, and valleys occur between lines. These defects compromise the quality of the top surfaces of parts. These ridges are shown in Figure 2.2.

Figure 2.2 Top surface of powder bed made by rastering nozzle with x-y positioning system

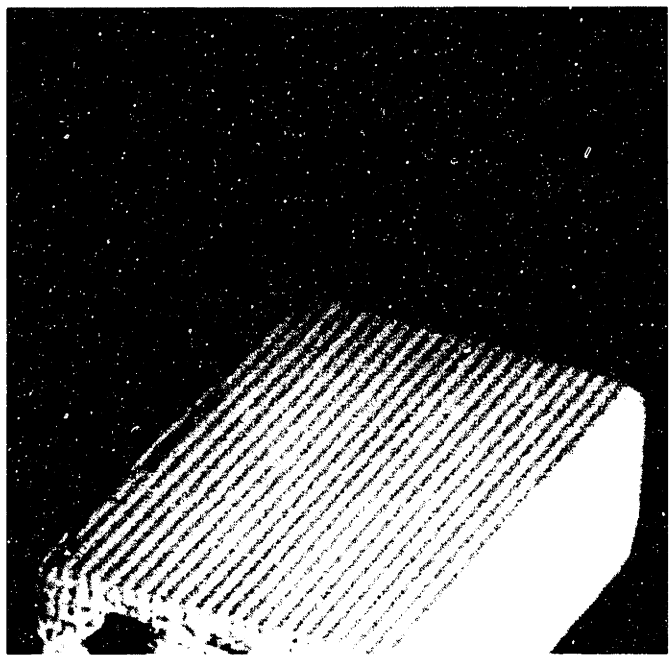

One flaw attributed to simple nozzle rastering is that line deposition always begins next to the wettest section of the previously deposited line (before the slurry from the previous line has had much of a chance to slip cast). Deposition then finishes up next to the driest section of the previous line (after the slurry has had more time to slip cast). The fact that inter-arrival time between lines changes along the length of a line, prevents a layer produced in this manner from being uniform.

Figure 2.3 Schematic showing that inter-arrival time between adjacent deposited lines

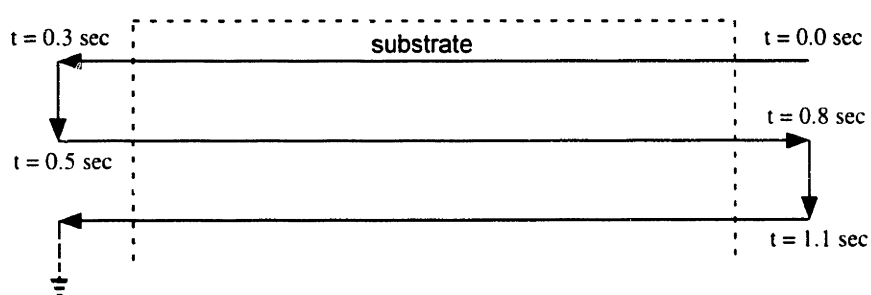

Inter-line defects are a product of nozzle rastering with an x-y positioning system (Figure 2.4). These defects appear as localized high porosity occurring along the interfaces between adjacently deposited lines. It is hypothesized that this porosity is caused when a wet line of slurry is deposited against a partially slip cast line of slurry (Line merging experiments, in which wet lines of slurry merge with no inter-line defects, support this idea). These porous defects compromise the strength of the final part. Furthermore, such defects are unacceptable in parts such as RF resonators, whose electromagnetic properties depend strongly on the uniformity of the constituent material.

Figure 2.4 Cross-section of powder bed made by rastering nozzle with x-y positioning system showing defects between lines

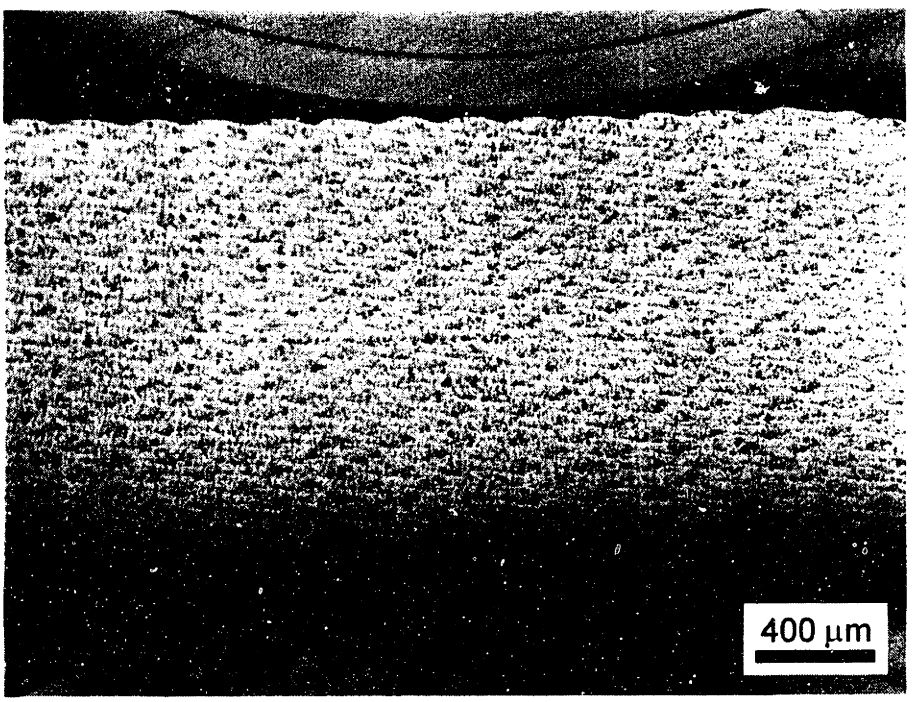

This thesis discusses four devices designed to eliminate line-stitching defects, all tested with a variety of 1 micron alumina slurries. The first device tested was a tape-casting unit, designed to spread an entire layer of slurry in one pass with a leveling blade. The remaining devices were designed to deposit individual lines of slurry very quickly,

and in the same direction. The first of these devices employed a spinning arm, and will be referred to as the "rotary apparatus;" the second employed a moving belt, and will be referred to as the "belt apparatus;" and the third employed an oscillating bicycle wheel, and will be referred to as the "bicycle wheel apparatus." This last device was very useful for experimenting with layer creation, and the results of experiments performed using this apparatus will be discussed in detail.

3. Tape Casting

3.1 Overview and Motivation

Tape Casting is a means of spreading a fluid by using a leveling edge called a "doctor blade." As the name indicates, the technique is used in the manufacture of tape, but it can also be used to manufacture objects composed of multiple layers. There are three main reasons tape casting may be a suitable way to make layers for ceramic 3DP™:

#1 In the tape casting process, layers are leveled with the doctor blade, so the operator knows that the steady-state layer height is equal to the distance the piston lowers the powderbed each layer. Thus z-axis resolution can be quite good.

#2 When tape casting, one spreads an entire layer in one pass. Thus throughput can be quite high. The process can be scaled up to larger powderbeds without adding significant amounts of time to the build cycle.

#3 Since the tape casting process does not rely on the joining of discrete lines of slurry, there are no defects associated with imperfect line stitching. Voids are minimized, and powderbed density is improved. Given the right operating conditions, layers produced by tape casting can be extremely smooth, level and dense.

The tape casting process in its simplest form is pictured in Figure 3.1. To avoid having to start with a very large puddle of slurry and finish with a very small puddle, it is expedient to attach a slurry feed system in front of the blade, which can dispense slurry continuously.

Figure 3.1: Tape casting schematic, side view

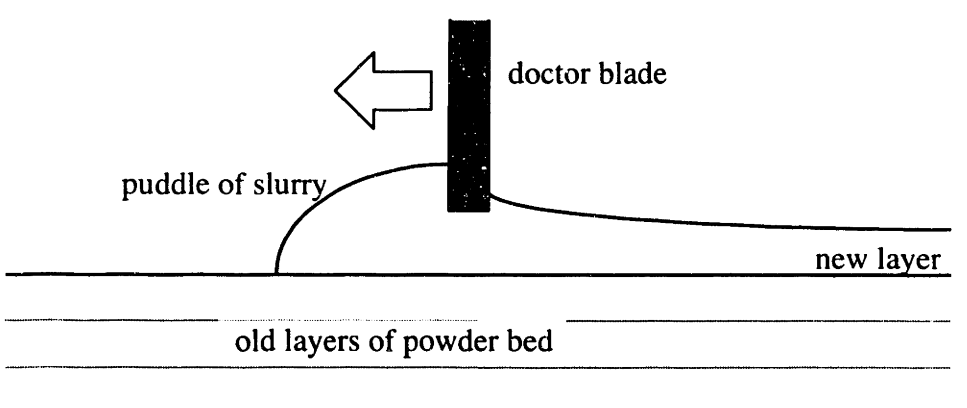

3.2 Method

The tape casting unit used in the experiments discussed in this chapter was attached to the slow axis of an x-y positioning system. A front blade was used to contain the slurry and prevent excessive slip casting ahead of the doctor blade. The bottom edge of the front blade was positioned approximately two mils below the bottom edge of the doctor blade. The gap between the two blades could be changed using spacers, but was normally set to be one millimeter. The slurry was fed into the space between the two blades with a 1600 micron nozzle. The tape casting unit was attached to the x-y positioning system by sliding it on to a pair of locating pins, and it was held in place by a magnet. The tape casting unit is pictured in Figure 3.2

Figure 3.2 Tape casting unit. Small screws are for adjusting blade positions. Curved blade is front blade; straight blade is doctor blade.

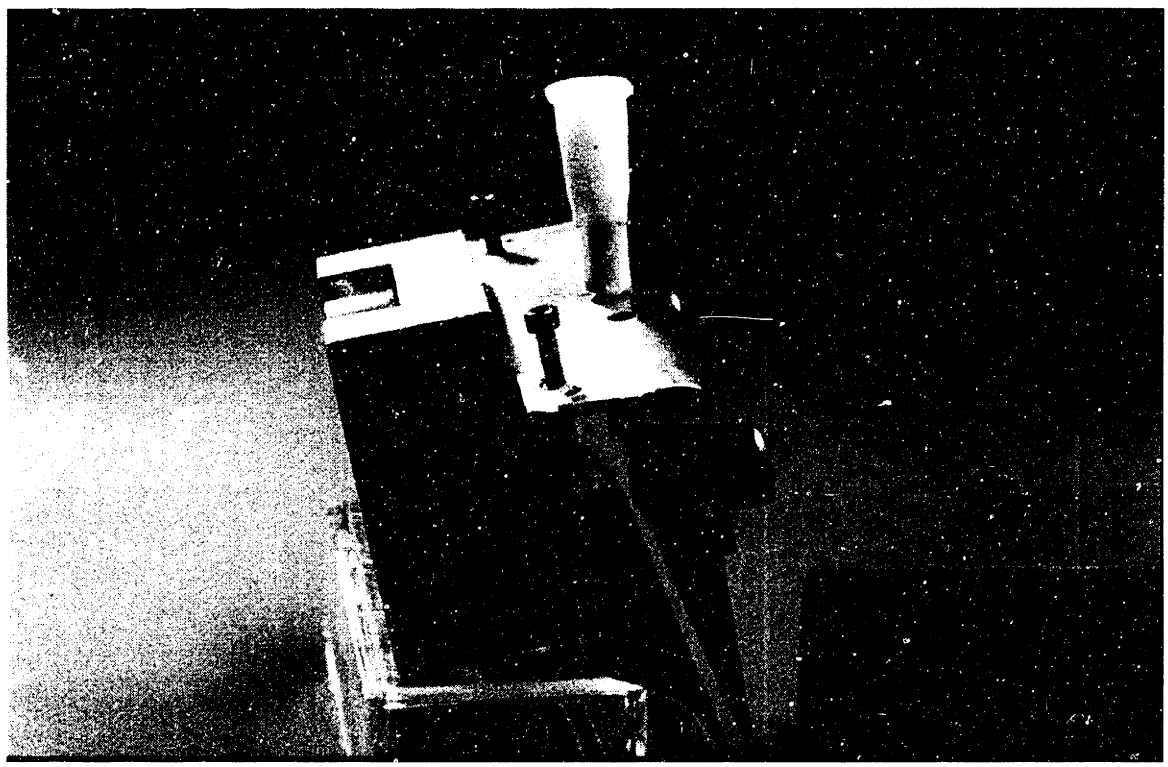

The blades were a little longer than the substrate, so it was possible to make powder beds just as wide as the substrate. Excess slurry poured down the sides of the

substrate, but this was minimized by adjusting flow rate, so as not to waste slurry. Plaster blocks were initially used as substrates, but they were phased out and replaced by E porosity borosilicate filters and bisque-fired alumina substrates, which had a much greater physical resemblance to slip-cast layers of alumina slurry.

The tape casting unit was traversed at speeds ranging from 0.05 m/s to 1.5 m/s. IPA, methanol and water were used in various combinations as solvent, and PEG was added to assist in redispersion. The PEG was always 400 MW, with the exception of a few experiments where higher molecular weight PEG's were used to thicken the slurry. a variety of solids loadings ranging from 20 to 40 volume percent were used. However, the slurry most frequently used was a 30 volume percent slurry containing a water to methanol ratio of 3:2. Further information on slurry production can be found in Appendix A.

Each layer was typically made in the following manner:

- The tape casting unit was positioned one inch in front of the powder bed, over a catch basin.
- The slurry was turned on and allowed to fill the space between the front and rear blades.
- When the flow of slurry reached steady state, the tape casting unit was moved over the powder bed. During the traverse, the newly deposited slurry was watched very carefully, so that the slip casting time could be estimated. Periodically, the front of the tape casting unit was watched during the traverse to ensure that no slurry was going out the front below the front blade.
- After the traverse, the slurry was turned off, and a record was made of the observed conditions.
- The tape casting unit was moved to the side, and then removed from the x-y positioning system.
- The drying lamp was moved over the powder bed and turned on, the powder bed was lowered to make room for the binder mask, and the binder jet was attached to the x-y positioning system.
- After 30 seconds of drying, the lamp was turned off and removed.

- The binder mask was placed over the powderbed, and the binder jet was rastered over the powder bed.
- The binder jet was removed from the x-y positioning system, the mask was removed, and the drying lamp was once again positioned over the substrate and turned on to dry the binder.
- During the binder drying step, the tape casting unit was cleaned and attached to the x-y positioning system.
- After 30 seconds, the lamp was turned off and removed.
- The tape casting unit was positioned one inch in front of the powder bed.
- The powder bed was raised back to its original height minus one layer thickness.
- The process was repeated. Note that three or four foundation layers were typically made before making layers containing binder.

To get layers of the desired thickness right from the start, the tape casting unit was not started with the tape casting unit one layer thickness above the surface of the substrate, but one thickness **plus** some extra distance (to make up for the fact that the slurry layer thickness decreased as slip casting occurred). This extra distance was be computed as:

$$extra = \frac{desired\ layer\ thickness(packing\ fraction - solids\ loading)}{solids\ loading}$$

However, the tape casting process is self-correcting as far as layer height is concerned, and if this distance was not achieved precisely, the layers eventually reached steady state thickness as shown in figure 3.3.

- the tape casting unit was watched during the traverse to ensure that no slurry was going out the front below the front blade.
- After the traverse, the slurry was turned off, and a record was made of the observed conditions.

- The tape casting unit was moved to the side, and then removed from the x-y positioning system.
- The drying lamp was moved over the powder bed and turned on, the powder bed was lowered to make room for the binder mask, and the binder jet was attached to the x-y positioning system.
- After 30 seconds of drying, the lamp was turned off and removed.
- The binder mask was placed over the powderbed, and the binder jet was rastered over the powder bed.
- The binder jet was removed from the x-y positioning system, the mask was removed, and the drying lamp was once again positioned over the substrate and turned on to dry the binder.
- During the binder drying step, the tape casting unit was cleaned and attached to the x-y positioning system.
- After 30 seconds, the lamp was turned off and removed.
- The tape casting unit was positioned one inch in front of the powder bed.
- The powder bed was raised back to its original height minus one layer thickness.
- The process was repeated. Note that three or four foundation layers were typically made before making layers containing binder.

3.3 Challenges

There are several issues which complicate the creation of layers using the tape casting process. The following section will discuss these problems and detail solutions to them.

3.3.1 Cracking

Powderbeds will crack upon drying if the depth of powderbed saturated with solvent (referred to as the saturation thickness) is too great. Cracking is caused by differential shrinkage due to differential drying, and can be avoided by preventing the saturation thickness from exceeding a critical saturation thickness. The saturation

thickness t_{sat} can be computed using the formula below. For 1 micron alumina slurry, the critical saturation thickness has been measured to be roughly 350 microns (Grau, p123).

$$t_{sat} = (\text{thickness of the deposited slurry while wet})\left(\frac{\text{Liquid fraction of the slurry}}{\text{Pore fraction of the powderbed}}\right)$$

3.3.2 Scraping

Slurry deposited in front of a doctor blade can slip cast in front of the blade. If too much builds up in front of the blade, the blade will scrape against it and mar the powderbed. This can be prevented by placing a blade in front of the doctor blade to contain the slurry and prevent it from pooling far in front of the doctor blade (see Figure 3.4).

Figure 3.4: Tape casting with a slurry nozzle and a front blade

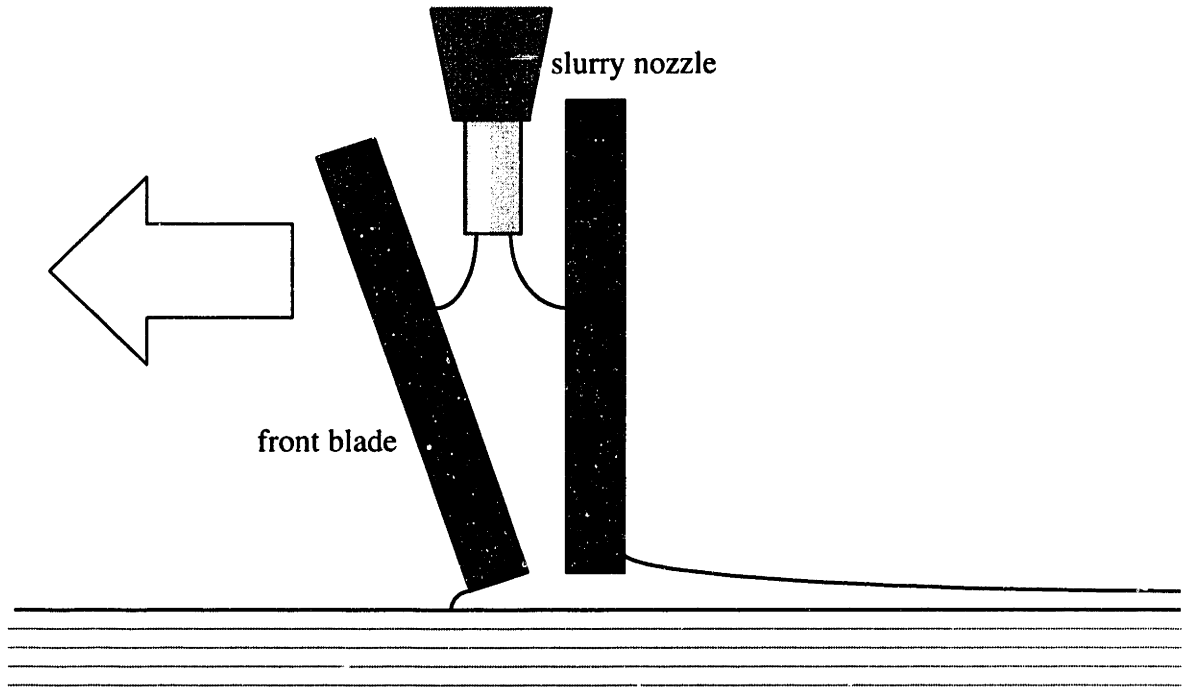

Scraping can also occur when slurry forms ridges at each edge of the powderbed due to differential slip casting, as shown in figure 3.5. Differential casting causes slurry to be drawn to edges of powderbeds because slip casting occurs faster at the edges. Ridges are created not only at the side edges, but also at the front and rear edges of the powder bed.

Figure 3.5 Close-up of tape cast powderbed, showing edge ridges. Photo courtesy of David Brancazio

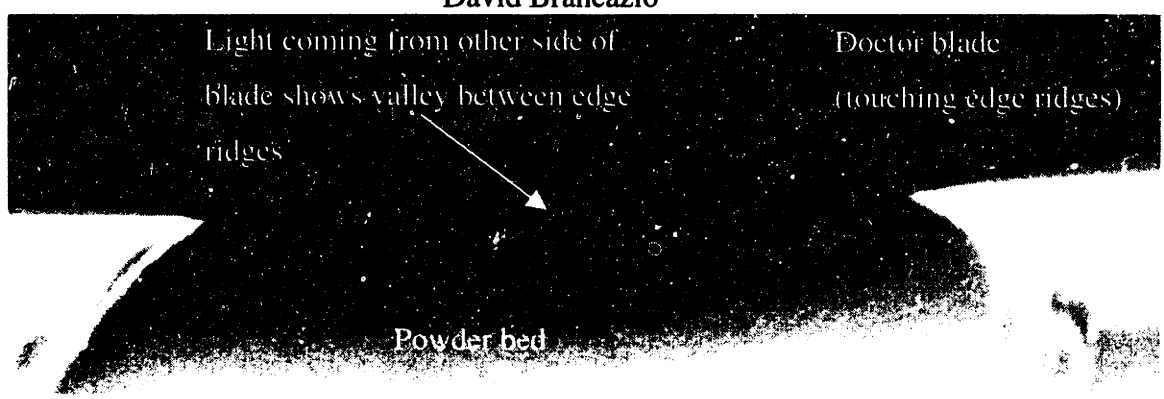

Ideally, edge scraping would not occur because the closer a powderbed surface is to the doctor blade, the less slurry is left behind in that area after the doctor blade passes over. For this reason edge ridges wouldn't be able to grow much, and the system would reach steady state without any edge scraping. The problem with this reasoning is that differential slip casting can move so much slurry to the edges **after** the doctor blade passes over, that the edges may grow by more than an entire layer thickness (despite the fact that they may start with hardly any slurry there at all due to the doctor blading). Clearly then, the way to stop such edge scraping is to prevent this transport of slurry from occurring, either by reducing the slip casting time or by reducing the slip casting at the edges (perhaps by loading the pores there with binder). Figure 3.6 shows in greater detail what is necessary for scraping of edge ridges to occur.

Figure 3.6 Scraping. Vertical dimensions exaggerated greatly for illustrative purposes. Drawing intended to represent formation of 50 micron thick layers.

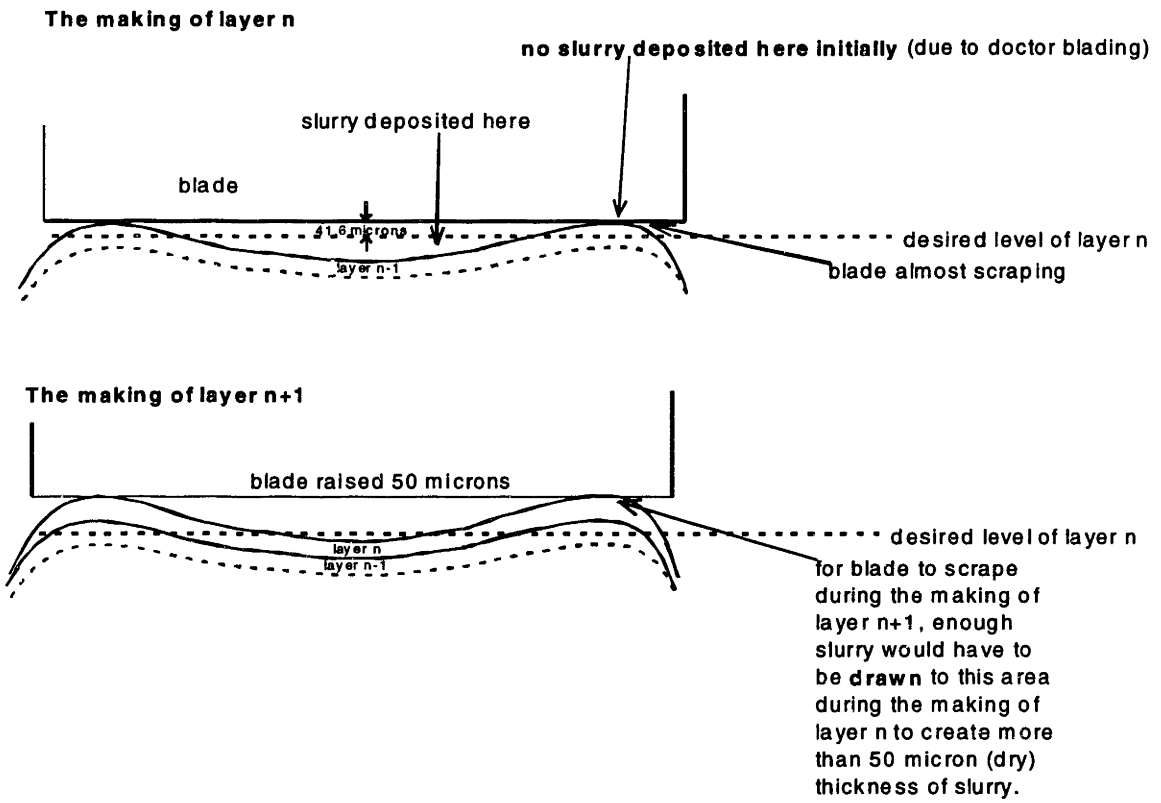

These cartoons assume the front blade is at the same height as the doctor blade. If the front blade is lower than the doctor blade, less slurry would have to be drawn to the ridge region for a scrape (of the front blade) to occur.

3.3.3 Bubbling

Slurry deposited quickly on a dry powder bed tends to bubble, as shown below.

Figure 3.7: Bubbles in a tape cast layer. Traverse speed was approximately 0.3m/s. Slurry was had solids loading of 30 volume percent. Solvent was 3:2 water to methanol.

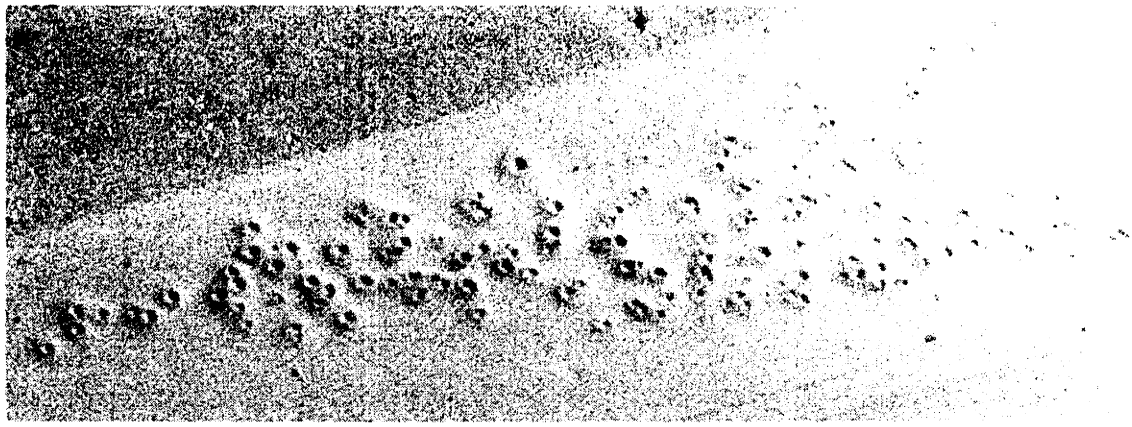

It is hypothesized that this occurs because air in pores beneath the new layer is forced upwards by infiltrating solvent. Here is why: the capillary pressure in a pore is

$$\Delta P = \frac{2\sigma\cos\theta}{R}$$

where σ is the surface tension, θ is the wetting angle, and R is the radius of the pore (Grau, p.115). Thus, smaller pores will experience higher capillary pressures than larger pores. If it is difficult for air to move very far through the powderbed, the solvent will push air down small pores and up large pores, creating a bubble (see Figure 3.8).

Figure 3.8: Why slurry bubbles

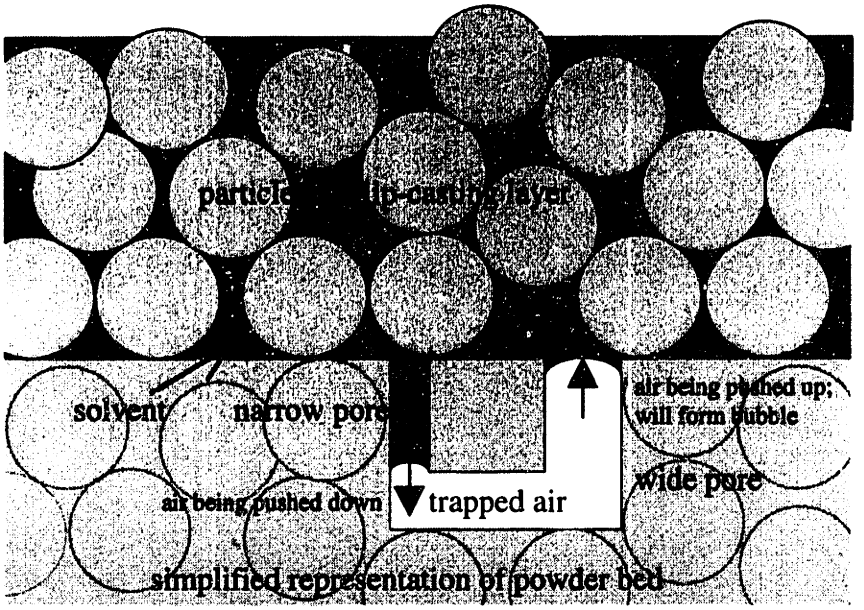

This hypothesis that trapped air displaced by infiltrating solvent is responsible for bubbling has been supported by experiments performed by Saxton, who observed the differences between powderbed layers deposited under vacuum and at ambient pressure respectively. Powderbeds made in a vacuum did not bubble, while powder beds made in the exact same manner at ambient pressure did (Saxton). Though Saxton did not actually tape cast the layers, but instead poured them without doctoring them, it appears that this approach would be a way to avoid bubbling in a tape cast layers. The problem with this approach would be the complexity of encasing the entire powder bed build area (including the binder jet and the lamp) in a vacuum chamber.

The idea that making it harder for air in pores under newly deposited slurry to escape might cause a previously robust system to experience bubbles is supported by experiments performed by Saxton, in which jetted lines of slurry were made progressively wider, until bubbling was observed (Saxton).

In these experiments 35 vol% alumina slurry with 1:1 water/IPA solvent was jetted through various-sized orifices and at different raster speeds to produce increasingly wider lines at a relatively constant jetting velocity. The narrowest lines were produced with a 127 micron wire bond nozzle, flow rate of approximately 2.25 cc/min, and traverse speed of 1.5 m/s. The widest lines were produced with a 500 micron syringe needle, flow

rate of approximately 29 cc/min, and raster speed of 1.0 m/s. Jet velocities for all lines were maintained between 2 – 3 m/s. The results indicated that lines greater than 800 microns in width bubbled, while those 650 microns or less tended not to bubble. There is a threshold in between in which bubbling may or may not occur. These results, shown in Figure 3.9, support the notion that bubbling is related to displaced air that forces its way back up through a slip casting slurry layer (Saxton).

Figure 3.9: Bubbling occurs in slurry lines as they get wider. Narrower lines of slurry (~390 microns shown at left) do not bubble because air can escape.

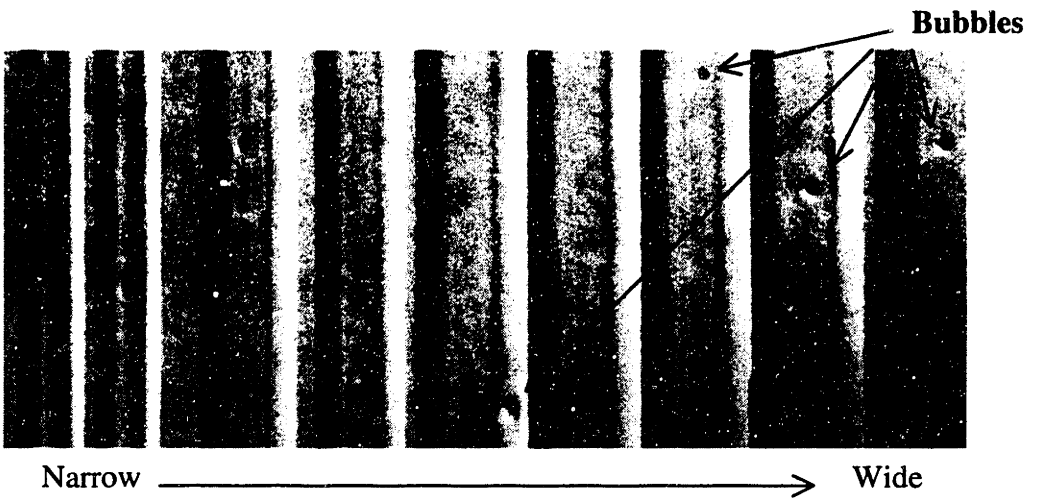

Bubbles created by tape casting often start out too small to see with the naked eye, but cause the evolution of progressively larger bubbles in subsequent layers (in the same location). This probably occurs because each bubble acts as a large pore, through which air can easily escape.

Bubbles are extremely undesirable because they become voids and stress concentrations in the final part. It may be possible to tape cast layers of slurry without experiencing bubbling by prewetting the powderbed or by traversing extremely slowly.

Prewetting the powderbed can prevent bubbling if it ensures that there is no trapped air to be driven out of the layer below the new layer. However, in prewetting the powderbed, one risks redispersing the top layer and exceeding the critical cracking thickness. Attempts to circumvent both problems by prewetting with a piezo atomizer have been unsuccessful.

Another way to prevent bubbling may be to suck air through the substrate and powder bed, but simple exploratory experiments indicate that the permeability of substrates and powderbeds is too low for this to be effective.

Yet another way to prevent bubbling would be to bathe the powderbed in carbon dioxide, which could be gettered (absorbed) by the water in the slurry (Kelley, p49). This approach would only be effective at low temperatures. The drying steps required to remove the solvent would make it very difficult to keep the powderbed cold.

The most promising way to eliminate bubbling in tape casting involves moving the tape casting unit much slower than was done in these experiments. Traversing very slowly may prevent bubbling by giving air time to escape out of the powderbed in front of the tape casting unit. For this to work with a slurry with 30 volume percent solids loading, the tape casting unit would have to traverse at around 1mm/sec. This hypothesis is supported by rotary apparatus and bicycle wheel apparatus experiments, in which conditions similar to tape casting were created, and bubbling was produced by high speed traverses, but not low speed traverses. These experiments will be discussed in greater detail in subsequent chapters.

The hypothesis that traversing slowly would eliminate bubbling has not been tested with tape casting because of concerns about scraping, and because the focus of the project shifted to layer fabrication techniques capable of supporting the creation of electronic vias, which tape casting would not (vias are metal junctions passing through a layer...to make a via through a tape cast layer would require the drilling of a hole).

Further information on bubbling in tape casting experiments is given in Appendix F.

3.3.4 Binder Bleeding

Binder deposited on a wet powder bed bleeds, because there are no dry pores for the binder to go into, and the binder dissolves in the surrounding solvent. Thus powder beds must be dry before binder is deposited. The four square parts shown in Figure 3.10 show the effects of binder bleeding.

The two squares on the top were made with a slurry with a solids loading of 32.5 volume percent and a 3:2 water to IPA ratio (no methanol). A traverse speed of 0.3 m/s was used and each layer was dried for 30 seconds. The binder was also dried for thirty seconds. These parts contained many bubbles.

The two squares on the bottom were made with a slurry with a solids loading of 32.5 volume percent and a 3:2 water to methanol ratio (no IPA). A traverse speed of 0.4 m/s was used and each layer was dried for ten seconds. The binder was dried for ten seconds. These squares experienced a greater degree of binder bleeding because of the reduced drying times.

Figure 3.10: Four square parts showing various degrees of binder bleeding. Parts were 3D printed; each layer was tape cast.

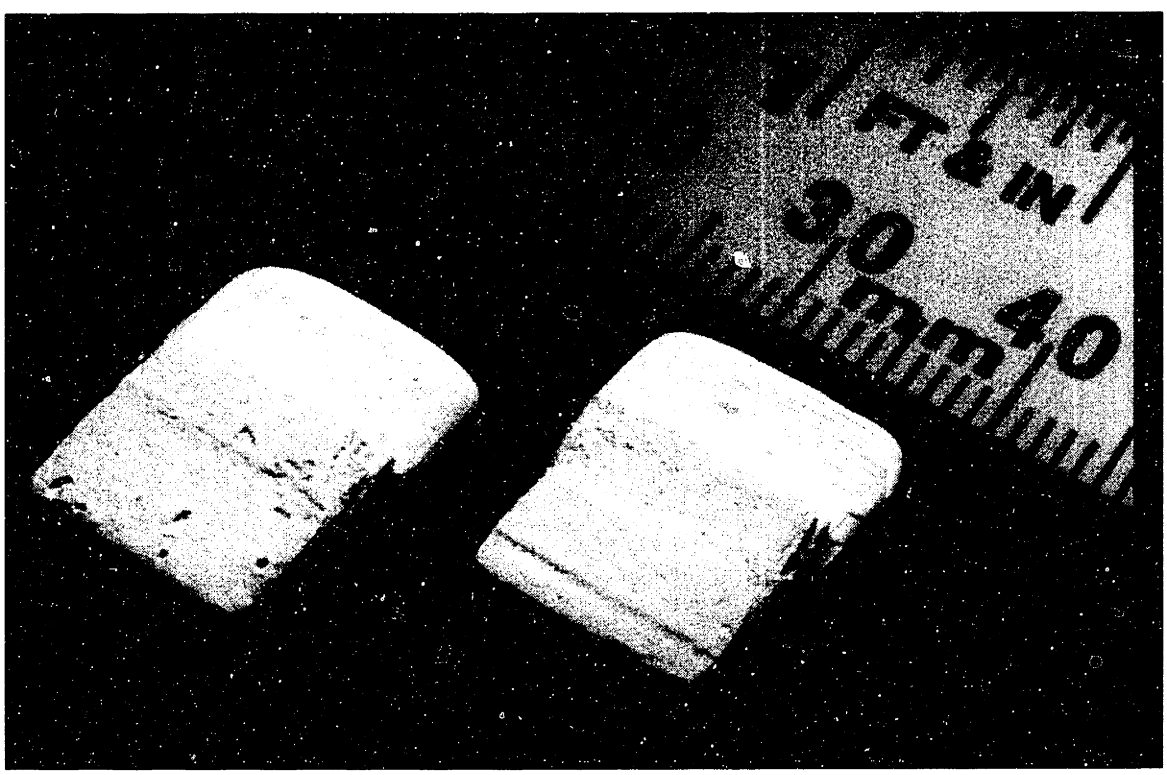

3.3.5 Slurry Migration

Slurry deposited on a damp powderbed tends form valleys and ridges, as shown in Figure 3.11. This is because slip casting occurs slowly on damp powder beds, and slurry is able to migrate to regions where solvent is infiltrating the powderbed faster. This process is highly undesirable, and makes it imperative to dry each layer thoroughly prior to depositing a new layer.

Figure 3.11: Slurry migration in tape cast bed. Random pattern due to very slow slip casting.

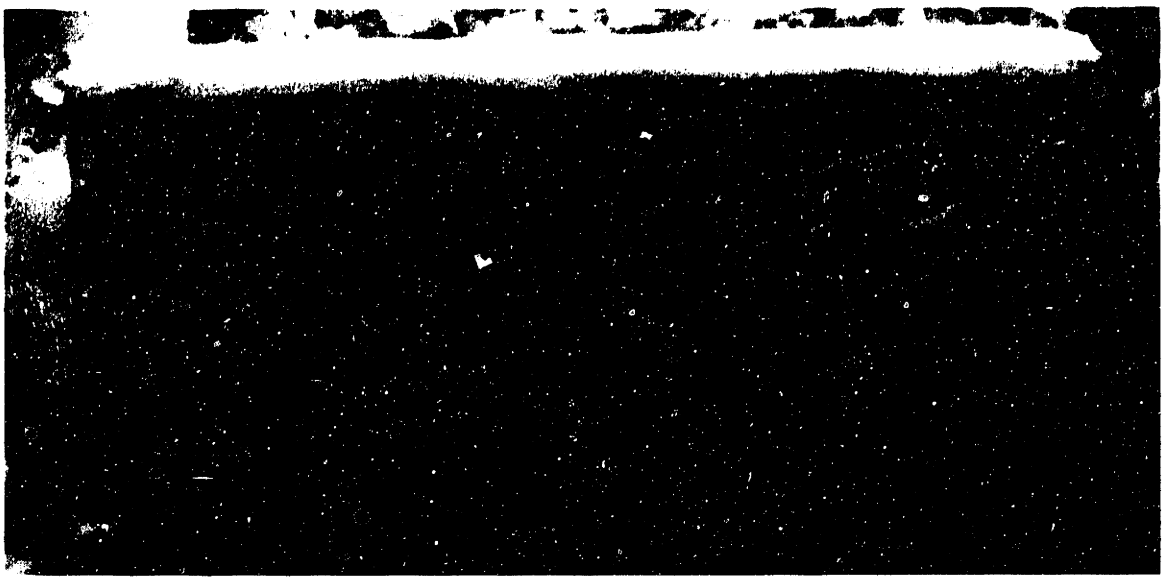

3.3.6 Cleaning

It is necessary to clean the blades thoroughly between passes to eliminate debris and to open up the slot between the blades. This can be tedious and might prove tricky to automate.

3.4 Powderbed Density Experiments

Experiments were done to determine the effect of layer thickness on particle packing. Powderbeds were made through tape casting, and the densities of the green powder beds were measured using porosimetry. As Figure 3.12 shows, thicker layers result in denser powder beds. This is due to the fact that slip-casting takes longer to occur when thicker layers are used, and particles have more time to settle in a tightly-packed configuration when slip-casting occurs slowly (see formula below). Thus there is some incentive to use the thickest layers possible when creating powderbeds. This incentive must be balanced against the desire to have very fine features and very fine stepping on non-horizontal surfaces, which of course points to the use of thinner layers.

Figure 3.12: Effect of interlayer defects on density of powderbed

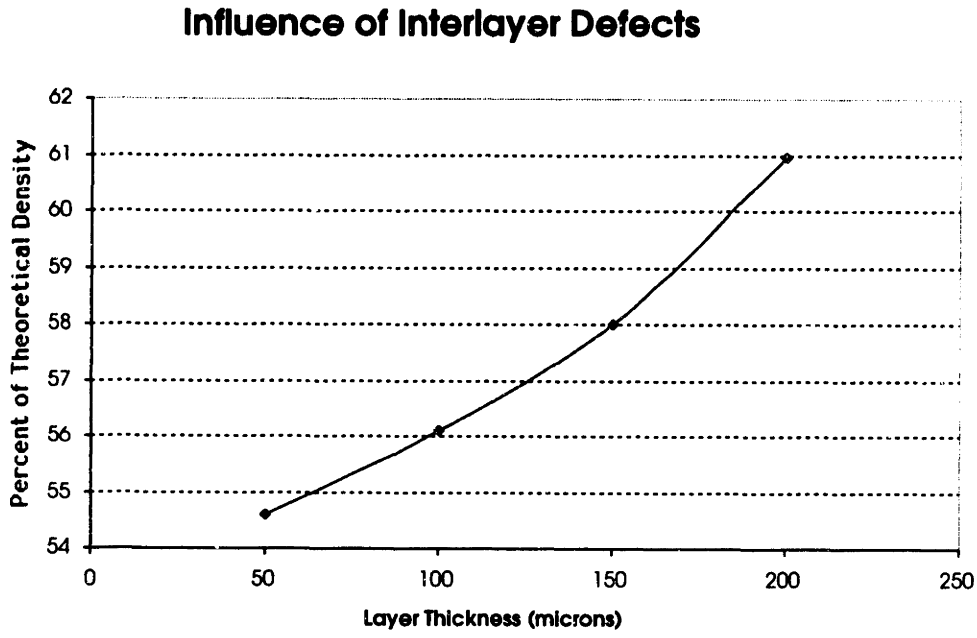

Time to fully slip cast can be expressed as:

$$t = \frac{\left(\frac{\xi_s}{n+1}\right)^2}{\Delta p}\left(\frac{\eta n}{2k_c} + \frac{\eta n^2}{2\varepsilon_m k_m}\right)$$

Where:
- Δp - the pressure drop across the porous mold
- n - factor (see below)
- η - solvent viscosity
- k_c - permeability of cast layer
- k_m - permeability of the mold
- ξ_s - initial wet slurry layer thickness
- ε_m - mold void fraction

The factor is n is defined as (reference):

$$n = \frac{(1 - x_s - \varepsilon_c)}{x_s}$$

Where:
- x_s - slurry solids loading
- ε_c - void fraction of cast layer

(Grau)

4. Rotary Apparatus

4.1 Overview and Motivation

It was hypothesized that a spiraling slurry deposition apparatus that made annular powder beds as illustrated in Figure 4.1 might avoid the bubbling problems encountered while attempting to tape cast powderbeds.

Figure 4.1: Spiraling deposition idea, top view

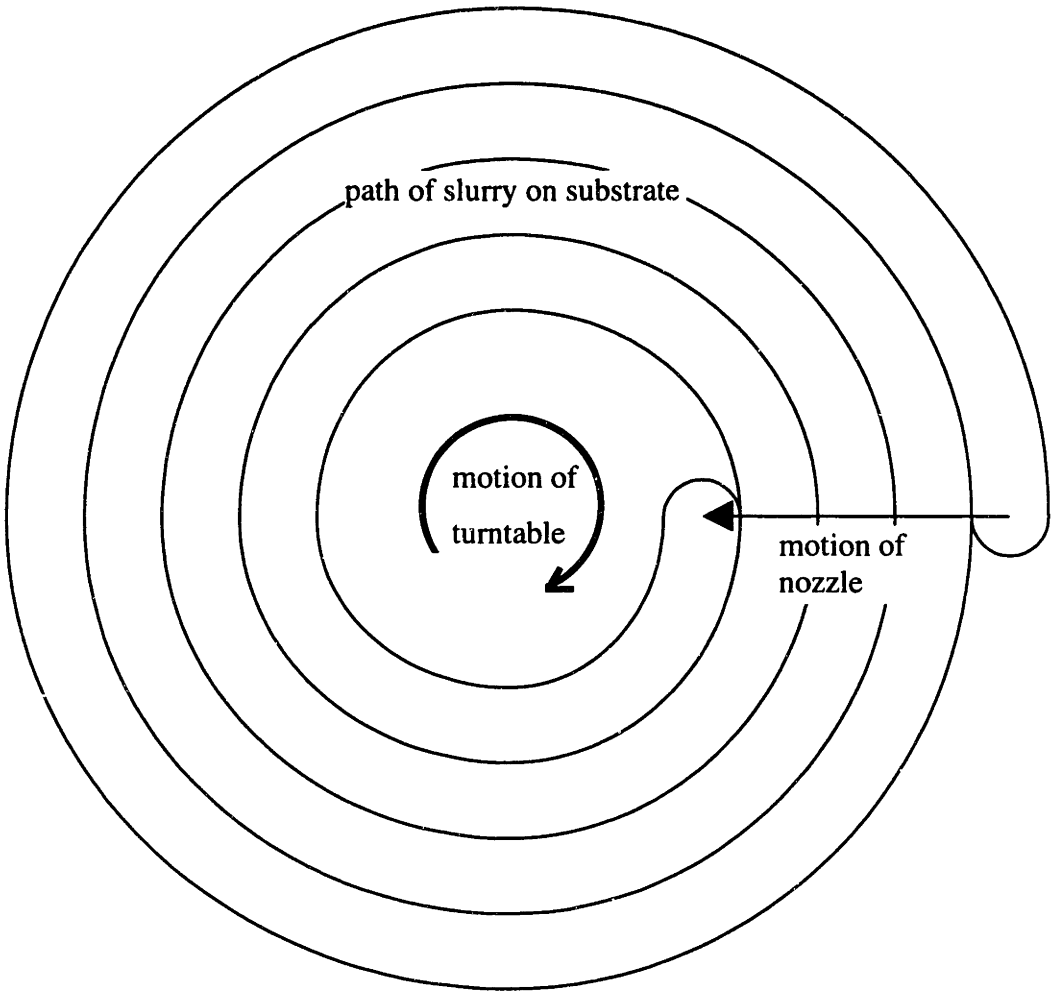

A spiraling slurry deposition apparatus could be built by putting an annular substrate on a turntable and mounting a slurry nozzle on a linear positioning slide above it. By rotating the turntable quickly and slowly moving the slide, the slurry nozzle would trace out a spiral path on the substrate. The bubbling problems would be avoided if the air being forced out by infiltrating solvent were allowed to escape ahead of the slurry front as shown in Figure 4.2.

Figure 4.2: Spiraling deposition idea, side view. cross-section

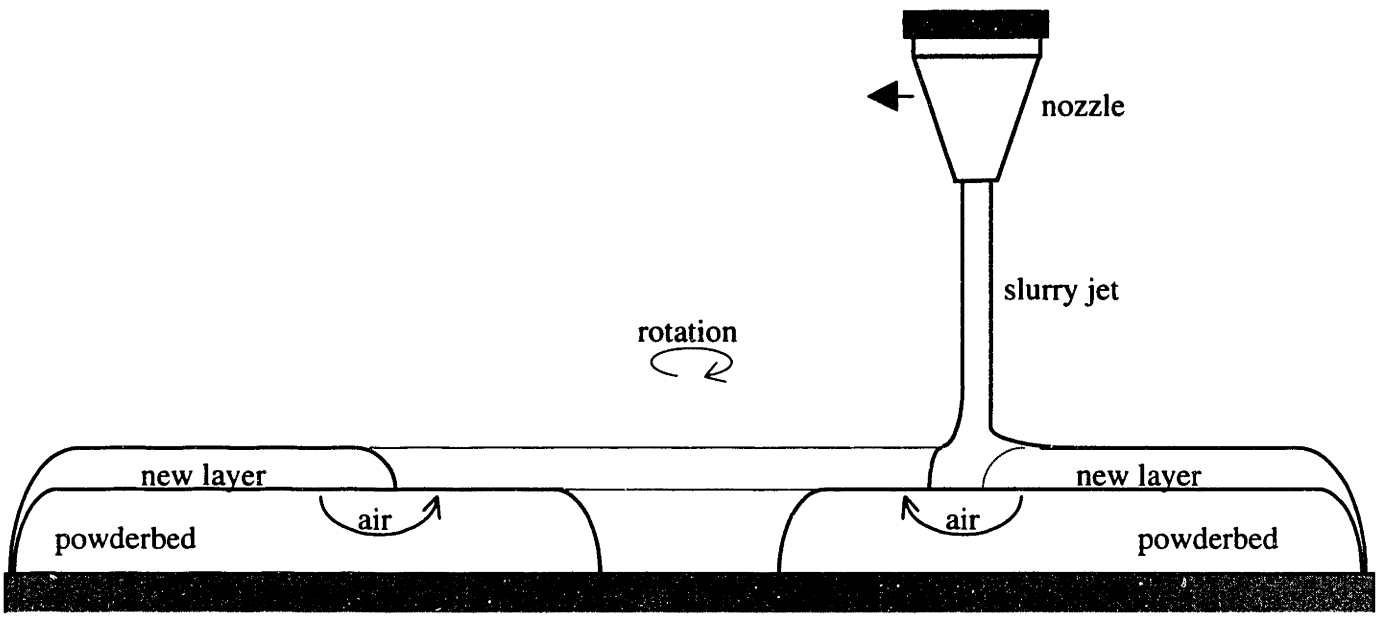

The spiraling slurry deposition apparatus idea had other merits besides having the potential to eliminate bubbling:

#1 Very fast line-stitching might eliminate the line-stitching defects associated with rastering a slurry nozzle on an x-y positioning system.

#2 A spiraling machine would not require the turn-around time required by a rastering machine, so higher throughput could be expected.

4.2 Proof of Concept

It was decided that the easiest way to test the hypothesis that a spiraling slurry deposition apparatus would simultaneously eliminate bubbling and line-stitching defects

would be to build a machine that deposited slurry in a circle. A substrate could then be moved slowly underneath, creating a pattern of side-by-side arcs, somewhat similar to a section of a spiral (see Figure 4.3)

Figure 4.3: Rotary slurry deposition apparatus, top view

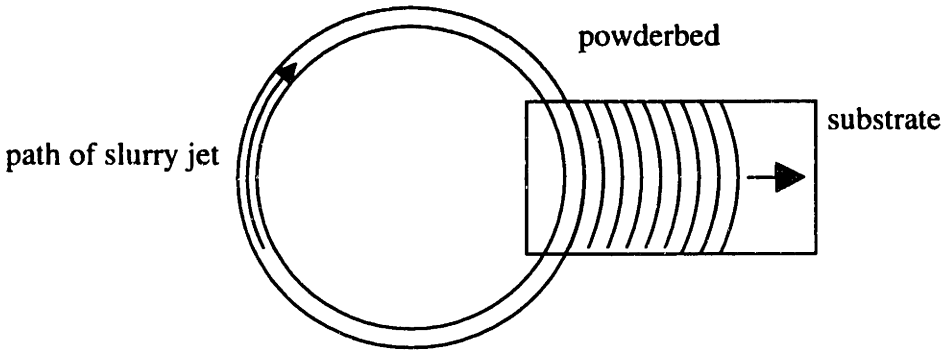

A rotary slurry deposition apparatus was constructed with a slurry jet at the end of a rotating arm, a substrate that moved radially underneath the slurry jet, and a z-stage, so that the substrate could be lowered for multiple layer builds (see Figure 4.4).

Figure 4.4: Rotary slurry deposition apparatus

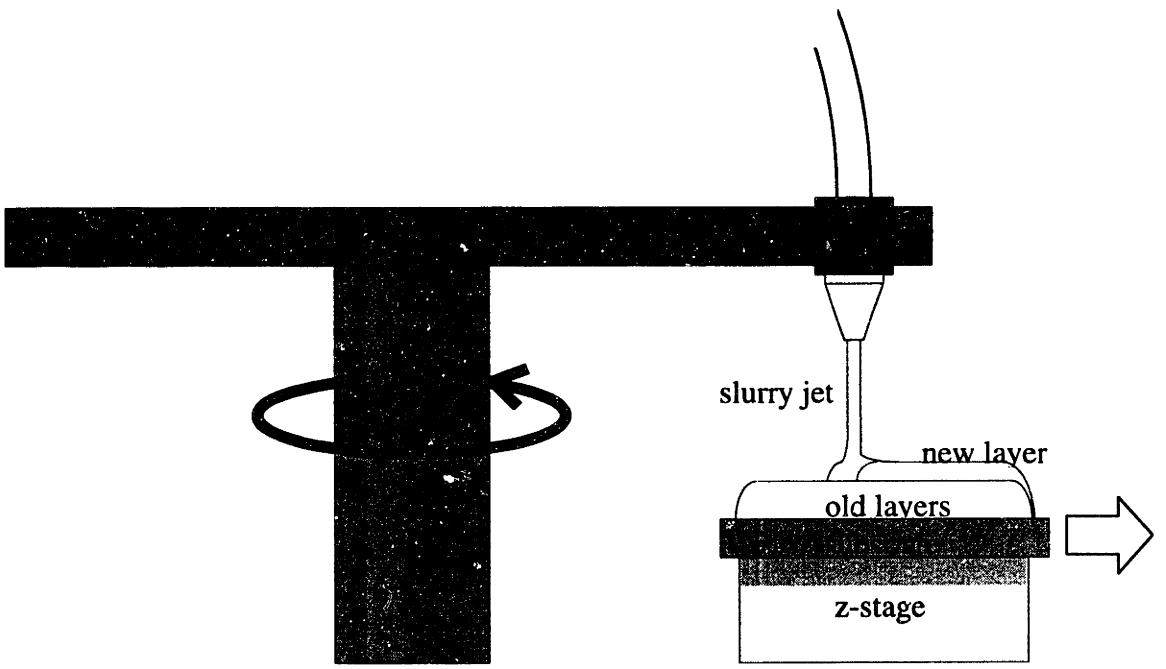

The arm rotated at speeds ranging from 300rpm to 1200rpm. The best results were gained when it was rotated at 600rpm, resulting in stitching times of a tenth of a second. Powder beds made at these stitching times were free of line-stitching defects (see Figure 4.5). To distinguish line-stitching that is so slow that it creates rows of defects from line-stitching that is so fast that it does not, the term "line merging" was adopted to describe the latter, more desirable process.

Figure 4.5 Comparison of powderbeds (transverse cross-sections)

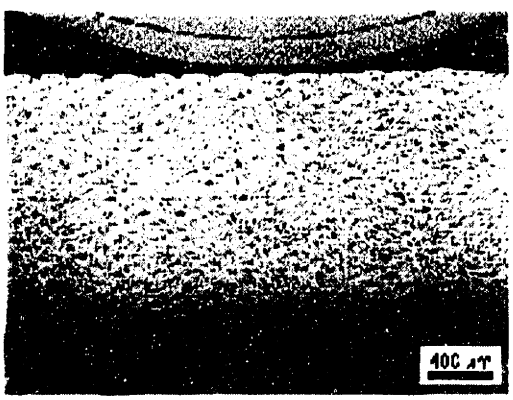

Layers produced by rastering nozzle using x-y positioning system

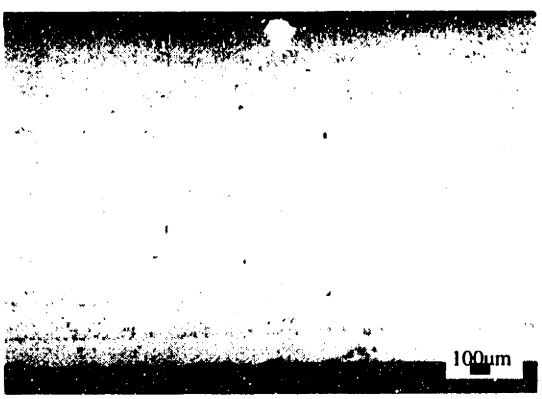

Layers produced by rotary apparatus. Each layer is 150 microns thick. Build details given below.

Experiments were performed with the substrates moved at a variety of speeds. The most successful builds, including the one pictured above to the right, occurred at slide speeds of 1mm/second, resulting in lines spaced 100 microns apart. Since the lines were around 300 microns wide, there was considerable overlap of lines. The radius of the path traced out by the nozzle was 2.39 centimeters. The flowrate was 4.5 grams/min, through a 127 micron nozzle. The tangential speed of the nozzle was 1.5 m/s. The top surface of a powderbed made under these conditions is shown in figure 4.6.

Figure 4.6: Top surface of powderbed made with rotary apparatus. Build details above.

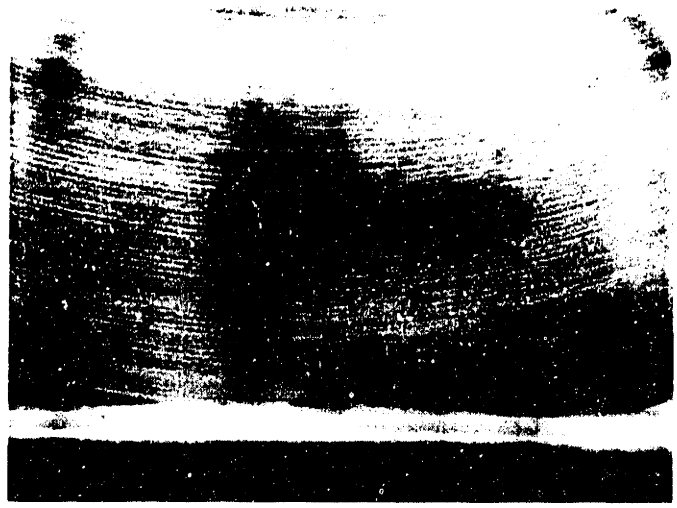

Despite the existence of a wet region that often exceeded three millimeters in width, the slurry deposited by the rotary printer rarely bubbled. Bubbling was usually confined to edge regions, or areas where a defect in the substrate propagated through. Apparently, the strategy for simultaneously eliminating bubbles and line defects was successful.

The sintered density of a powderbed created with the rotary printer was measured to be 96.8% of theoretical. Mercury porosimetry showed the powderbed to be free of large pores (see Figure 4.7)

Figure 4.7: Pore size distribution for green, debound powderbed fired at 1600 degrees Celsius. Powderbed made with rotary printer.

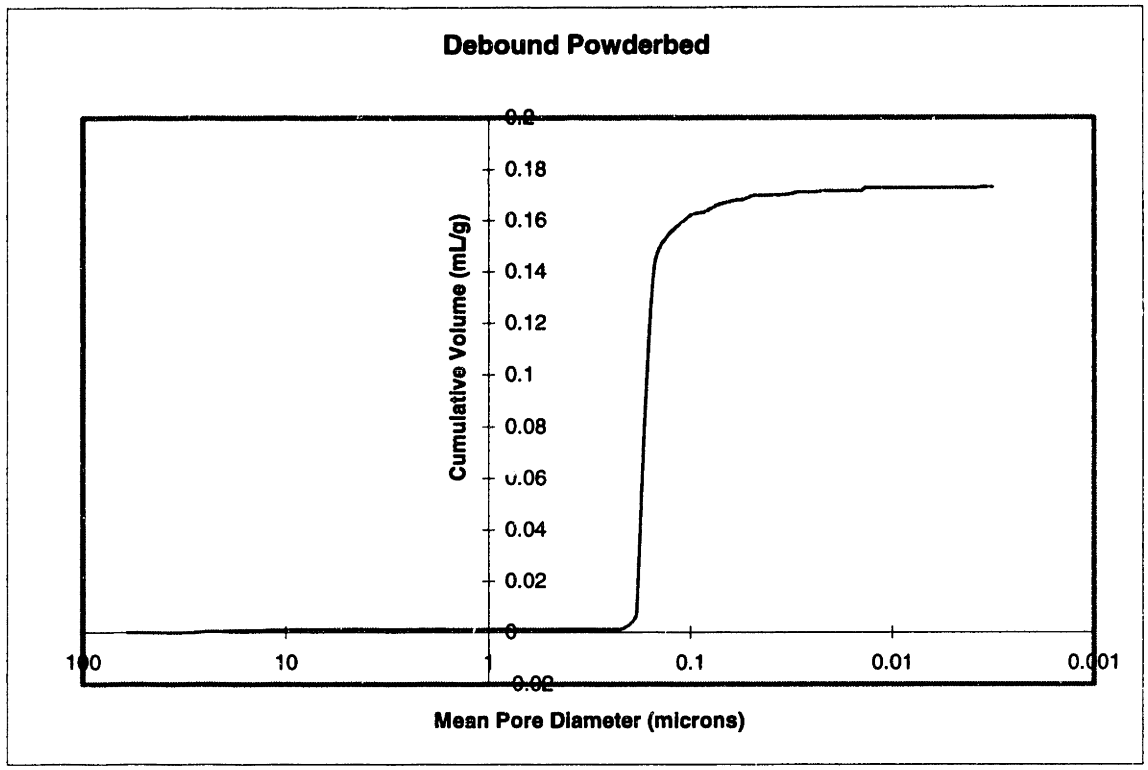

4.3 Problems with Rotary Apparatus

The rotary apparatus we constructed had several drawbacks:

#1 It could only make half-inch wide powderbeds (the arm axle was in the way of longer substrates)

#2 Every powderbed it made had a raised edge at the outside because the motors were just starting up when the lines constituting that area were deposited: consequently, the slide was moving slower, and the arm was moving slower, and a lot more slurry was deposited there than elsewhere.

#3 Our slide could not go slower than 1mm/sec. Consequently, we were not able to experiment with very low flow rates, and we were not able to make any smooth layers less than 150μm thick.

#4 Since the slurry was not laid out in an actual spiral pattern, but instead deposited in a pattern of side-by-side arcs, there was more slurry deposited at the sides of the powderbed than in the middle (see Figure 4.8). This caused a slurry build-up at the sides.

Figure 4.8: The problem with depositing side-by-side arcs

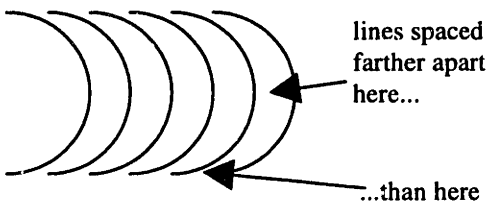

#5 Given certain operating conditions, deposited slurry would arrange itself into a pattern resembling wagon spokes radiating out from the inside edge of the powderbed (see Figure 4.9). The ridges and valleys of this pattern were *perpendicular* to the slurry lines. Slurry migration of this nature was different from that observed to occur during deposition on a damp powderbed, as described in the section on tape casting. Unlike this *randomly* patterned manifestation of slurry migration, *perpendicular* migration appeared to occur when **insufficient** slurry was deposited. It was hypothesized that surface tension caused the slurry to bead up instead of forming a smooth line of constant cross-section. This hypothesis was marginally supported by the fact that changing to a solvent with a higher surface tension made a previously robust system produce slurry migration. More convincing support for this hypothesis lies in a comparison to unstable varicose disturbances observed in fluid jets. In these disturbances, the instabilities are known to arise from the surface tension of the jet interface (Middleman, p484).

Figure 4.9: Slurry migration, perpendicular

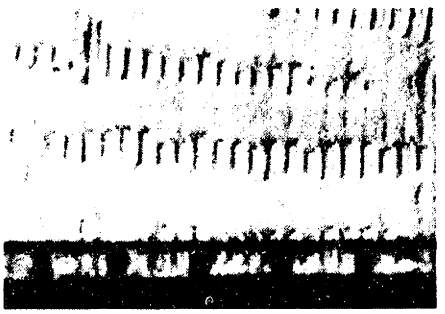

Slurry lines deposited in vertical direction.
Scale is in millimeters.

Some of the equations governing disturbances in fluid jets provide insight into the occurrence of perpendicular migration during powder bed formation. In particular, it appears that the wavelength of the disturbance can be predicted in the same way that the wavelength of a fluid jet's instability can be predicted. The disturbance that will grow most rapidly in a fluid jet has a wave number of

$$(kR)_{max} = 0.69$$

(Middleman, p487)

Since $k=2\pi/\lambda$ (Holman), the wavelength of the disturbance that will grow most rapidly will be

$$\lambda = \frac{2\pi R}{0.69}$$

When R is taken to be the radius of a slurry line instead of the radius of a fluid jet, the equation can be used to predict the wavelength of the perpendicular migration. This, of course is not the same thing as preventing it from happening, and is presented here only as a curiosity.

5. Belt Apparatus

5.1 Motivation

In order to maintain a constant linewidth and flowrate, a spiraling slurry deposition apparatus would have to change the rotational velocity of the turntable, and would subsequently have to change the velocity of the nozzle slide. These complications and the fact that the stitching time would change if the rotational velocity were changed, provided an impetus to shift the focus of the project from a spiraling apparatus to a belt apparatus that would function like the rotary apparatus. This apparatus would involve a belt on which a slurry nozzle would be mounted, and a substrate which would move underneath it (see Figure 5.1).

Figure 5.1: Belt Apparatus

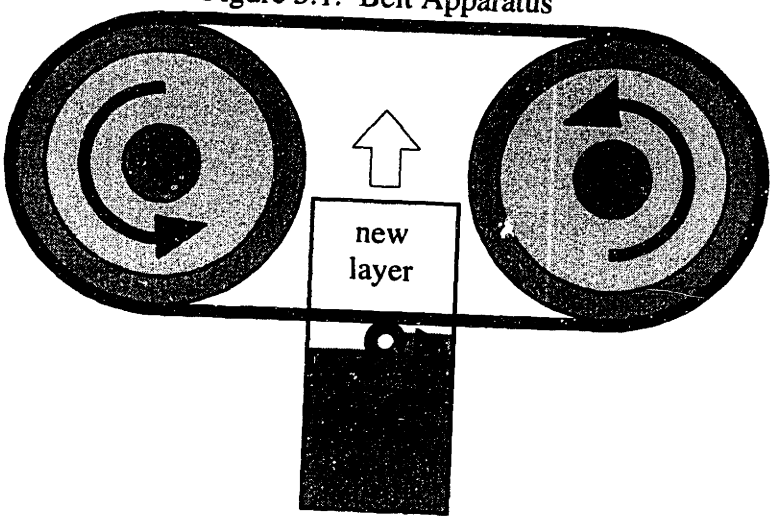

The belt apparatus would retain the positive aspects of the rotary apparatus (fast stitching and lack of bubbling) while simultaneously avoiding it's shortcomings (raised edges due to the fly-cutting pattern and limited print distance). A large, multiple-nozzle belt apparatus could create powderbeds of considerable width.

5.2 Implementation

Figure 5.2 is a schematic of the belt apparatus that was constructed. The nozzle was seated in a bearing so that it could rotate with respect to the belt. A thick plastic tube acted not only as a slurry feed line but also as a flexible coupling to fix the angular position of the nozzle with respect to the powderbed.

Figure 5.2: Belt apparatus

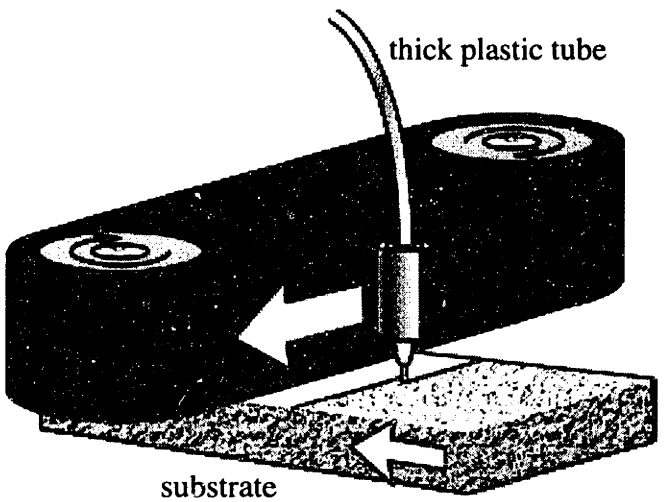

Since the experiments were all performed on short powderbeds that did not extend to the back of the apparatus, there was no need to put a slurry-catching trough on the back to prevent sections of the powderbed from being deposited on twice. We realized that creating long powderbeds would require the addition of such a slurry catcher as illustrated in figure 5.3

Figure 5.3 Creation of long powderbeds with the belt apparatus

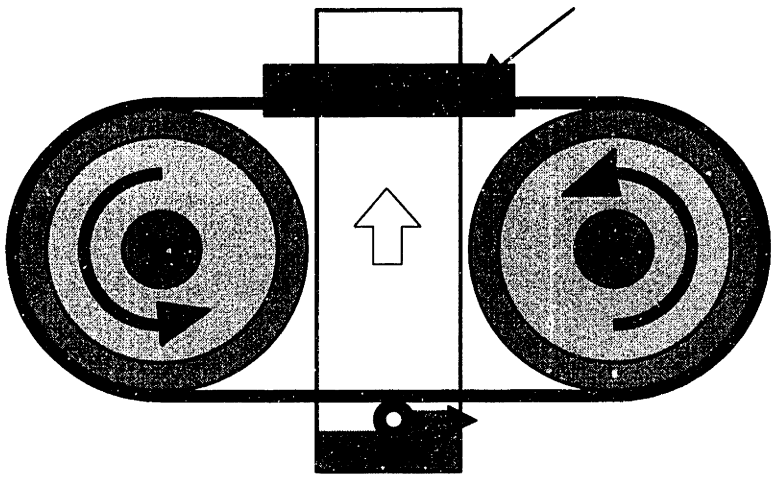

5.3 Results

Unfortunately, there was a disturbance which compromised the quality of the layers made with the belt apparatus. Each line of slurry that was deposited had a wavy shape, as shown in figure 5.4. At first the disturbance was believed to be due to the rotation of the nozzle in the bearing. The thinking was that if the jet of slurry were a little crooked, and the nozzle were to be rotate during the deposition phase, then the lines of slurry would not be straight. It was possible that the thick plastic tube was not performing its duty as flexible coupling in a satisfactory manner.

Figure 5.4 Disturbance in lines created with the belt apparatus.

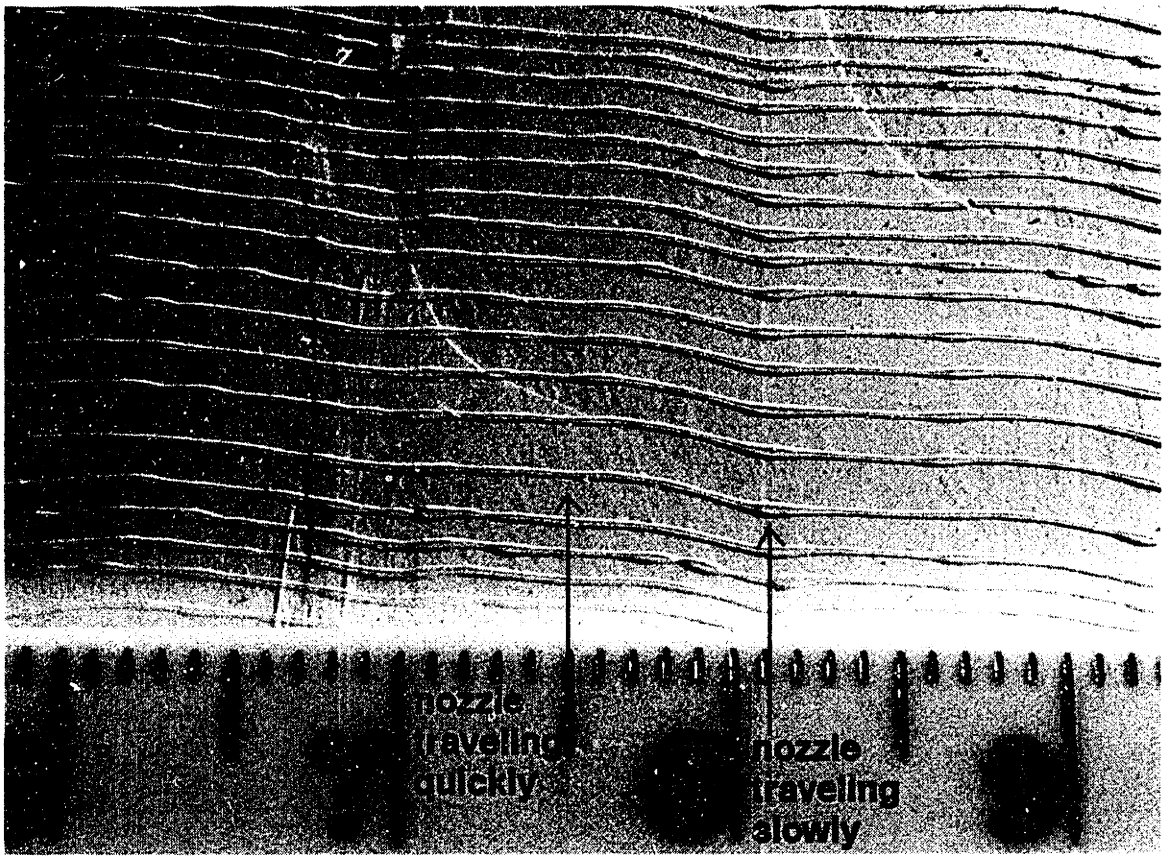

Individual lines of slurry produced by the belt apparatus, showing a repeating disturbance. Please note that the lines of slurry are spaced at irregular intervals because the substrate was pulled by hand.

In an attempt to correct this problem, the plastic tube was replaced with a flexible coupling constructed of four layers of wound brass wire with an alternating 45 degree bias. The slurry was fed to the nozzle through a thinner tube that was taped to the outside of the flexible coupling. Unfortunately, this did not solve the problem either. After trying other solutions, such as tightening the belts as much as possible, it was decided that the disturbance was likely due to unavoidable pressure pulses in the slurry line, and another approach to line-merging was undertaken.

6. Bicycle Wheel Apparatus

6.1 Overview and Motivation

The wiggles in the slurry path of the belt apparatus prompted an effort to design a mechanism that would be certain to deposit slurry in straight lines. A mechanism consisting of a bicycle wheel with two protrusions that bounce between springs was constructed as shown in figure 6.1.

Figure 6.1: Bicycle Wheel Apparatus

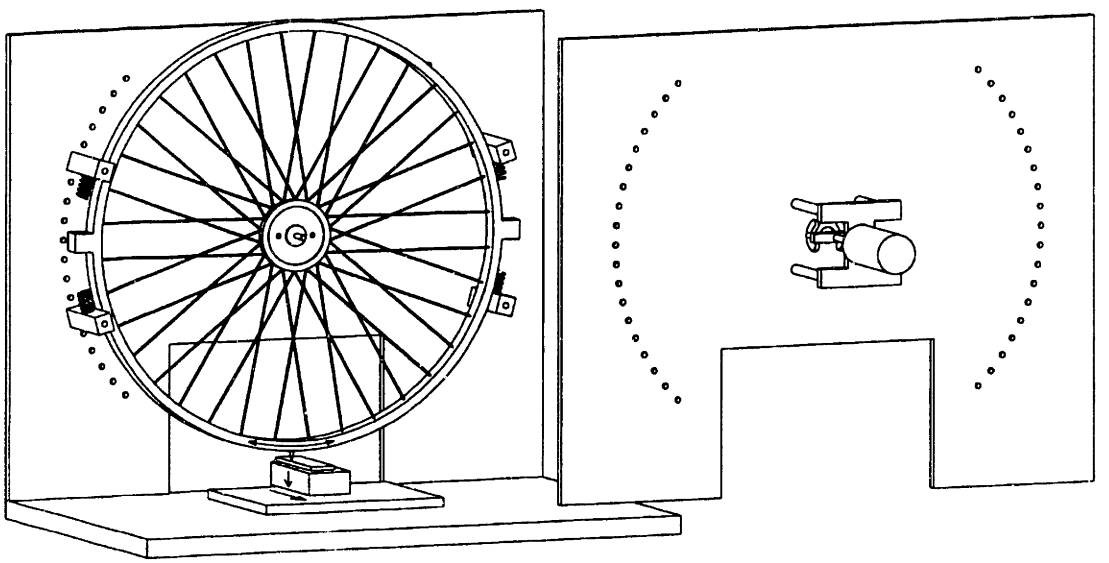

A nozzle on the rim of the wheel deposits slurry on the powderbed when moving in one direction only. When the nozzle is moving in the other direction, it is pivoted towards a trough, which catches the slurry (see Figure 6.2). The ability to turn slurry on and off will be important when a similar device is built to fabricate electronic components such as RF filters. In such devices it will be imperative for the slurry jet to be able to turn off at any given moment so that vias may be created *through* the layer with metal slurry.

Figure 6.2: Slurry on/off mechanism, side view. Nozzle assembly moves in and out of page

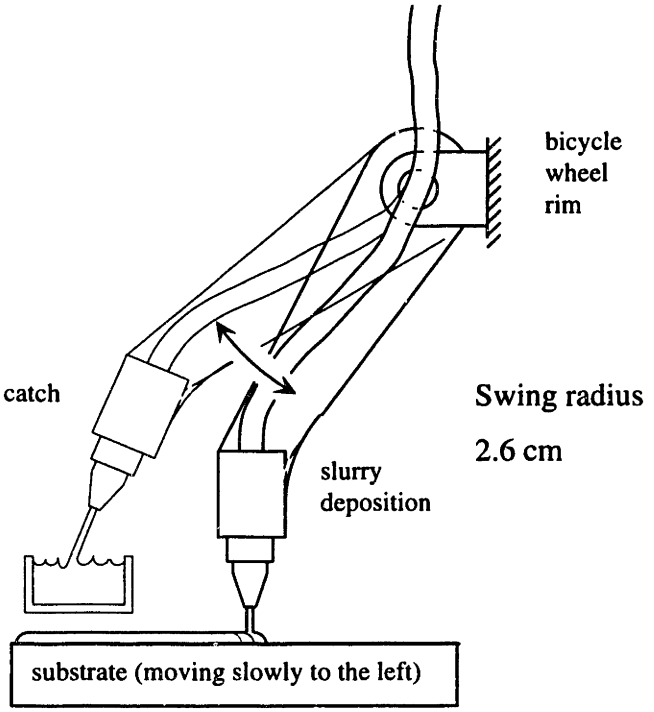

The powder bed is moved under the nozzle by a linear slide. By this means, lines of slurry are deposited next to each other on the powder bed as the bicycle wheel bounces back and forth. The springs can be moved closer or farther apart, resulting in cycle times ranging from 100ms to 550ms (assuming a nozzle speed of 1.5 m/s). The motion of the bicycle wheel is sustained by a DC motor which provides enough torque during each return pass to counteract the energy losses associated with friction, air resistance, and (most importantly) bouncing on the springs. The motor is rated for 24V maximum, and it's armature resistance is roughly 2.4ohms. Since it moves at low velocities (for an ungeared motor) the motor uses at most $24^2/2.4=240$ Watts. A muffin fan is used to cool the motor off.

The wheel's turn-around while in contact with the springs can be modeled as the period of a harmonic oscillator:

$$T = 2\pi\sqrt{\frac{m}{k}} \tag{6.1}$$

Where m is the mass that is oscillating, and k is the spring constant. The time that the wheel spends in one turn-around would be half the period of the full cycle. In the bike wheel system, contact is made with two springs at end of travel (two sets of springs for each wheel block), so the effective k in the above equation is doubled. The equation for predicting time spent in one turn-around follows:

$$Turn\ around\ time = \pi\sqrt{\frac{m}{2k}} \tag{6.2}$$

In this case, m is the effective mass of the wheel (and anything mounted to the rim of the wheel) acting at the radius from the center of the wheel to the spring. For the bicycle wheel apparatus m is 1.3kg. A specialized bicycle wheel was custom made for this set-up. The wheel has a double walled rim and large hub to provide extra rigidity. Additionally, the spokes are tensioned much higher than the spokes on an average bicycle wheel. These extra measures were taken to reduce vibration caused by spring collisions, which could affect the accuracy of slurry deposition. Additional information regarding the springs used with this device is given in Appendix C.

Though the nozzle actually moves in an arc (being mounted on the rim of a wheel) the path is close enough to a straight line that experiments to test the concept of line merging can be performed efficaciously, since the wheel is of a large radius and the path traveled by the nozzle is very short. If experiments indicate that line merging will eliminate line-stitching defects without adversely affecting powderbed quality, then a sliding version of the bike-wheel apparatus will be built, which will really move the nozzle in a straight line (see Figure 6.3).

Figure 6.3 Future version of device (concept)

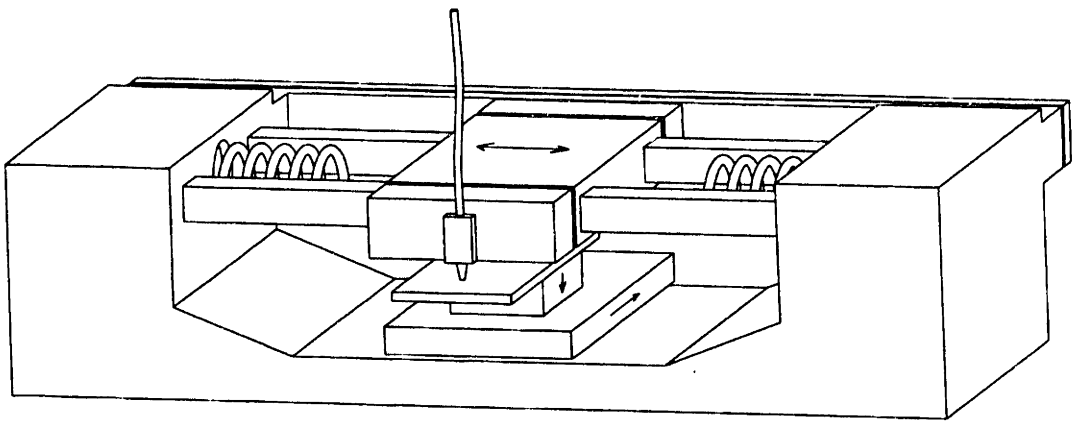

6.2 Initial Characterization

6.2.1 Parameters

6.2.1.1 Ratio of Line Width to Line Spacing

The ratio of the line width to the line spacing was used to measure the degree of overlap in each experiment. For a given set-up, line width is defined by the width of lines deposited individually (i.e., not touching). Line spacing is defined by the distance from the centerline of one line to the centerline of another, as seen from the top. The higher the ratio, the more the lines are overlapped. Ratios less than one indicate an absence of overlap. Line width was generally kept around 450μm, so the different values appearing in this chapter are mostly a reflection of the different line spacings used in the experiments.

6.2.1.2 Ratio of Cycle Time to Casting Time

The ratio of cycle time to casting time is used in this thesis in so that results for different slurries (with different slip casting times) can be compared more easily. Cycle times of approximately 100 msec, 300 msec, and 550 msec were explored to produce the results detailed in this thesis.

6.2.2 Method

Experiments were conducted to identify the ideal operating parameters to achieve successful line merging. One slurry was used for all experiments discussed in this chapter: 30 volume percent alumina (1 micron particle size) in a solvent of equal parts water and isopropyl alcohol. Two weight percent (based on solids) polyethylene glycol was added to enable powder bed redispersion. The slurry was 40 millimolar in nitric acid to stabilize the particles. Flow rates were held relatively constant across the full range of experiments to ensure that the jetting velocity remained constant throughout. As a result, slurry line widths were similar for all experiments (roughly 450μm).

Experiments focused on varying the cycle time and the line spacing. Before any set of experiments, the apparatus was operated with a rapid substrate slide speed so that individual lines could be examined for straightness and line width could be measured. The cycle time to slip-casting time ratio was based on observed slip cast times. Individual lines were video taped as they slip cast. The video was then replayed frame-by-frame to determine an approximate time for complete slip casting.

6.2.3 Experimental Results

6.2.3.1 Stitching

Powderbeds made with very little overlap and/or large cycle times had parallel ridges identical to those made by rastering a nozzle with an x-y positioning system. A layer with such stitched lines is shown in Figure 6.4.

Figure 6.4: Stitched lines. 500 μm wide lines at 325 μm spacing, 310 millisecond cycle time, visible peaks occur in regions of line overlap

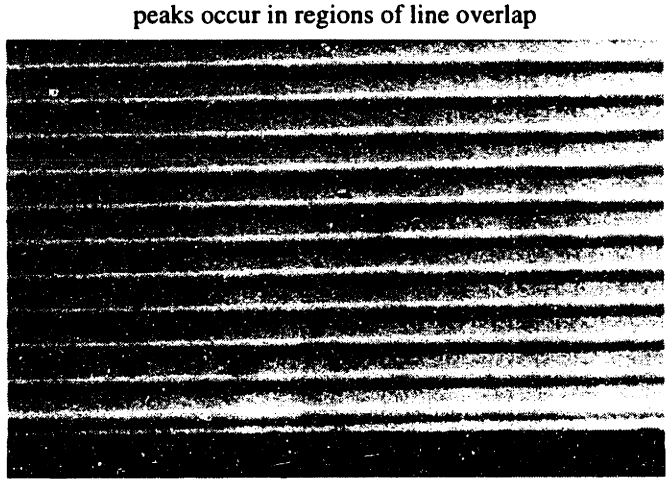

6.2.3.2 Perpendicular migration

As cycle time was gradually decreased, and overlap was gradually increased, lines made by the bike wheel apparatus started to reach back and cover previously deposited lines, forming a pattern of perpendicular slurry migration identical to that described in the Rotary Apparatus section (see Figure 6.5).

Figure 6.5: Perpendicular migration. 500 μm wide lines at 150 μm spacing, 310 msec cycle time, Lines start out looking nice and straight but quality degrades as perpendicular migration sets in.

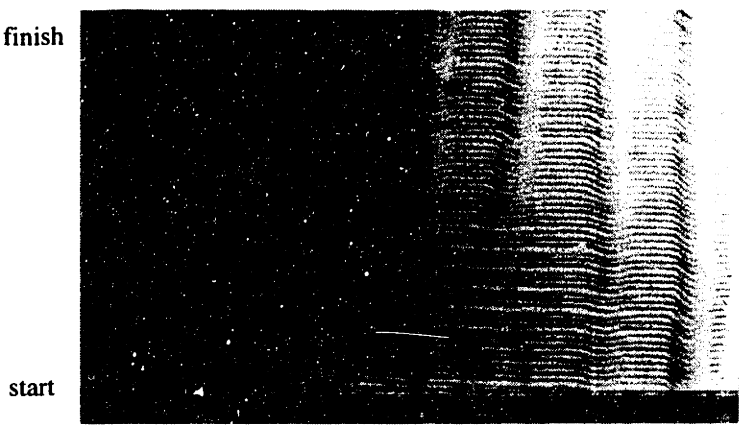

As the cycle time continued to be decreased and the degree of overlap continued to be increased, the perpendicular slurry migration pattern gave way to lines that were almost merged, but still showed some ridges in the direction of the nozzle's travel (see Figure 6.6).

Figure 6.6: Lines almost merged

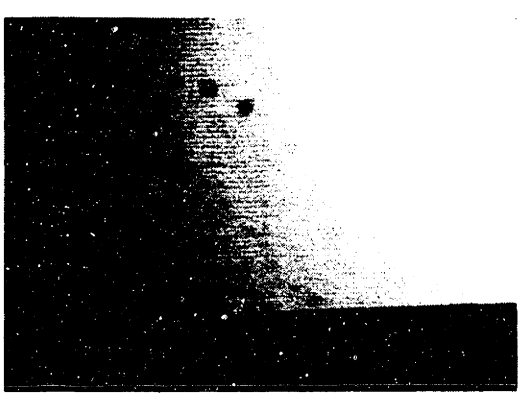

6.2.3.3 Oversaturation

On the other extreme, when lines were closely spaced, and the degree of overlap was very large, the substrate would become saturated with liquid and the slurry would migrate randomly, as shown in Figure 6.7. This migration was due to the long slip-casting times resulting from the soaking of the substrate and differential slip casting effects.

Figure 6.7: Oversaturated powderbed

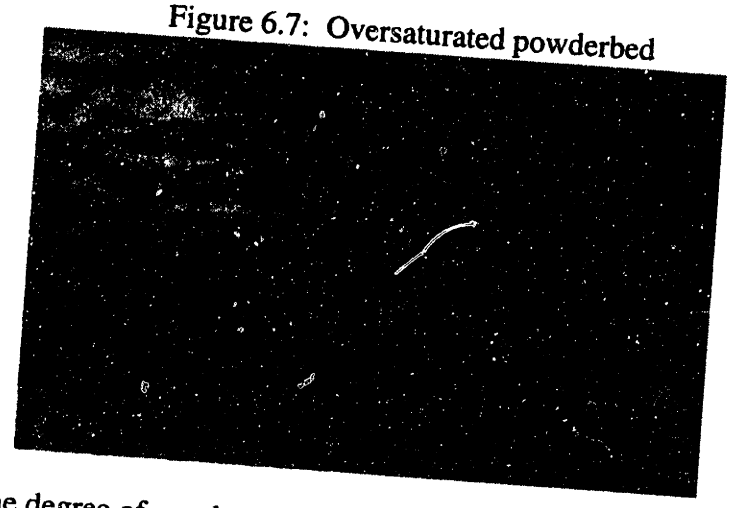

When the degree of overlap was slowly decreased, the pattern of random migration slowly gave way to a pattern of thick, ununiform lines, as shown in Figure 6.8.

Figure 6.8: Ununiform lines

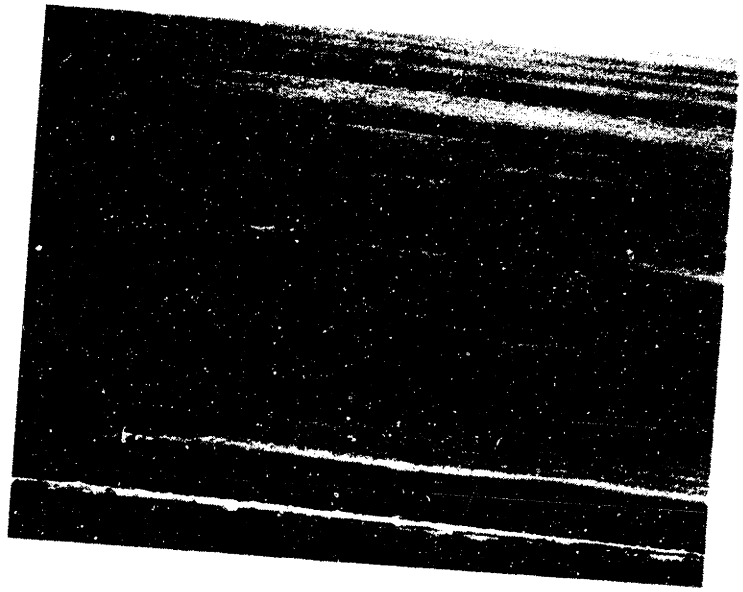

6.2.3.4 Bubbling

Very fast slide speeds resulted in powder beds containing bubbles. These bubbles were created by the same capillary pressure differences that created bubbling during the tape casting experiments. Greater overlap of lines resulted in larger, but fewer, bubbles. Powder beds made at substrate slide speeds below 1.3 mm/sec never bubbled, as long as the solids loading was not decreased below 30 volume percent. A powder bed containing bubbles is shown in Figure 6.9.

Figure 6.9: Bubbling

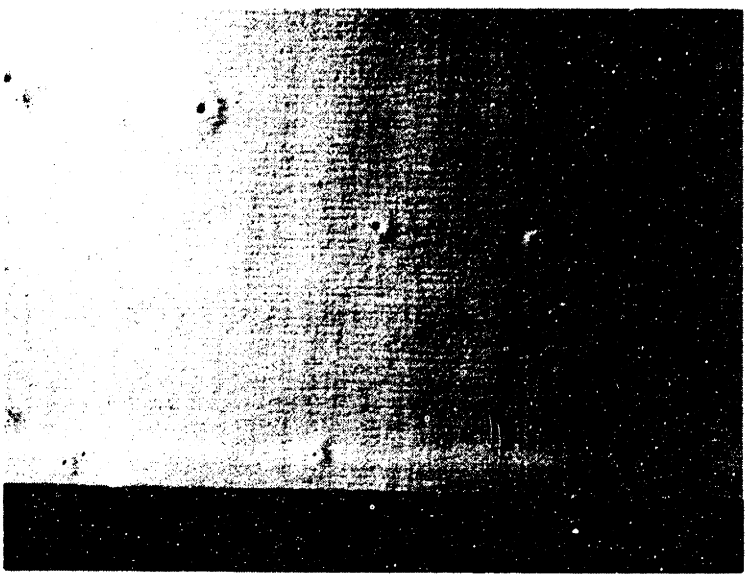

This powderbed was made with 22v/o slurry

6.2.3.5 Line merging

Finally, there was an operating window between the undesirable regions described above in which smooth layers with hardly any ridging were created. A powderbed made in this operating window is shown in Figure 6.10

Figure 6.10: Powderbed made by line merging

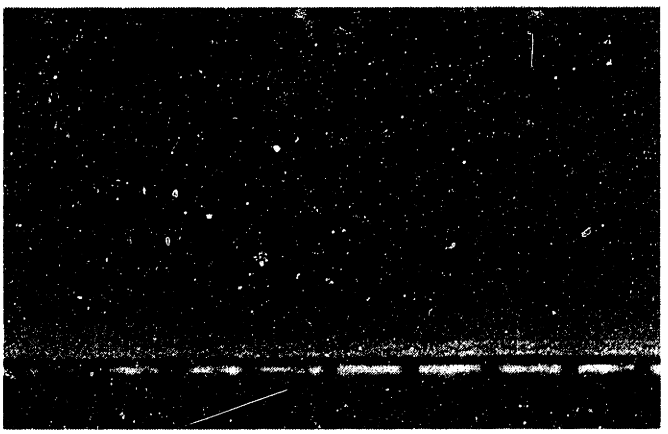

6.2.3.6 Summary

The results for the experiments performed on the bicycle wheel apparatus with 30 volume percent slurry are given below in graphical form. These experiments were done with 1:1 water to IPA slurry, jetted at 3m/s through a 127μm nozzle traveling at 1.5m/s. Under these conditions, the slurry slip-cast in 500ms when deposited in individual lines.

Figure 6.11: Results of bicycle wheel experiments. Line width generally held constant at 450 microns, Slip Casting Time assumed to be constant at 500msec. Axes non-dimensionalized for the sake of comparison with other slurry systems.

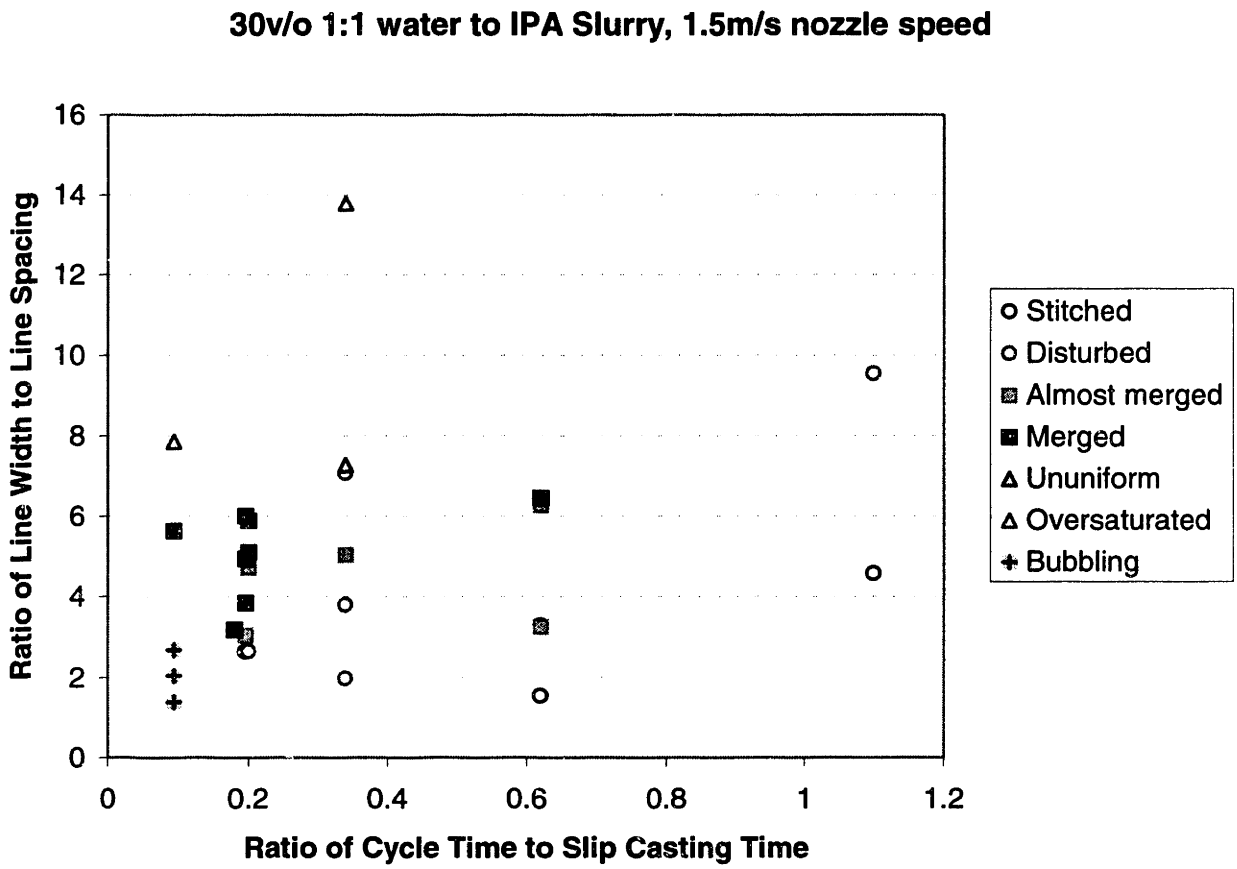

Conclusions

The seven different operating regions described above are plotted out in Figure 6.12. The best results were obtained with 90-100 millisecond cycle times, and width ratios of approximately 5.5.

Figure 6.12: Operating Regions for 30v/o water to IPA slurry, 1.5m/s nozzle speed. Line width generally held constant at 450 microns, slip casting time assumed to be constant at 500msec. Axes non-dimensionalized for the sake of comparison with other slurry systems.

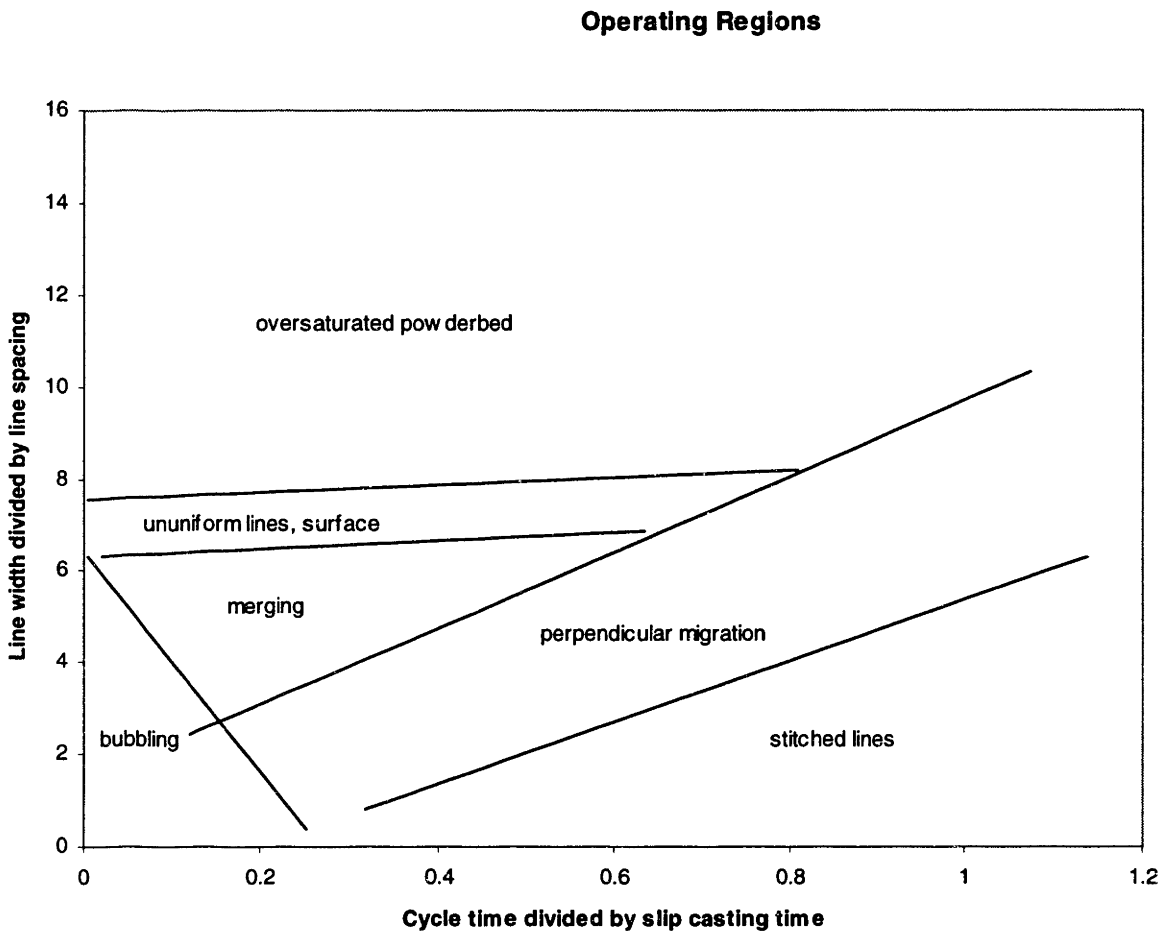

7. Line Merging Modeling

Ceramic layer fabrication by line merging was first explored with the rotary apparatus (Chapter 4). Rotary deposition was merely a quick exploration that proved the concept. More in depth study was required before layer fabrication via line merging could be used to build powder beds for parts.

Practical implementation of line merging requires that ideal deposition parameters be identified. Rotary deposition was essentially a trial-and-error approach to layer deposition. After one layer was deposited, the results were used to tweak the parameters until an ideal ceramic layer was produced. To be able to predict successful line merging, rough models are required to relate the many parameters: slurry loading, cycle time, line width, line spacing, flow rate, nozzle velocity, etc. The parameter space needs to be mapped out so that ideal conditions can be identified.

7.1 Notation

Throughout this chapter many variables, relationships, and equations will be used to identify ideal operating parameters for successful line merging. The following notation will be used:

Table 7.1 Notation to be used in line merging modeling

d	distance
k_c	permeability of slip cast alumina slurry layers
l	line spacing
L_{slurry}	width of wet slurry front that traverses substrate
p	packing fraction of slip cast alumina layer
P_c	capillary pressure
Q	slurry volumetric flow rate

s	slurry solids loading (volume fraction)
S_f	safety factor of 0.8
t	time
t_{crit}	critical saturation thickness before layers crack
t_{sat}	saturation thickness
t_w	wet slurry layer thickness
t^*	target dry layer thickness
T_c	cycle time between deposited slurry lines
T_s	slip casting time for a layer of slurry
v	nozzle velocity (traverse speed)
v_{slurry}	velocity at which wet slurry front moves across substrate
$v_{solvent}$	velocity at which solvent moves through pore space of substrate
w	line width
ε	void fraction of slip cast alumina slurry layers
η	slurry solvent viscosity

7.2 Critical Relationships

7.2.1 Slip Casting Time Versus Cycle Time

For line merging to occur, the second line must be deposited before the first line has fully slip cast. The degree of line merging will be influenced by how large the ratio is between slip casting time and cycle time. If a line takes approximately 0.5 seconds to slip cast and the cycle time for line deposition is 0.1 seconds, then 5 lines can be deposited before the first line has fully slip cast.

Once lines are merging, the time that it takes a region of a layer to slip cast will no longer be reflected by an individual line's slip casting time. A better measure of slip casting time is the time that it takes the total wet layer thickness to slip cast. The wet layer thickness is determined from the slurry volumetric flow rate, line spacing, and nozzle velocity:

$$t_w = \frac{Q}{lv} \tag{7.1}$$

The ratio of slip casting time over cycle time can be expressed as:

$$\frac{T_s}{T_c} = \frac{C_1}{T_c}\left[\frac{Q(1-s)}{lv}\right]^2 \tag{7.2}$$

where C_1 = 7.35E7 s/m^2 (Saxton)

7.2.2 Line Width Versus Line Spacing

For line merging to occur, the lines must partially overlap. The degree of overlap can be looked at as the ratio between the width of an individual line and the spacing between deposited lines. The degree of overlap will influence how thick the final layer is; high levels of overlap will result in thick layers. The line width to line spacing ratio can be expressed as:

$$\frac{w}{l} = \frac{1}{l}\left(\frac{C_2}{s} + C_3\right)\sqrt{\left(\frac{Q}{v}\right)} \tag{7.3}$$

Where C_2 = 4.7 and C_3 = -0.065 (Saxton)

7.2.3 Line Width and Wet Front Advance Versus Bubbling

It has already been determined that wide slurry lines (> 800 microns) have a tendency to bubble, most likely because air is trapped during slip casting. To avoid bubbling in line merging, the lines must be narrower than this critical width.

The rate at which the wet slurry front advances across a dry porous substrate also influences the occurrence of bubbling. The velocity at which the wet slurry advances across the substrate is:

$$v_{slurry} = \frac{l}{T_c} \tag{7.4}$$

Line merging is able to avoid bubbling because a solvent front fills the pore space ahead of an advancing wet layer. If this wet front advances across the substrate more rapidly than the solvent can penetrate the pore space ahead of the front, air will be trapped and bubbling will occur. The time required for a given solvent to permeate a distance d through the powder bed pore space can be determined by integrating the Washburn equation:

$$\frac{dl}{dt} = \frac{kP_c}{\varepsilon \eta d} \tag{7.5}$$

$$t = \frac{\varepsilon \eta d^2}{2k_c P_c} \tag{7.6}$$

The rate at which solvent can travel through pore space is given by a restatement of the Washburn equation in terms of the line spacing:

$$v_{solvent} = \frac{2k_c P_c}{\varepsilon \eta l} \tag{7.7}$$

For typical values of k_c = 4.18 E-16 m^2, P_c = 362 kPa, ε = 0.41, η = 2.69 cP, and l = 150 microns, $v_{solvent}$ = 1.82 mm/s. Due to viscous drag effects as the solvent advances through the pores, the average velocity of the solvent front depends on the length through which it travels. Since each deposited line represents a new source of solvent that can advance before the next deposited line, the critical length is the spacing between lines. To prevent bubbling, the solvent from a line must travel a distance equal to the line spacing before the next slurry line is deposited.

7.2.4 Width of Wet Front Versus Migration

The amount of slurry comprising the wet front will influence its propensity to migrate. Large amounts of slurry take longer to slip cast, allowing more time for migration to occur. The amount of wet slurry present in the wet front is most easily measured as the width of the wet front:

$$L_{slurry} = \frac{T_s l}{T_c} \tag{7.8}$$

This equation is merely the number of lines that are partially wet at one time (T_s/T_c) times the incremental spacing between each line.

Additionally, an extremely large wet front is symptomatic of over-saturation. Large wet fronts (> 5mm) can only occur (for reasonable cycle times > 0.1 sec) if slip casting is occurring slowly. Slow slip casting is a sign that the pore space of previous layers is becoming filled with solvent. Over-saturation can lead to wide scale migration due to differential casting rates.

7.2.5 Solvent Flux Versus Layer Cracking

To avoid layer cracking, the solvent flux reaching the powder bed must be such that the saturation thickness is less than the critical saturation thickness. The solvent flux is directly related to the thickness of the slurry layer deposited and inversely related to the solids loading of the slurry. The packing fraction of the powder bed layer will influence the saturation thickness (Figure 7.1). The saturation thickness for a deposited layer of slurry is as follows:

$$t_{sat} = \frac{Q(1-s)}{l v \varepsilon} \tag{7.9}$$

Figure 7.1 Schematic showing saturation thickness, which is the thickness of the region of pore space that is 100% saturated by the solvent from a slip cast layer

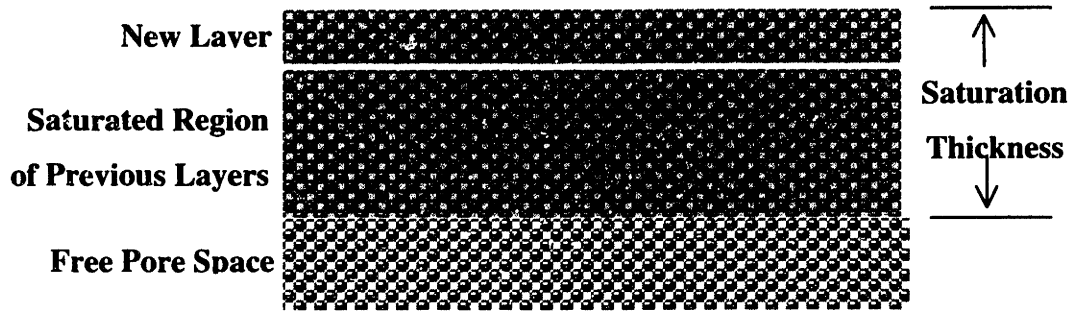

7.3 Analyzing the Critical Relationships

The critical relationships described above are interesting, but not very useful by themselves. Further analysis reveals that all of the equations can be tied to one another through four independent variables. The other variables are constant for a given slurry.

7.3.1 Target Layer Thickness

In 3DP the layer thickness determines the maximum resolution that can be expected in a finished part. Any surface not parallel to one of the axes will display a stair-stepping pattern reflective of the individual layers that comprise it. Accordingly, layer formation through line merging must be analyzed with a target layer thickness in mind. This target dry layer thickness can be expressed as:

$$t^* = \frac{Q s}{l v p} \tag{7.10}$$

This target dry thickness is merely the thickness of the deposited wet slurry layer from equation 7.1 times the solids loading of the slurry divided by the final packing fraction of the particles in the slurry. It is important to note that Q and v always appear together

when expressing the amount of slurry deposited in a given region (equations 7.2, 7.3, 7.9), thus Q/v can be treated as one independent variable. The equation for target dry layer thickness specifies that for a given thickness only two of the three variables Q/v, s, and l, can be independent. The layer packing fraction p is considered constant for a given slurry. It is typically 0.55 for 1 micron particle size alumina slurries. The line spacing is typically the easiest setting to adjust on 3DP deposition machines, so it is selected as the dependent variable. The other variables (Q/v and s) are bounded, so they are chosen as the independent variables.

7.3.2 Independent Variables

Q/v and s were selected as independent variables for line merging analysis in the previous section. Additionally, T_c is an independent variable that is typically bounded by the limits of the 3DP deposition machines themselves. These three variables will be used to analyze and optimize the line merging parameter space. Though independent, these three variables do have bounds.

7.3.2.1 Bounds on cycle time

The bounds on cycle time are primarily driven by the machine used to deposit the lines. As the desired cycle time decreases, it is much more difficult to build a machine that can uniformly deposit slurry without being adversely affected by speed irregularities and vibration. The bicycle wheel apparatus (Chapter 6), is capable of operating between 0.1 sec and 0.5 sec cycle times, given a minimum speed of 1.5m/s.

7.3.2.2 Bounds on solids loading

The solids loading of slurries used in line merging has both upper and lower bounds. The minimum solids loading is related to layer cracking. If the solids loading is too low, too much solvent causes the layer's saturation thickness to exceed the critical saturation thickness. An expression can be derived for this lower bound by combining a

safety factor with equations (7.9) and (7.10) for a given target dry layer thickness to express saturation thickness as:

$$t_{sat} = \frac{pt^*(1-s)}{s\varepsilon} < S_f\, t_{crit} \tag{7.11}$$

Which leads to the expression:

$$s > \frac{\dfrac{pt^*}{\varepsilon S_f\, t_{crit}}}{1 + \dfrac{pt^*}{\varepsilon S_f\, t_{crit}}} \tag{7.12}$$

Assuming $p = 0.55$, $t^* = 50$ μm, $\varepsilon = 0.41$, and a $S_f = 0.8$, then the minimum solids loading varies as a function of critical saturation thickness as shown in Figure 7.2. For 1 micron alumina slurries with all water solvent, the critical saturation thickness has been observed to be approximately 350 microns. The reduced solvent surface tension of slurries formulated with 1:1 water to isopropanol (by volume) solvents will only increase the critical saturation thickness.

Figure 7.2 Plot relating the minimum slurry solids loading that will produce crack-free layers

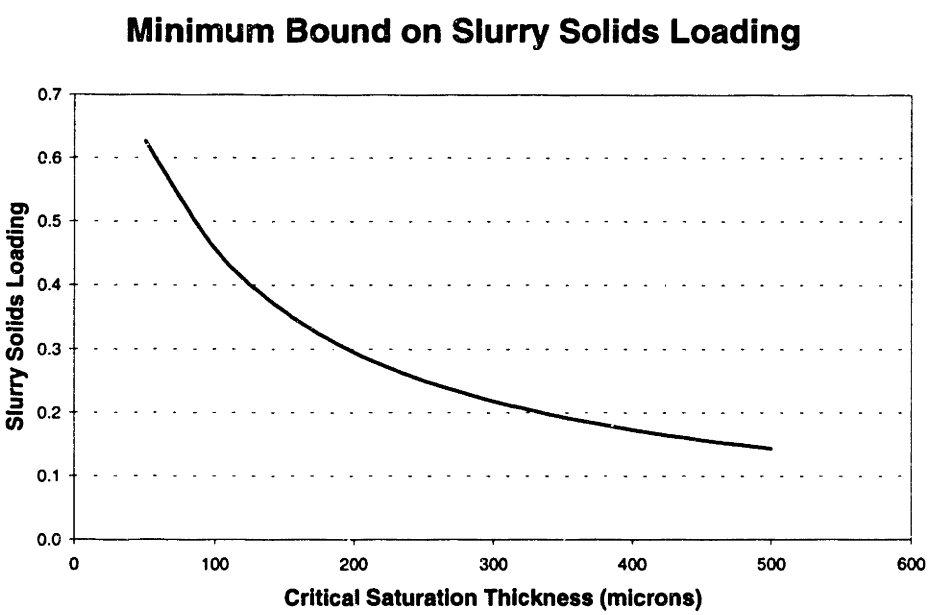

The upper bound on solids loading is determined by jetting conditions. Slurries with solids loadings above 0.40 are very difficult to jet. They have a tendency to fully or partially clog nozzles. Jet stability is critical; a jet deflection due to a partial nozzle clog is enough to ruin a ceramic layer, and consequently ruin the entire powder bed. For these reasons, the upper bound for solids loading was set at 0.40.

7.3.2.3 Bounds on Q/v

Q/v is bounded by the combination of individual bounds on Q and v. The lower bound of the volumetric flow rate Q is determined by jet stability. A minimum jetting velocity of approximately 2.5 m/s is required to produce a stable jet. This jetting velocity and 127 micron orifice size combine to yield a Q of approximately 3.2E-8 m^3/s (1.9 cc/min). The upper bound of the volumetric flow rate is likewise related to the jetting velocity. A jetting velocity that is too high will cause the slurry to splatter on the powder bed surface, resulting in irregular lines and surface finish. The maximum jetting velocity is approximately 8 m/s, which corresponds to a Q of 1.0E-7 m^3/s (6.0 cc/min).

The upper and lower bounds on the nozzle velocity v are determined by the slurry deposition apparatus (Chapter 6). The maximum v is approximately 2.8 m/s at a 0.1 sec cycle time and the minimum v is approximately 0.25 m/s at a 0.5 sec cycle time.

7.4 Summary of Relationships

The critical relationships were expressed as functions of only the independent variables and the target dry layer thickness. The effects of changing one of the independent variables could then be easily seen.

7.4.1 Slip Cast Time Divided by Cycle Time

Rotary deposition revealed that in most cases, maximizing the ratio of slip cast time divided by cycle time produced the best layers. The best merging typically occurred when many lines were able to merge into one front. Combining equations (7.2) and

(7.10) yields one equation for T_s/T_c relating it to the independent variables and target dry layer thickness:

$$\frac{T_s}{T_c} = \frac{C_1}{T_c}\left[pt^* \left(\frac{1}{s} - 1 \right) \right]^2 \tag{7.13}$$

7.4.2 Line Width Divided by Line Spacing

Rotary deposition revealed that to an extent maximizing the line overlap produced the best layers. Combining equations (7.3) and (7.10) yields one equation for *w/l* in terms of the independent variables and the target dry layer thickness:

$$\frac{w}{l} = pt^* \left(\frac{C_2}{s} + C_3 \right) \left(\frac{Q}{v} \right)^{\frac{-1}{2}} \tag{7.14}$$

7.4.3 Width of Slurry Wet Front

In order to reduce the chances of slurry migration, the width of the wet front must not be excessive. The wet front can not be minimized because a certain width of wet front is required for the slurry to slip cast as a uniform layer rather than separate lines. The width of the slurry wet front can be expressed in terms of the independent variables and dry layer thickness by combining equations (7.8), (7.10), and (7.13):

$$L_{slurry} = \frac{C_1 pt^*}{T_c} \left(\frac{Q}{v} \right) \frac{(1-s)^2}{s} \tag{7.15}$$

7.4.4 Velocity of Slurry Wet Front

To avoid bubbling the slurry wet front must not traverse the powder bed faster than the solvent can travel through the pore space of the substrate. In terms of the independent variables and dry layer thickness, combining equations (7.6) and (7.10), the expression is:

$$v_{slurry} = \frac{s}{pt^{*}T_c}\left(\frac{Q}{v}\right) < v_{solvent} \tag{7.16}$$

To increase throughput, the objective is to increase v_{slurry} up to the limiting value of $v_{solvent}$.

7.5 Trends

The complex relationships between the previous equations (7.13-7.16) and the independent variables can best be summarized in the Table 7.2. This table lists the four primary equations that are to be optimized and shows what direction the independent variables should be adjusted to move towards optimization. The relationships assume a fixed target dry layer thickness and slurry composition.

Table 7.2 How to adjust independent variables to approach optimum conditions for line merging

		Independent Variables		
Optimization Eqn	**Objective**	**T_c**	**Q/v**	**S**
T_s/T_c	Increase	↓	_	↓
w/l	Increase	_	↓	↓
L	Reduce	↑	↓	↑
v_{slurry}	Increase up to $v_{solvent}$	↓	↑	↑

The trends shown in the table above can be transformed into a plot (with T_c and Q/v as the independent variables) that shows generally where layer defects are likely to occur (Figure 7.3). The actual position and slope of the lines on the plot depends on the slurry solids loading, but the general relationships hold for any solids loading. Ideally the thresholds for each defect would intersect to form some valid operating window where good layers could be produced. It should be noted that bubbling occurs when v_{slurry}

exceeds $v_{solvent}$, so from the perspective of avoiding bubbling, v_{slurry} should actually be minimized.

Figure 7.3 General parameter map showing trends where layer defects are likely to occur in relation to Q/v and T_c

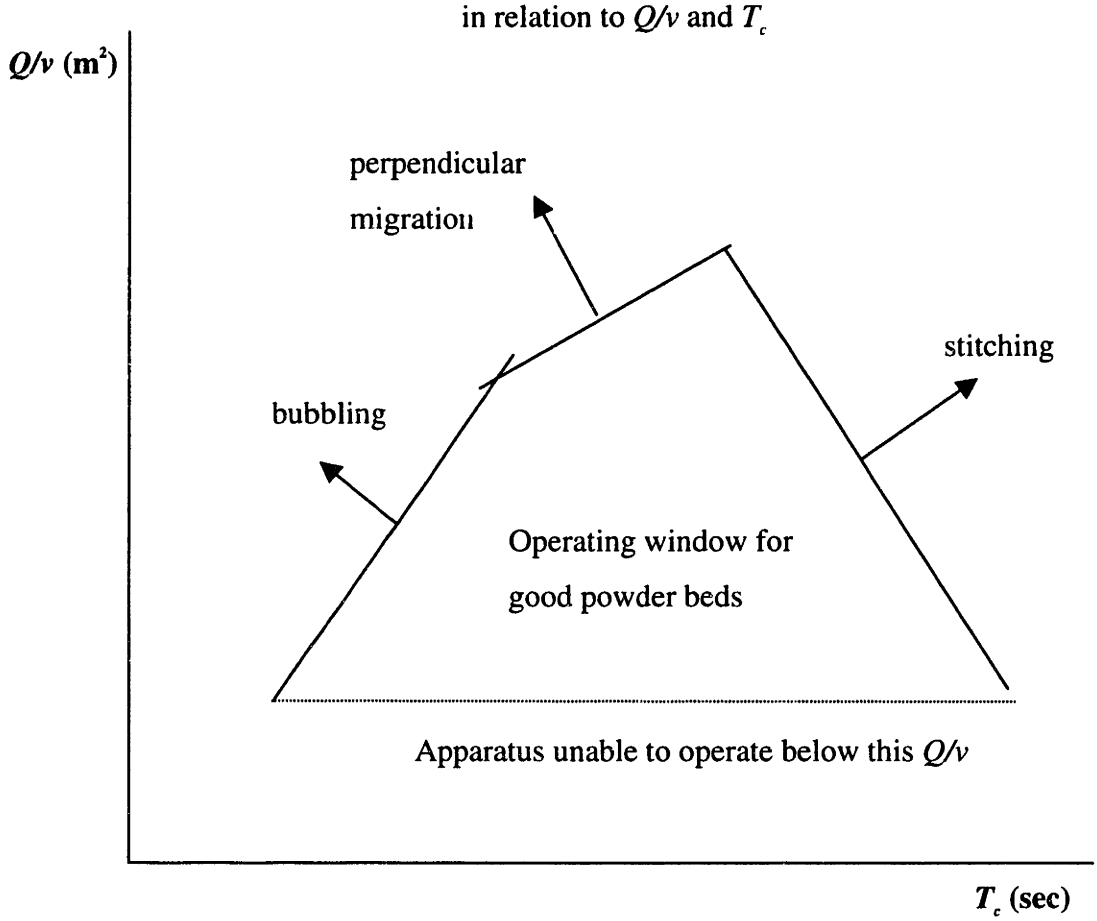

7.6 Optimization

The independent variables, constraints, and relationships were entered into an Excel spreadsheet. Four separate three-dimensional plots were constructed to depict the magnitudes of three of the four different objective functions versus T_c and Q/v. The solids loading and target dry layer thickness was held constant for each plot. No plot was constructed for v_{slurry} because the object is to maximize it below a limiting value ($v_{solvent}$) in order to increase throughput. Regions in the plot where the objective function is zero

reflect the bounds set forward in section 7.3.2. These bounds require that $0.1 < T_c < 5.0$, $t_{sat} < S_f t_{crit}$, and 3.33 E-8 m^2 $< Q/v <$ 1.0 E-7 m^2.

7.6.1 Optimization Plot for T_f/T_c

The first plot displays the magnitude of T_f/T_c over the range of Q/v and T_c that fell within the constraints for a given solids loading and target dry layer thickness. This plot clearly showed that T_f/T_c peaked for low T_c and low Q/v. Figure 7.4 shows the plot for a target thickness of 50 μm and slurry loading of 20 vol%.

7.6.2 Optimization Plot for *w/l*

The second plot displays the magnitude of the *w/l* ratio over the same range. This plot showed that *w/l* increased for low Q/v, and was independent of T_c as expected. Figure 7.5 shows the plot for a target thickness of 50 μm and slurry loading of 20 vol%.

7.6.3 Optimization Plot for L_{slurry}

The third plot displays the inverse of the magnitude of L_{slurry} versus the same variables. The peak occurs at high cycle times, exactly the opposite of T_f/T_c. Figure 7.6 shows the plot for a target thickness of 50 μm and slurry loading of 20 vol%.

7.6.4 Combined Optimization Plot

The three separate objective functions were combined into the last plot. The objective function was the sum of T_f/T_c, *w/l*, and $1/L_{slurry}$ (mm^{-1}). Figure 7.7 shows the plot for a target thickness of 50 μm and slurry loading of 20 vol%. This plot indicates that operating at low Q/v is ideal. What T_c to operate at is less certain. As long as all factors are equally weighted low T_c appears to be favorable. Experiments may reveal that one or two factors are the most important, in which case weighting factors would be needed to better indicate what T_c is optimum.

Figure 7. 4 The ratio *Ts/Tc* as a function of cycle time and *Q/v* for a 20 vol% slurry and 50 micron target layer height

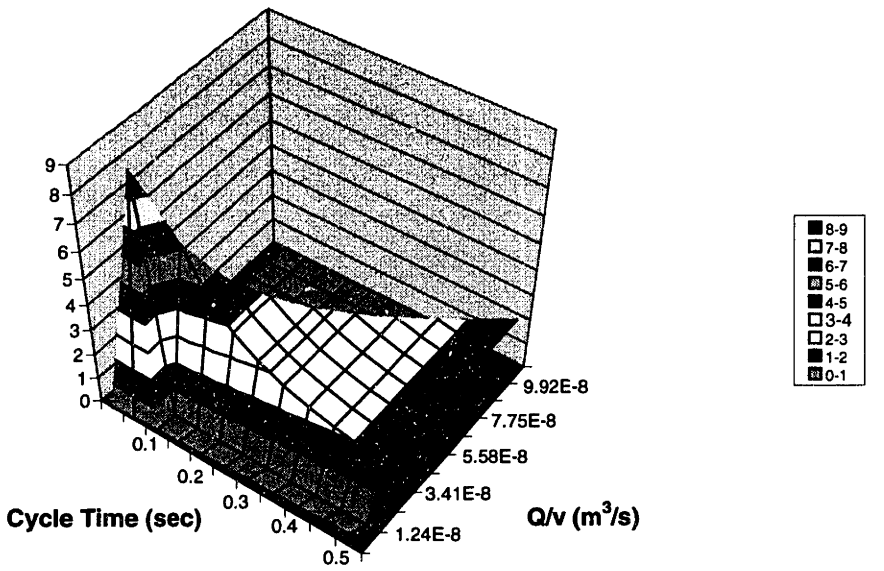

Figure 7.5 The ratio *w/l* as a function of cycle time and *Q/v* for a 20 vol% slurry and 50 micron target layer height

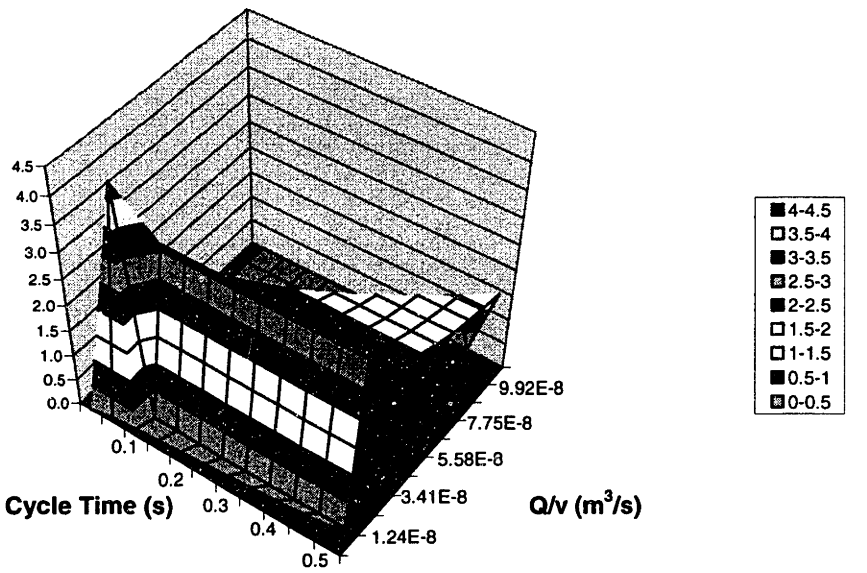

Figure 7.6 The ratio $1 / L_{slurry}$ as a function of cycle time and Q/v for a 20 vol% slurry and 50 micron target layer height

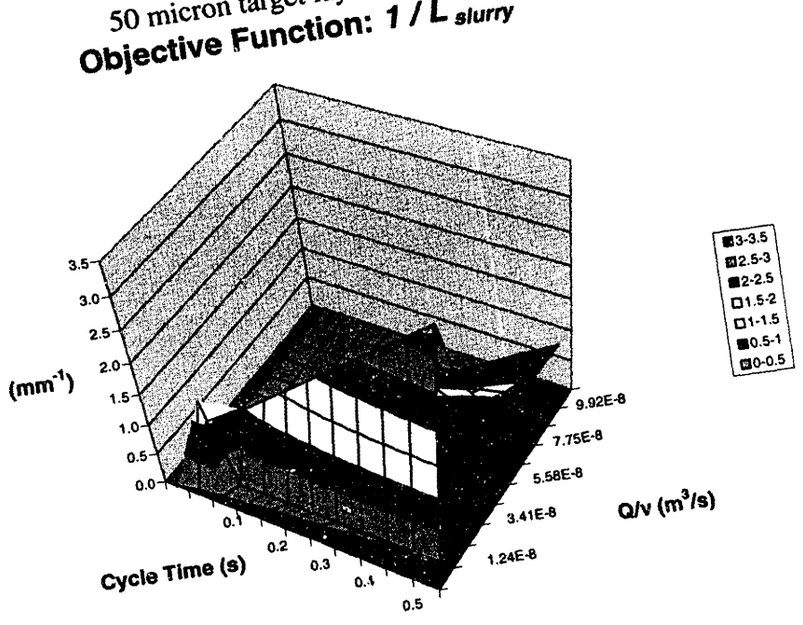

Figure 7.7 The combined objective as a function of cycle time and Q/v for a 20 vol% slurry and 50 micron target layer height

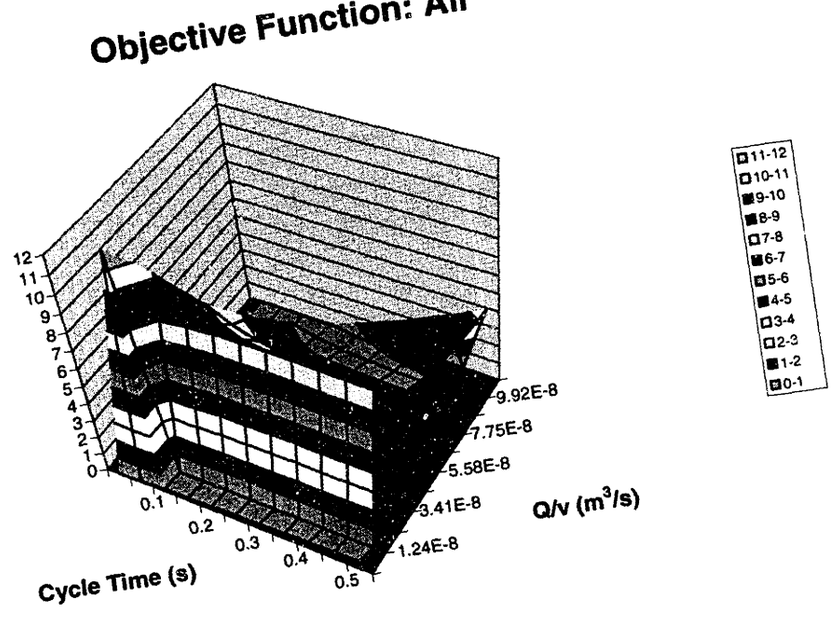

7.7 Summary

The critical relationships for successive line merging were identified and modeled. The ratio of T_s/T_c should be maximized to ensure that several lines of slurry merge together prior to slip casting. Maximizing the line overlap ratio w/l ensures that peaks and valleys between lines do not appear in the forming layer. The width of the wet front L_{slurry} should not be excessively large (> 5mm), otherwise slurry migration is more likely to occur. The velocity at which the wet slurry front advances across the substrate v_{slurry} should be less than the rate at which solvent is able to penetrate the pore space of the top layer in order to prevent bubbling in the layer.

These equations were then expressed in terms of three independent variables Q/v, T_c, and s, and the target dry layer thickness t^*. Relationships between the independent variables and their overall effect on the critical equations could then be identified. A table and plot showing the general trends between the critical relationships and the independent variables Q/v and T_c is useful in generalizing where layer defects should occur. Ideally there should be some operating window in which no layer defects occur. These relationships can also be visualized in a series of three-dimensional plots that show the different objective functions versus T_c and Q/v. For a given plot s and t^* is held constant. Changes in s change the magnitude of the objective function but not the trend shown in the plots.

There are both strong and weak aspects of the combined line merging model. The importance of the T_s/T_c was verified with rotary experiments. Line merging clearly can not occur if the ratio is below one and it is logical that below some limiting value only partial line merging will occur. The existence of a fundamental upper limit on T_s/T_c is not present in the model. The ratio w/l is also fundamentally important. Line merging can not occur for a value below one, but again an upper limit is not obvious. The relative importance of l/L_{slurry} is the weakest part of the model. When L_{slurry} is large, more wet slurry is present on the powder bed surface and available to migrate. Most likely perpendicular slurry migration is caused by an instability. A large L_{slurry} might enable perpendicular migration but it would not cause the instability that triggers the migration.

8. Line Merging Experiments

Experiments were conducted to identify the best operating parameters to achieve successful line merging. The experiments were designed around the model presented in Chapter 7. A target dry layer thickness of 50 microns was selected, which corresponded to the thinnest layers used in slurry-based 3DP. All slurries used a solvent of equal parts water and isopropanol. The solids loading of the slurry remained as one of the independent variables.

Several plots were generated for the combined objective function at different solids loadings. The optimum conditions (where the objective functions peaked) all occurred in the same region of Q/v and T_c, although the magnitudes of the peaks varied. The magnitudes of the peaks increased as the slurry solids loading decreased. According to the model, once the best operating parameters were identified for a given slurry, similar parameters would also yield the best possible layers for other solids loadings. Since the peak of the objective function increases with lower solids loading, it was expected that the best layer possible would occur for the lowest achievable solids loading. The lowest achievable solids loading can be determined by the critical saturation thickness in equation (7.10). It is important to note that if good layers can be produced for several different solids loadings, the higher solids loading would be preferred because for a given Q/v and T_c it will produce a higher throughput, since more solids is deposited per unit Q.

General information describing the individual trials for different slurry compositions is provided in the following sections. Detailed information on each trial is located in Appendix I.

8.1 22 Vol% Trials

The first experiments were conducted with a 22 vol% alumina slurry. These experiments had two key objectives. The first objective was to deposit slurry layers at several different locations on the objective function parameter map. The idea was to link regions of the map to the defects observed in rotary printing and predicted by the line

merging model. The second objective was to locate the region in the map where the best possible layer was produced. The combined objective function parameter map for 22 vol% slurry is shown in Figure 8.1

Figure 8.1 The parameter map of the combined objective function for a 22 vol% slurry

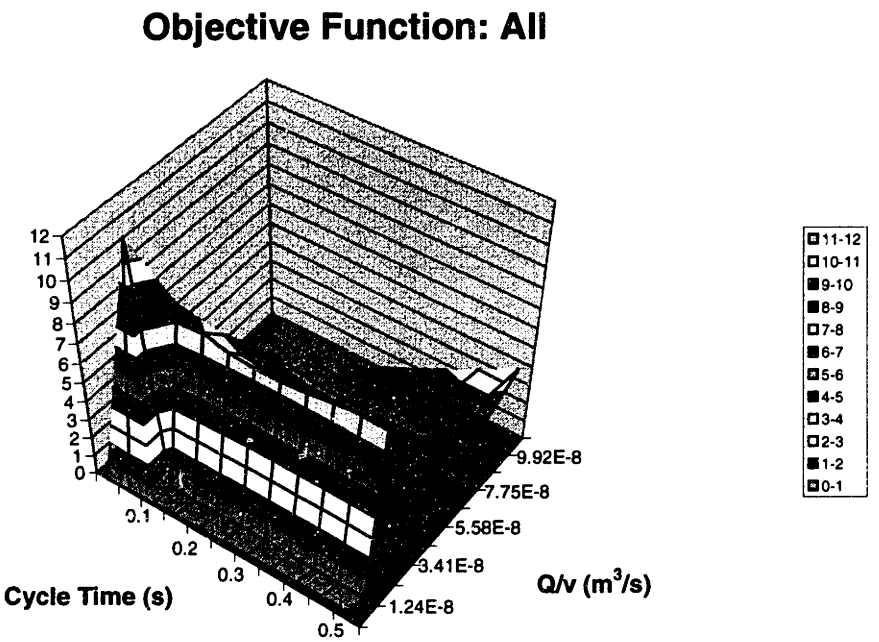

8.1.1 Parameter Mapping for Individual Trials

Initial trials were conducted for 0.1 sec < T_c < 0.3 sec for different Q/v. As it turned out only Q/v < 2.5E –8 m^2 were attempted because both initial results and the model predicted that low Q/v was required. The results of the 22 vol% trials with respect to the different parameter maps are best explained in Figures 8.2 – 8.5.

Figure 8.2 Parameter map for the T_s/T_c objective function detailing experiments conducted with an 22 vol% slurry

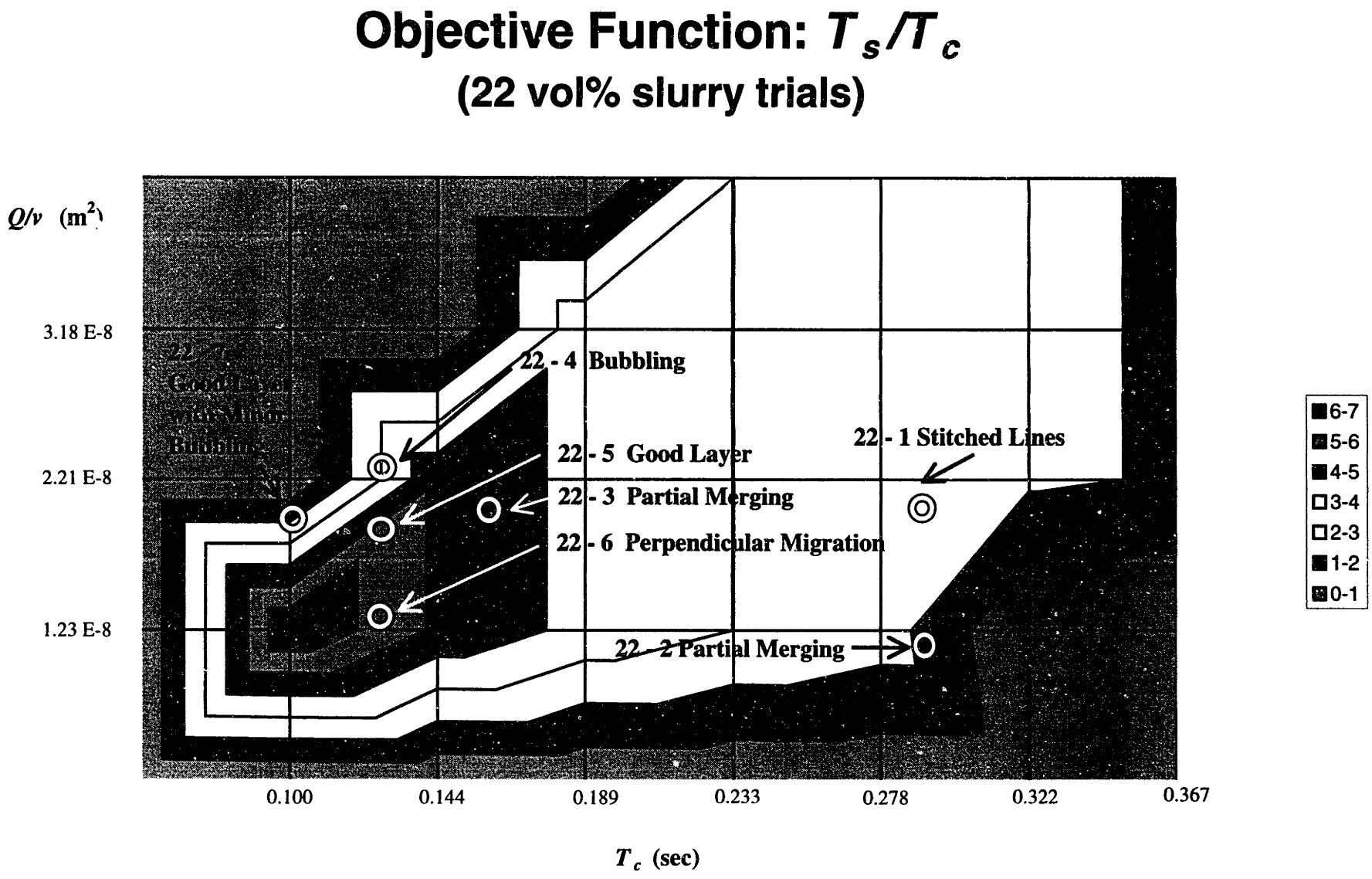

Figure 8.3 Parameter map for the *w/l* objective function detailing experiments conducted with an 22 vol% slurry

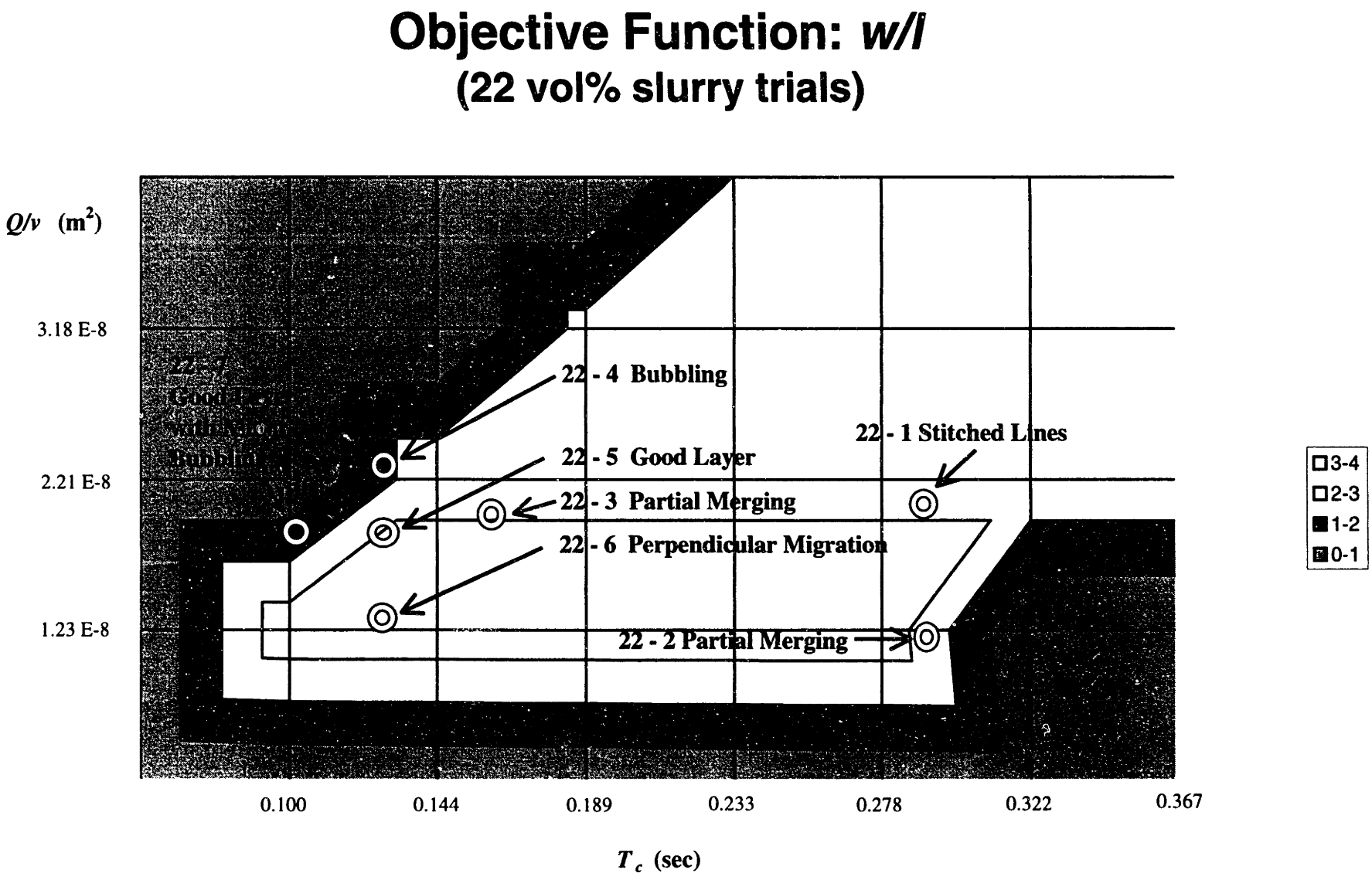

Figure 8.4 Parameter map for the $1/L_{slurry}$ objective function detailing experiments conducted with an 22 vol% slurry

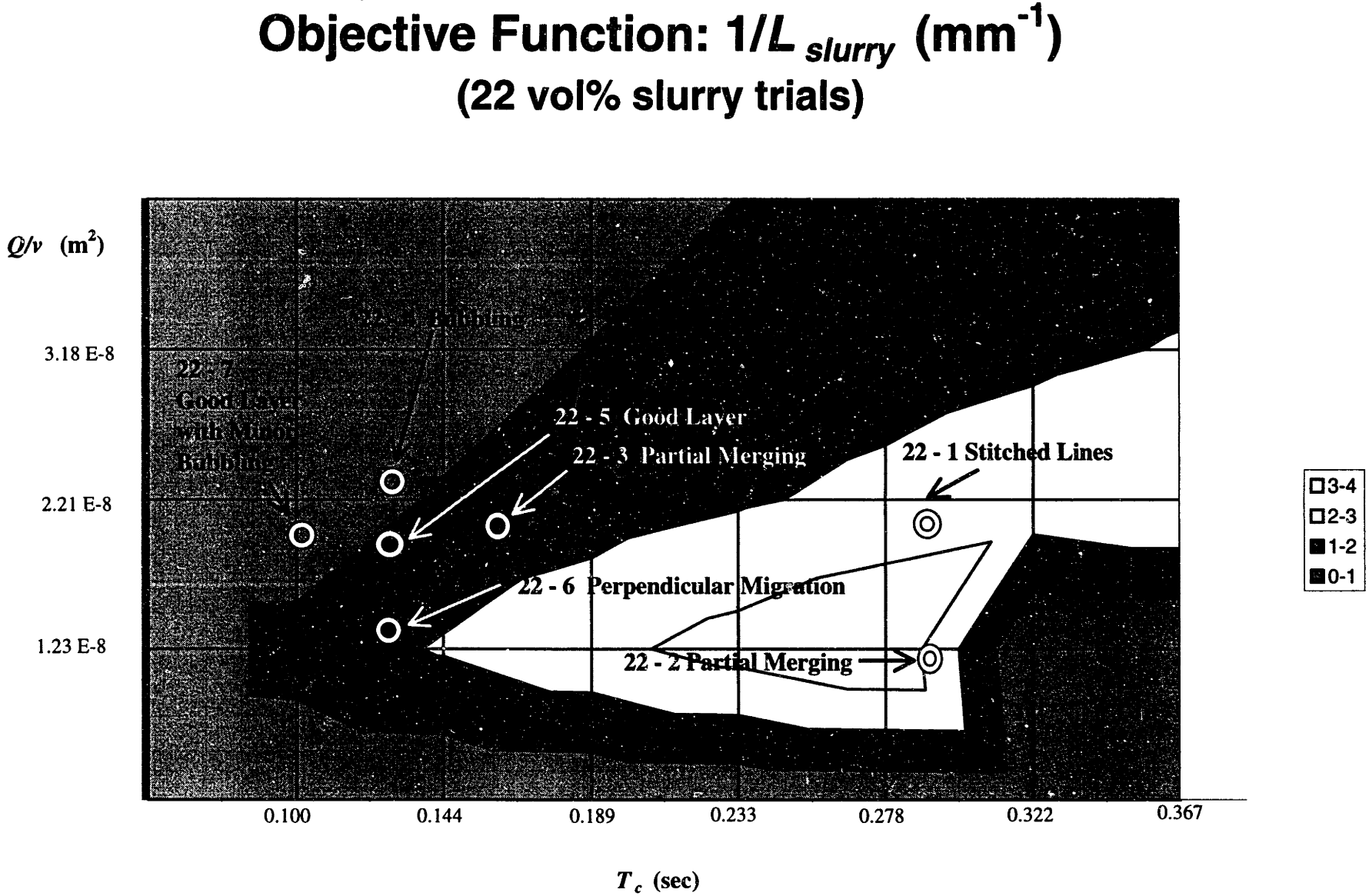

Figure 8.5 Parameter map for the combined objective function detailing experiments conducted with an 22 vol% slurry

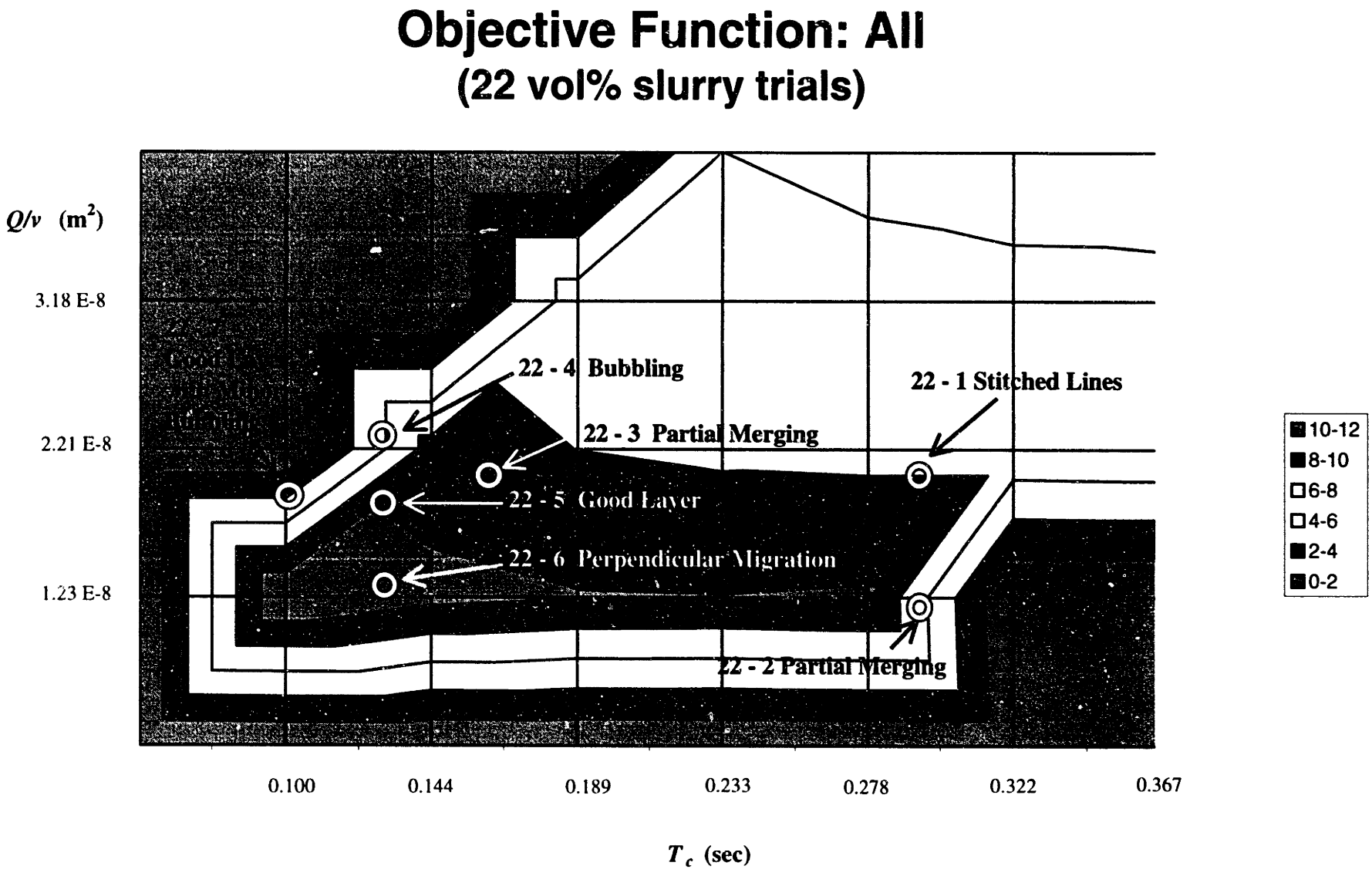

8.1.2 Interpreting the Results

8.1.2.1 Parameter map for T/T_c

The results of the seven trials agree with the trends of the parameter map based on the objective function T/T_c. The best results (Trial 22-5) occur very near the objective function's maximum. At the same time, perpendicular migration (Trial 22-6) also occurs very near the maximum. In both cases though, line merging did occur, which is what the T/T_c ratio is expected to predict. As expected, little line merging occurred in regions where the objective function was relatively low in magnitude.

The trends outlined in Table 7.2 indicate that T/T_c is dependent on T_c but independent of Q/v. This is difficult to see in the map because of the bounds that are imposed by the limits of the bicycle wheel apparatus. The unusual shape of boundaries is caused by the spreadsheet program interpolating between "real" values and the artificial zero that is imposed outside the bounds of the apparatus. Trials 22-4 through 22-6 indicate that Q/v has an important effect on the outcome of the layer. The ratio of T/T_c appears to be sufficient to predict whether lines will merge prior to slip casting, but it does not appear sufficient to predict the appearance of a merged layer.

8.1.2.2 Parameter map for w/l

The results of the seven trials partially reflect the parameter map based on the objective function *w/l*. The best layer (Trial 22-5) falls near the maximum of the objective function. Perpendicular migration (Trial 22-6) and partial merging (Trial 22-2) also occur near the maximum.

The trends outlined in Table 7.2 indicate that the ratio w/l is dependent on Q/v but independent of T_c. As with the previous plot, bicycle wheel operating boundaries and interpolation create artificial gradients at the boundaries. In reality, trials 22-5 and 22-7 have equal chances of success according to the *w/l* objective function. This parameter map appears useful for determining the amount of line overlap that is required to produce

a merged layer, but it is not very useful for predicting the success of the layer once it is merged.

8.1.2.3 Parameter map for $1/L_{slurry}$

The results from the seven trials suggest that the relationship between the inverse of the width of the slurry wet front and the occurrence of perpendicular migration was questionable. After making a line-merged powder bed without perpendicular migration, Q/v was reduced, while T_c was held constant. According to the model, this should have reduced the likelihood of perpendicular migration. However, these conditions resulted in the creation of a powder bed with perpendicular migration. This portion of the model appears to be the weakest.

8.1.2.4 Parameter map for combined objective function

The results from the seven trials compare favorably to the parameter map based on the combined objective function. The best results occur near the peak of the objective function as predicted. A majority of the defects occur away from the peak, with one exception. Perpendicular migration appears very near the peak of the objective function near the conditions where the good layer was produced. The combined objective function does not adequately predict the occurrence of perpendicular migration. This is not surprising since the individual model for perpendicular migration ($1/L_{slurry}$) has already been questioned.

8.1.3 Best Results

The best results with an 22 vol% slurry occurred in trial 22-5. For this trial the key ratios were $T_s/T_c = 5.37$, $w/l = 3.02$, $1/L_{slurry} = 1.27$ mm^{-1}. Figure 8.6 shows the top surface of this layer.

Figure 8.6 Good layer produced with a 22 vol% slurry (scale mm)

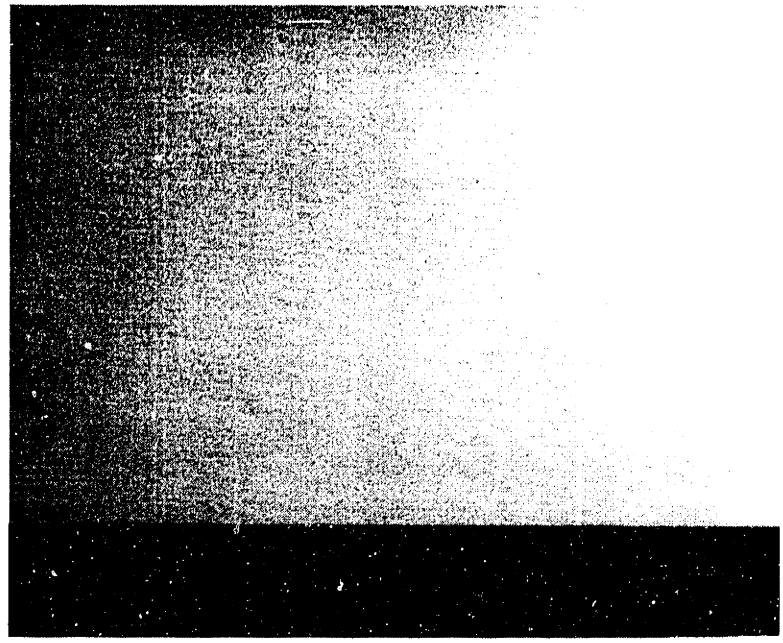

8.1.4 Multiple Layers

An attempt was made to build a multi-layered powder bed (Trial 22-8) at the same conditions at which trial 22-5 was conducted. The procedure was to deposit the a merged slurry layer, dry it under a 500W halogen lamp at full power for 30 sec, cool the surface for 30 seconds with a small DC box fan, and repeat. The first layer looked just as good as the layer in trial 22-5. The second layer displayed subtle signs of perpendicular migration. The perpendicular migration became more pronounced with subsequent layers. Figure 8.7 shows the powder bed after depositing 10 layers.

Figure 8.7 10 layer powder bed produced with a 22 vol% slurry, showing signs of perpendicular migration

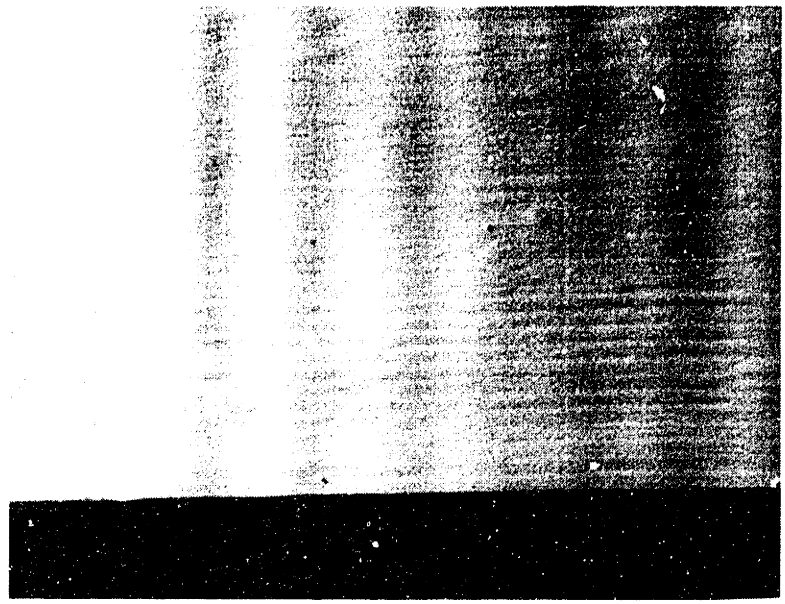

Perpendicular migration developed too rapidly and too severely to consider making multiple layer powder beds under these conditions. A decision was made to explore slurries with lower solids loadings since the parameter map had previously indicated that the magnitude of the combined objective function for a given Q/v and T_c increases as slurry solids loading decreases.

8.2 18 Vol% Trials

Since the 22 vol% trials successfully mapped out the parameter space and demonstrated the accuracy of the different aspects of the model, 18 vol% trials were only conducted in an effort to produce the best possible layer. The 22 vol% trials indicated that low cycle times on the order of 0.1 sec were required to produce the best layers, so all trials were conducted for $T_c = 0.1$ sec. The parameter map for the combined objective function for a 18 vol% slurry also revealed that the peak occurred at low cycle times (Figure 8.8)

Figure 8.8 The parameter map of the combined objective function for a 22 vol% slurry

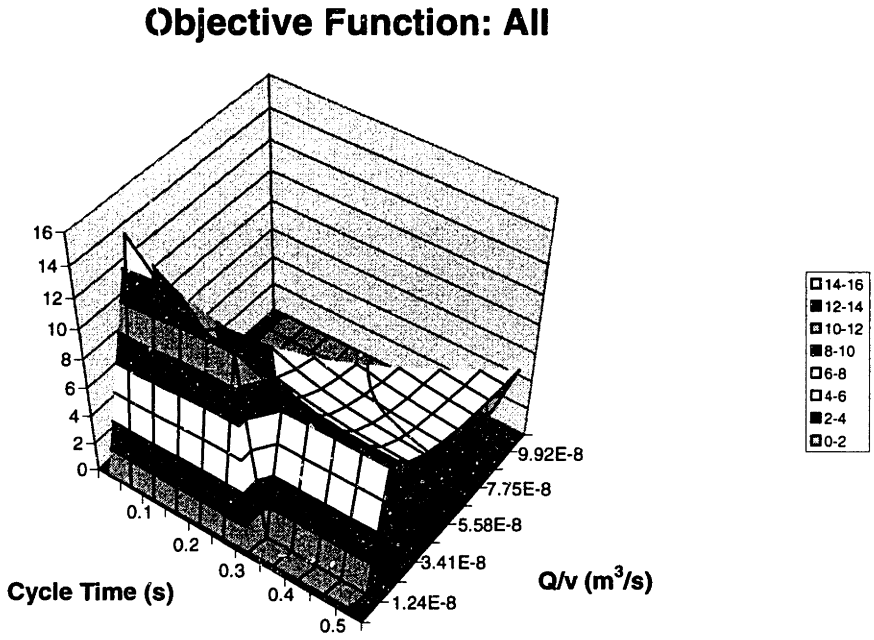

8.2.1 Parameter Mapping for Individual Trials

Figure 8.9 shows the 18 vol% trials and their results plotted on a topological view of the parameter map for the combined objective function.

Figure 8.9 Parameter map for the combined objective function detailing experiments conducted with an 18 vol% slurry

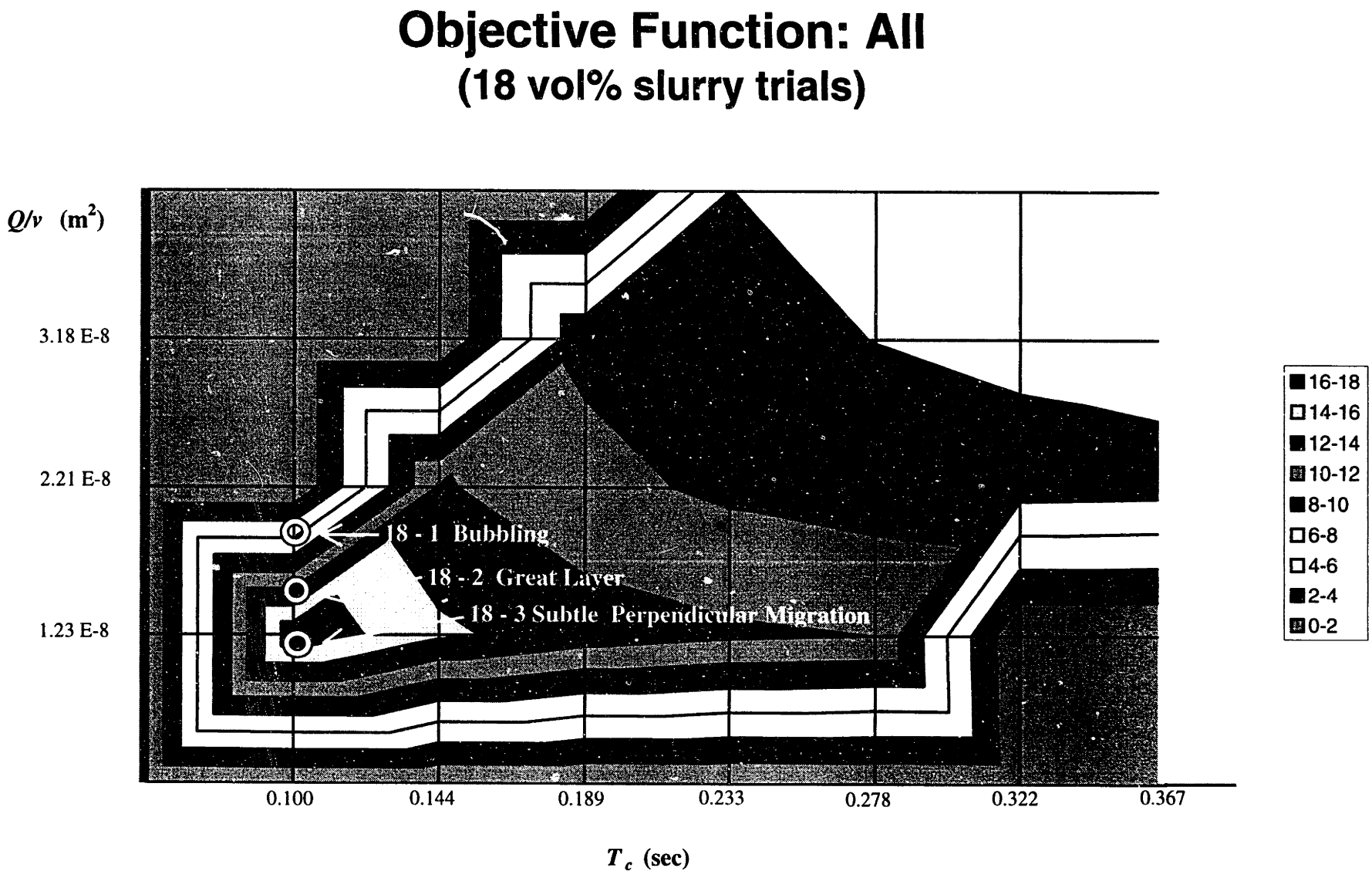

8.2.2 Interpreting the Results

The best layers occurred very near the peak of the combined objective function in the parameter map. As with the 22 vol% results, perpendicular migration and bubbling also occurred very near the peak. The boundaries separating the bubbling regime and perpendicular migration regime from the good regime are subtle. Overall, the combined objective function model is very useful for determining initial target operating conditions. After that, a process of trial and error may be required to shift from a poor regime to the good regime where defect-free layers can be produced.

8.2.3 Best Results

The best results occurred for trial 18-2. For this trial the key ratios were T_s/T_c = 11.54 , w/l = 4.56 , l/L_{slurry} = 0.95 mm^{-1}. Figure 8.10 shows the top surface of this layer.

Figure 8.10 Best layer produced with an 18 vol% slurry (scale mm)

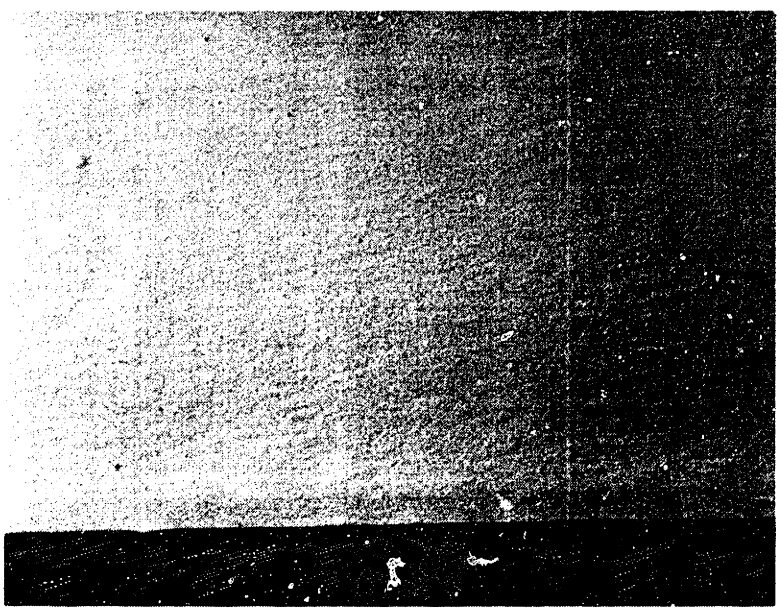

8.2.4 Multiple Layers

8.2.4.1 Standard procedure

A multiple layer powder bed (Trial 18-4) was attempted at the same conditions as trial 18-2. The same procedure was followed for these layers as was followed for the 22 vol% multiple layer build (Section 8.1.4). A twenty layer powder bed was successfully built at these parameters. Slight signs of perpendicular migration began appearing at layer 15, but they did not grow significantly by layer 20. The migration could present a problem in a larger build however. The top of this powder bed is shown in Figure 8.11.

Figure 8.11 20 layer build with 18 vol% slurry showing perpendicular migration

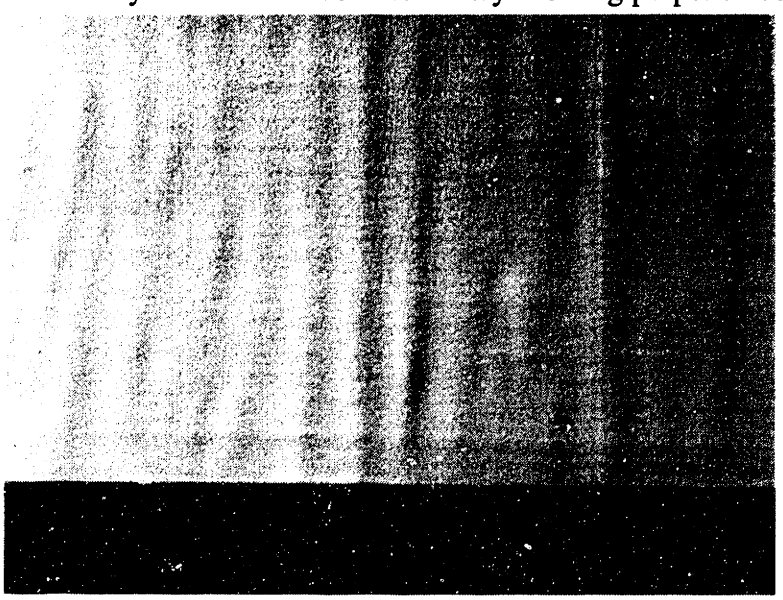

8.2.4.2 Rotating 90 degrees

Another multiple layer powder bed (Trial 18-5) was constructed for similar parameters. This time the procedure was slightly changed. After a layer was deposited the powder bed was rotated 90 degrees, first clockwise then counter-clockwise so that only two powder bed orientations were used. This was done in an effort to cut-off perpendicular migration before it could develop. Perpendicular migration begins subtly and propagates through layers. It was believed that stacking layers with lines of

perpendicular migration at 90 degree angles would effectively keep it from propagating through.

Another twenty layer powder bed was constructed for these conditions. The final surface finish was much better than that of the previous trial. Rotating the powder bed 90 degrees between layers kept subtle perpendicular migration from propagating into severe migration (Figure 8.12).

Figure 8.12 20 layer build with 18 vol% slurry. Perpendicular migration was stemmed by rotating the bed 90 degrees between layers (scale mm)

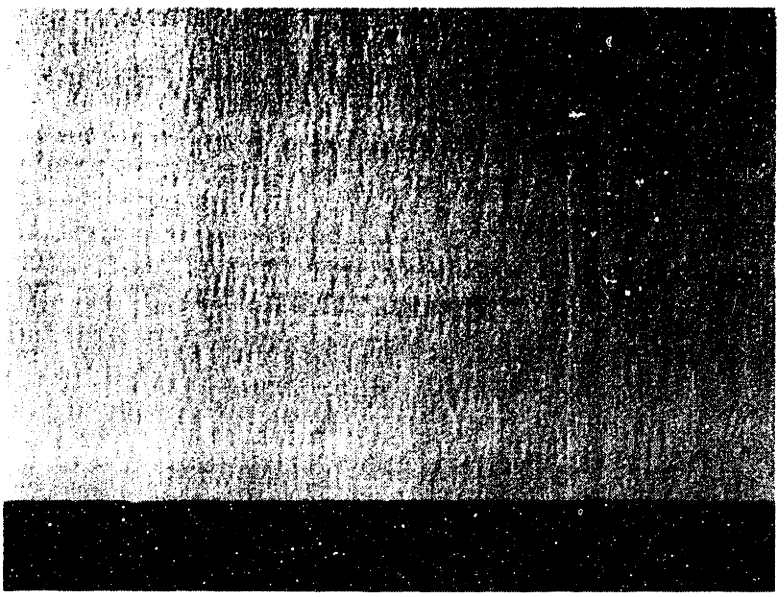

8.3 15 Vol% Trials

Trials were conducted with a 15 vol% slurry in an effort to further improve the results obtained with the 18 vol% slurry. The parameter map for the combined objective function of the 15 vol% slurry had an even higher peak than for the 18 vol% slurry, suggesting that even better layers might be produced (Figure 8.13).

Figure 8.13 The parameter map of the combined objective function for a 15 vol% slurry

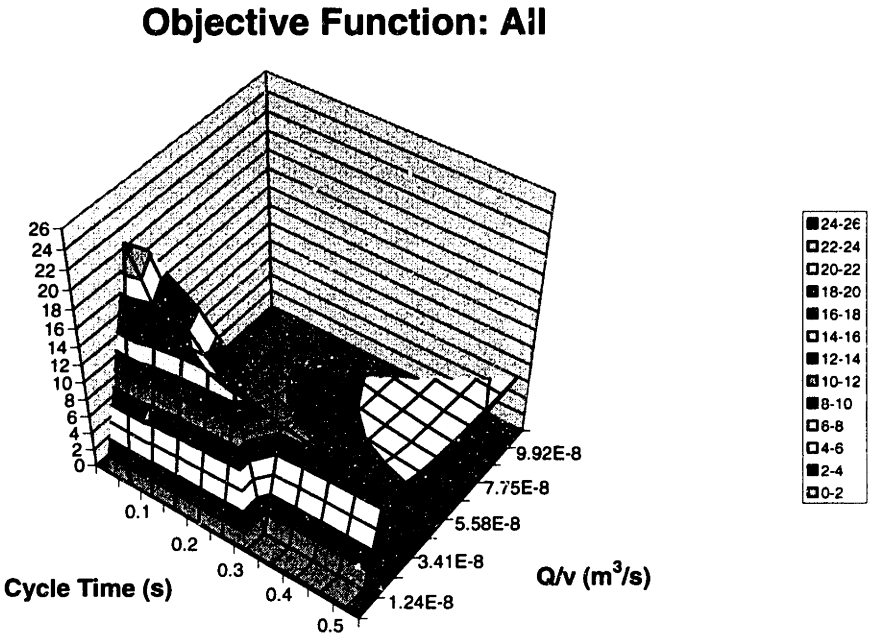

8.3.1 Parameter Mapping for Individual Trials

Figure 8.14 shows the 15 vol% trials and their results plotted on a topological view of the parameter map for the combined objective function.

Figure 8.14 Parameter map for the combined objective function detailing experiments conducted with an 15 vol% slurry

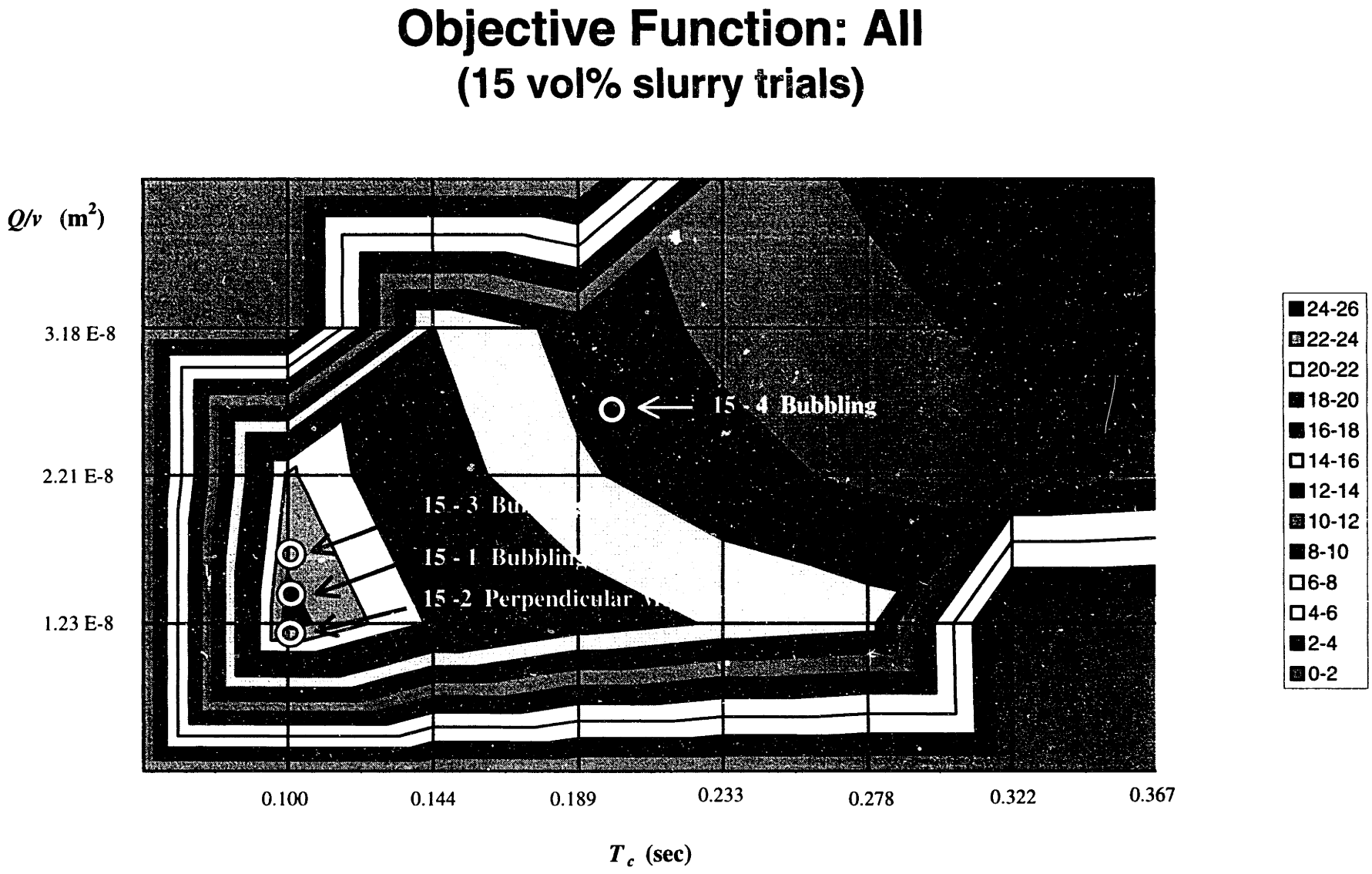

8.3.2 Interpreting the Results

No layers were successfully deposited without significant bubbling or perpendicular migration. Apparently the window between bubbling and perpendicular migration steadily narrows as slurry solids loading is reduced. This is not the only limiting factor because critical saturation thickness also limits the slurry solids loading to a minimum near 15 vol% to avoid layer cracking. Bubbling appears to become more prominent as slurry loading is reduced, suggesting that the current model of bubbling is not exact. It is possible that bubbles have an easier time emerging through a less viscous layer of slurry. The viscosity of alumina slurry varies significantly with solids loading. For example, a 45 vol% alumina slurry with all water solvent has a viscosity of approximately 20 cP, while a 25 vol% slurry with all water solvent has a viscosity of approximately 5 cP.

8.4 Optimum Conditions

The best layers were produced with an 18 vol% slurry. Additionally, perpendicular migration was limited by rotating the powder bed 90 degrees between layers.

8.4.1 Large Build

A sixty layer powder bed (Trial 18-6) was produced at conditions similar to those in Section 8.2.4.2. The exact conditions were T_c = 100 msec, Q/v = 1.33 E-8 m2, and slide speed = 0.86 mm/s. These conditions yielded T_s/T_c = 11.54, w/l = 4.68, and l/L_{slurry} = 1.00 mm^{-1}. Very subtle perpendicular migration was first detected at layer 7, but the 90 degree rotation scheme appeared to keep it from propagating. A few micro-bubbles appeared between layers 45-60 (Figure 8.15). These bubbles suggest that the threshold between producing good layers and bubbling is very small. Slight variations in the saturated pore space or the packing density of a layer during the build could be enough to trigger these micro-bubbles.

Figure 8.15 Photograph showing micro-bubbles that appeared in approximately the last 15 layers of the 60 layer build

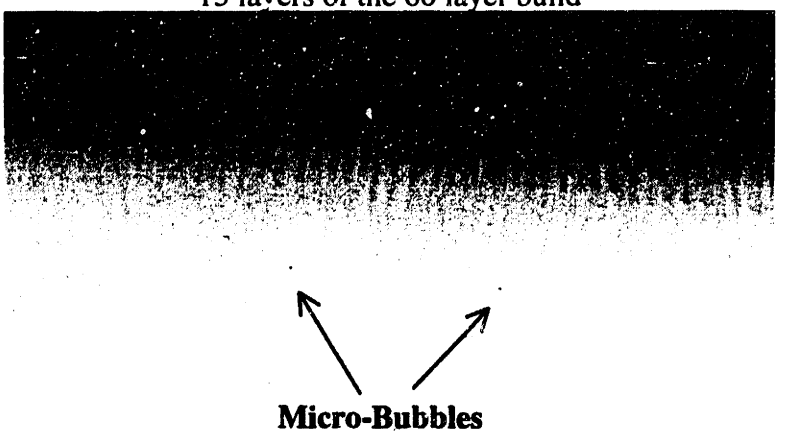

Figure 8.16 shows the entire build: 60 alumina layers on a bisque-fired alumina substrate. Figure 8.17 shows a photo-micrograph of the powder bed surface revealing a smooth surface finish and a few micro-bubbles.

Figure 8.16 Top view of 60 layer powder

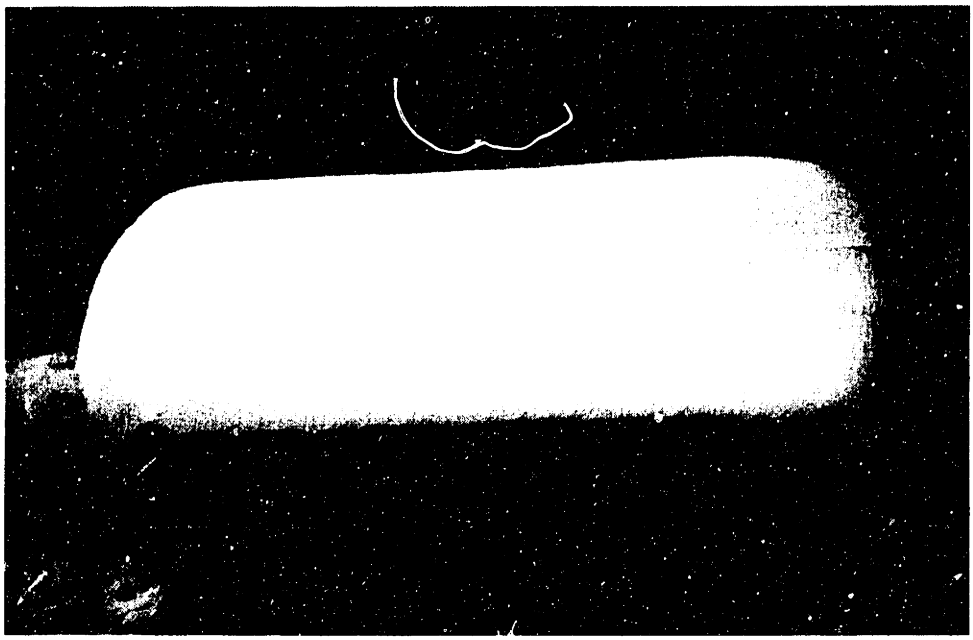

Figure 8.17 Photo-micrograph showing smooth top surface of 60th layer. Micro-bubbles are just barely evident

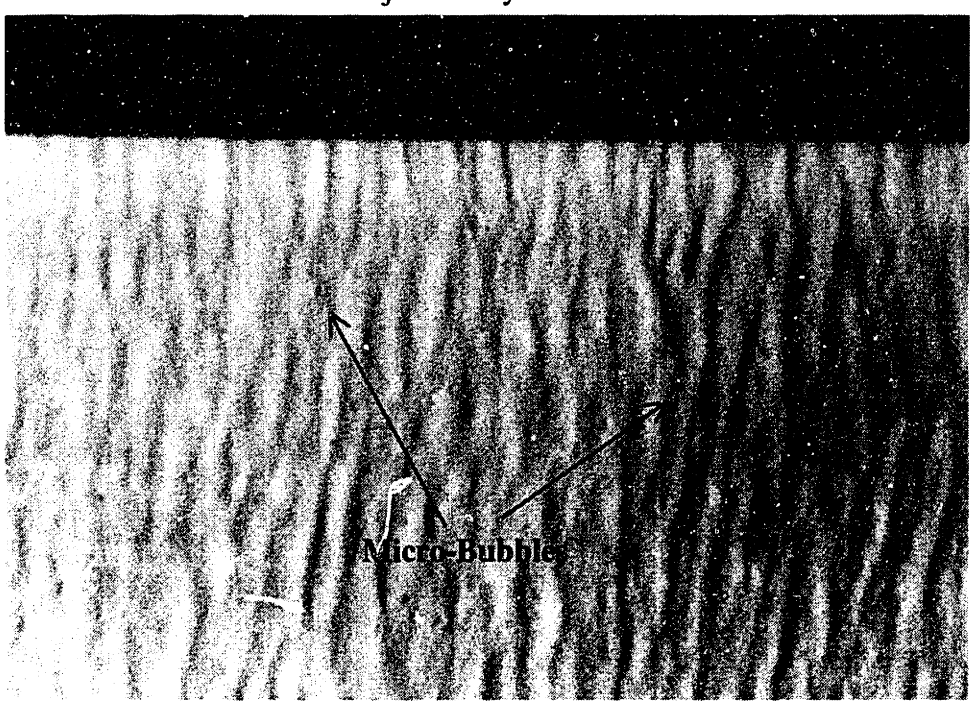

8.4.2 Characterization

8.4.2.1 Surface profilometry

Surface profilometry was performed at the midpoint of the top surface of the powder bed. A 3 mm pass was taken in both deposition directions (at 90 degree angles to each other). The orientation of the top layer was such that the nozzle traversed the narrow width of the substrate, meaning that lines of perpendicular migration in the top layer would extend along the length of the top layer. These lines of migration appear in a surface profilometry pass across the narrow width of the powder bed. Across the narrow width of the powder bed the surface profile varied approximately 11 microns peak to valley (Figure 8.18). A profilometry pass along the length of the powder bed shows residual perpendicular migration from the previous layers. Along the length of the powder bed, the surface profile varied approximately 6 microns peak to valley (Figure 8.19). These values compare favorably to the approximately 40 micron peak to valley variation that can be seen between stitched rastered lines.

Figure 8.18 Surface profile of 60 layer powder bed across narrow width showing a maximum variation of 7 microns peak to valley

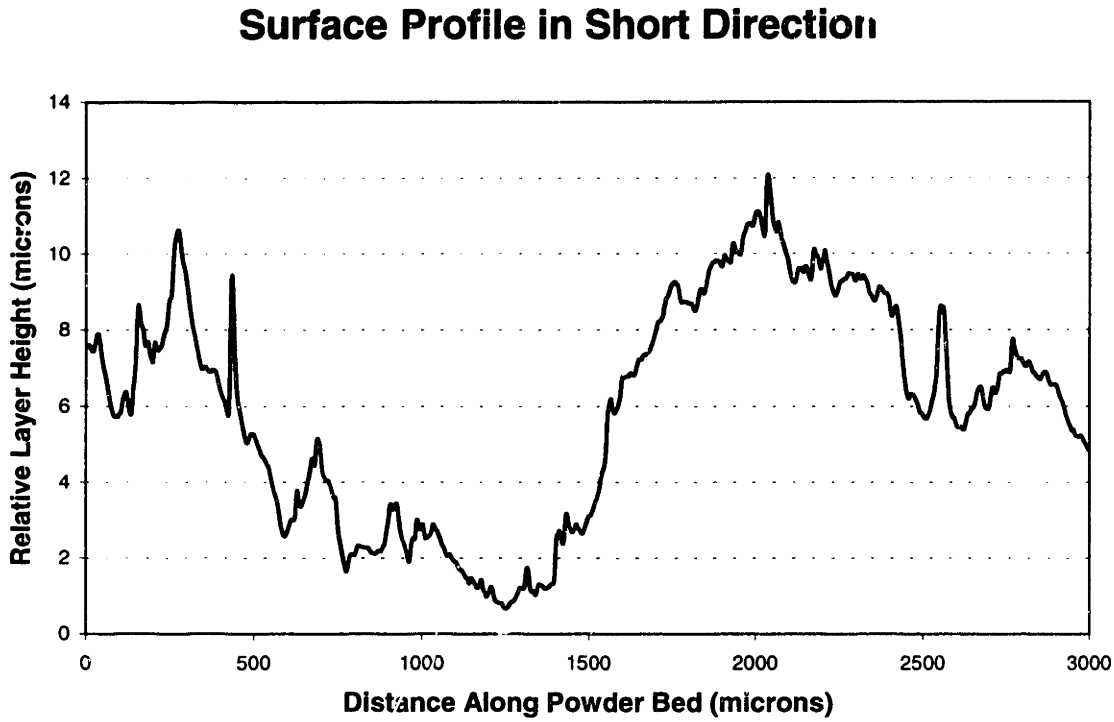

Figure 8.19 Surface profile of 60 layer powder bed along length showing a maximum variation of 7 microns peak to valley

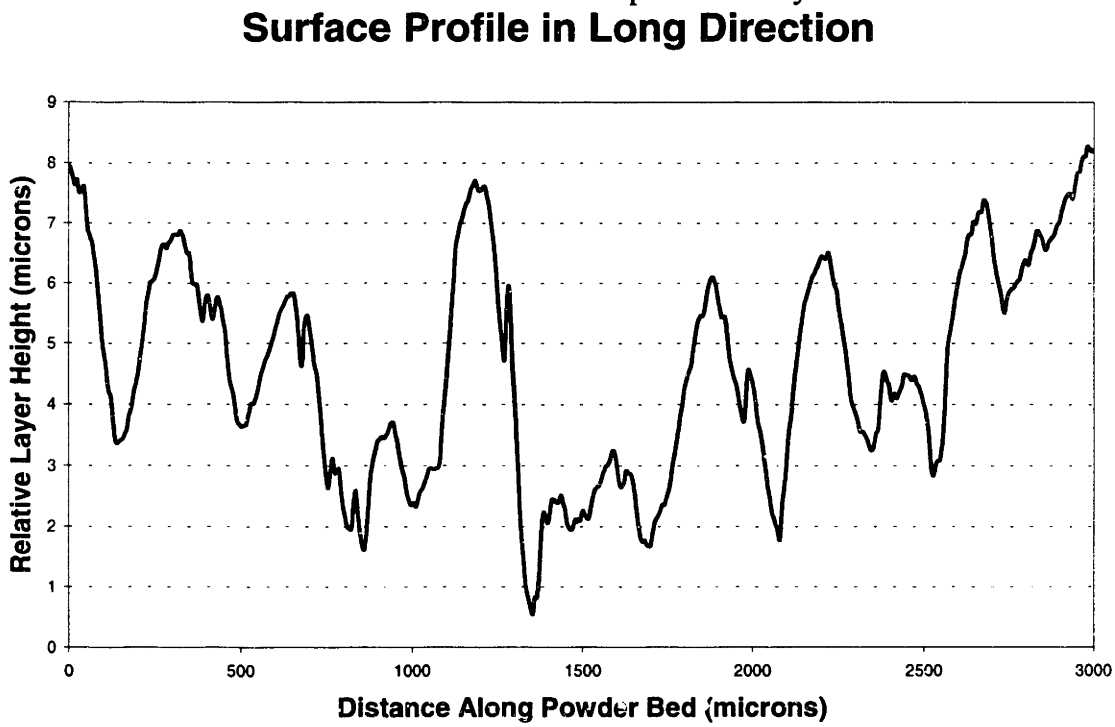

8.4.2.2 Cross-section SEM

The powder bed was cross-sectioned, mounted, and evaluated by SEM. Although the individual layers from which the 60 layer powder bed was constructed looked good on the surface, SEM revealed many internal inter-layer bubbles. These bubbles appear to have nucleated at the bottom of deposited layers. Rather than rising through the slurry layer and leaving an obvious defect at the surface, these were so small that they were captured at the bottom of the layer during slip casting. These defects can be seen in Figure 8.20. The small size of the bubbles suggests that this particular trial was run right near the threshold of bubbling. In order to conclusively prove that successful line merging could occur without the nucleation of micro-bubbles at the interlayer boundary, an additional substrate needed to be cross-sectioned and analyzed with SEM.

Figure 8.20 SEM photos of cross-section of 60 layer powder bed. Small bubbles appear to have nucleated near the bottom of deposited layers. These bubbles did not rise and break through to the surface.

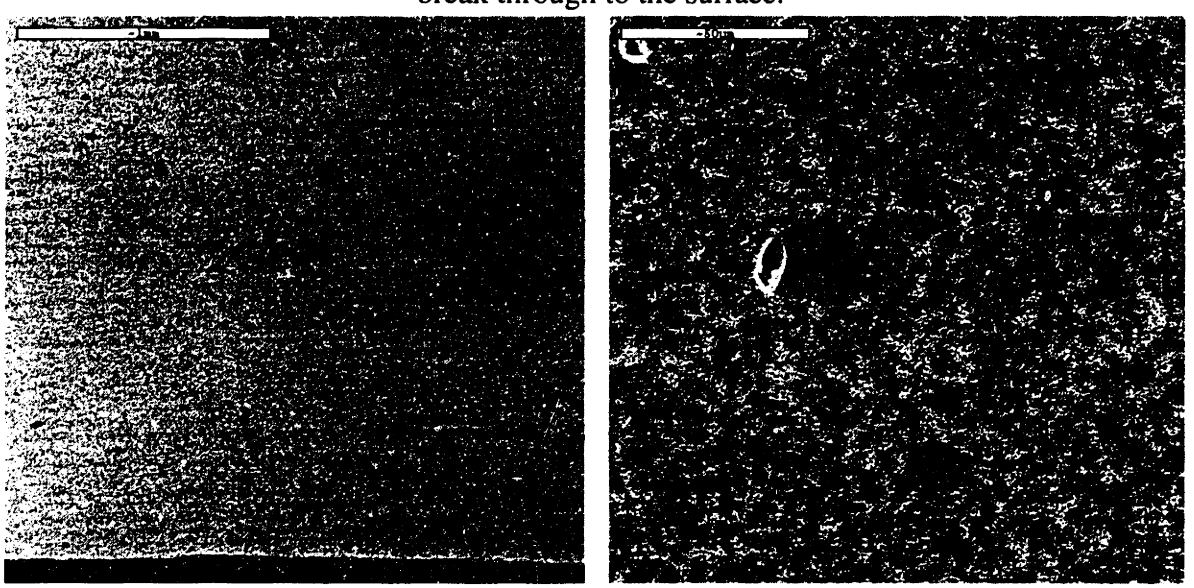

8.4.2.3 Cross-section and SEM analysis of Trial 22-9

In order to demonstrate that merged layers could be deposited without micro-bubbles occurring along inter-layer boundaries, the five layer powder bed from Trial 22-9 (see Appendix I) was cross-sectioned. This powder bed was produced with a 22 vol% slurry. The SEM photos of the cross-section appear in Figure 8.21.

Figure 8.21 Cross-sections of Trial 22-9

Only slight signs of density gradient at layer interfaces

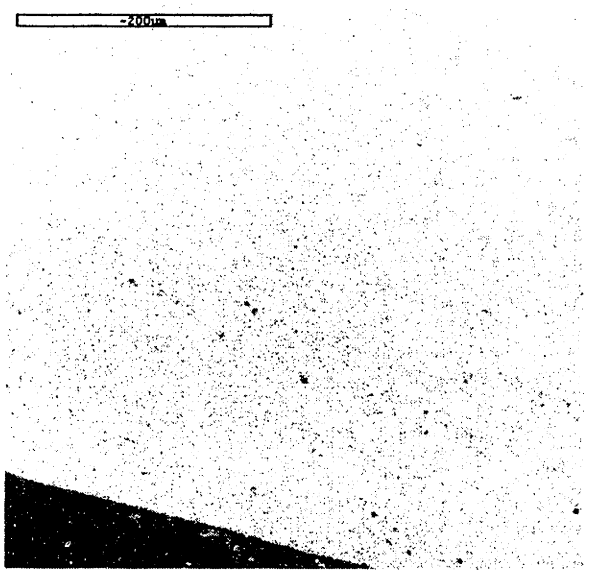

Very little porosity evident

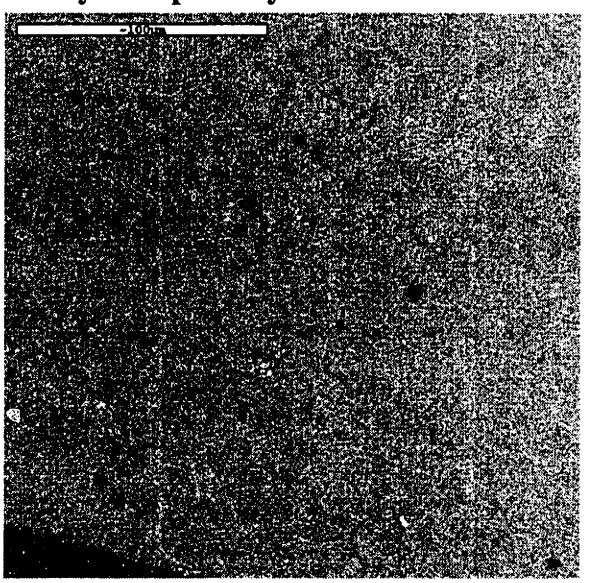

Porosity appears uniformly distributed and no larger than approximately 1-2 microns in diameter

High magnification reveals that dark spots are most likely surface contamination of the mounted specimen

The SEM photos demonstrate that the presence of inter-layer micro-bubbles is not a necessary condition for successful line merging to take place. Most likely the micro-bubbles seen in Trial 18-6 were a result of just crossing over the threshold into a bubbling regime. These photos do demonstrate that the threshold between bubbling and not bubbling may be very small. According to the theory, if the advance of the slurry wet front were slightly slowed these micro-bubbles should go away.

8.4.3 Long Build

Perpendicular migration is most likely a product of instabilities in the advancing slurry wet front. These instabilities are more likely to occur in large area powder bed layers because they would have more time to grow since deposition takes longer. Additionally the fingers of perpendicular migration might have a more dramatic effect since there would be a longer length of powder bed through which they could extend and grow.

In an effort to verify that line merging could resist instabilities and produce a long uniform merged layer, a longer bisque substrate was constructed (Trial 18-7). This substrate measured approximately 1.5" wide and 4 inches long. Layers were deposited on this substrate for the same parameters as the 60 layer build. Five layers were successfully deposited without significant signs of perpendicular migration. There was one instance in the third layer where the slurry jet wandered, resulting in a straight line defect across the substrate. This defect was partially obscured upon depositing the fourth and fifth layers, but it did not fully heal itself (Figure 8.22).

Figure 8.22 Pictures of the first layer, third layer, and fifth layer of the long build

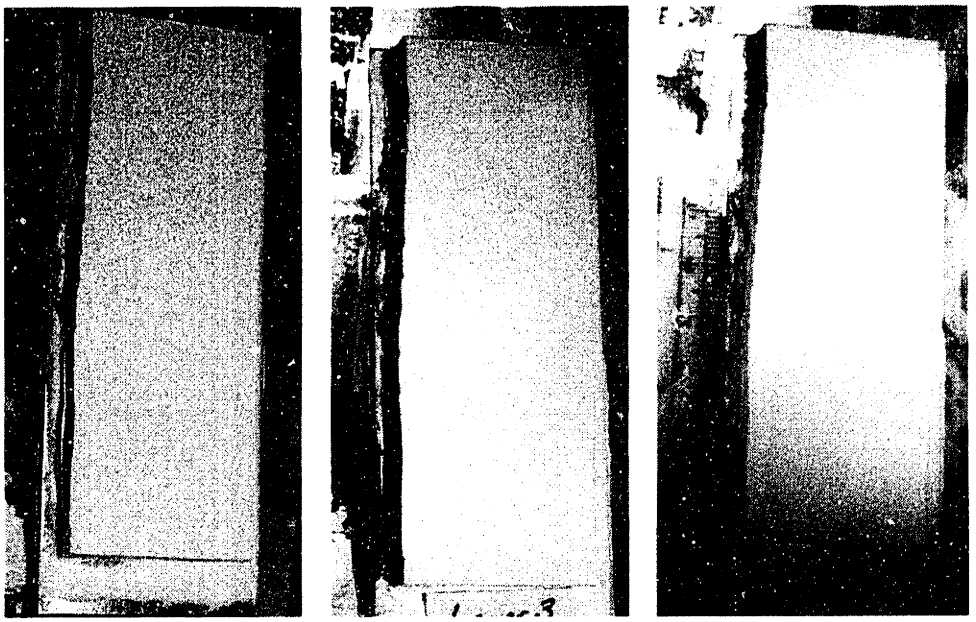

8.5 Summary

Experiments were conducted to verify the line merging model developed in Chapter 8 and to identify the optimum operating parameters for multiple layer builds. The parameter map was explored with a 22 vol% slurry to determine in what regions defects occurred and whether these results matched the model. Figure 8.23 shows the 22 vol% trials indicated on the a plot similar to the one shown in Section 8.5. This plot demonstrates that the line merging model accurately reflects the trends toward bubbling and stitching within a layer. The model is not as accurate in its predictions of slurry migration. It predicts that the chances of perpendicular migration should increase with high Q/v, but experimental observations suggest that the occurrence of perpendicular migration is linked to low Q/v.

Figure 8.23 Parameter map showing trends where layer defects are predicted to occur in relation to Q/v and T_c with experimental results from 22 vol% trials plotted

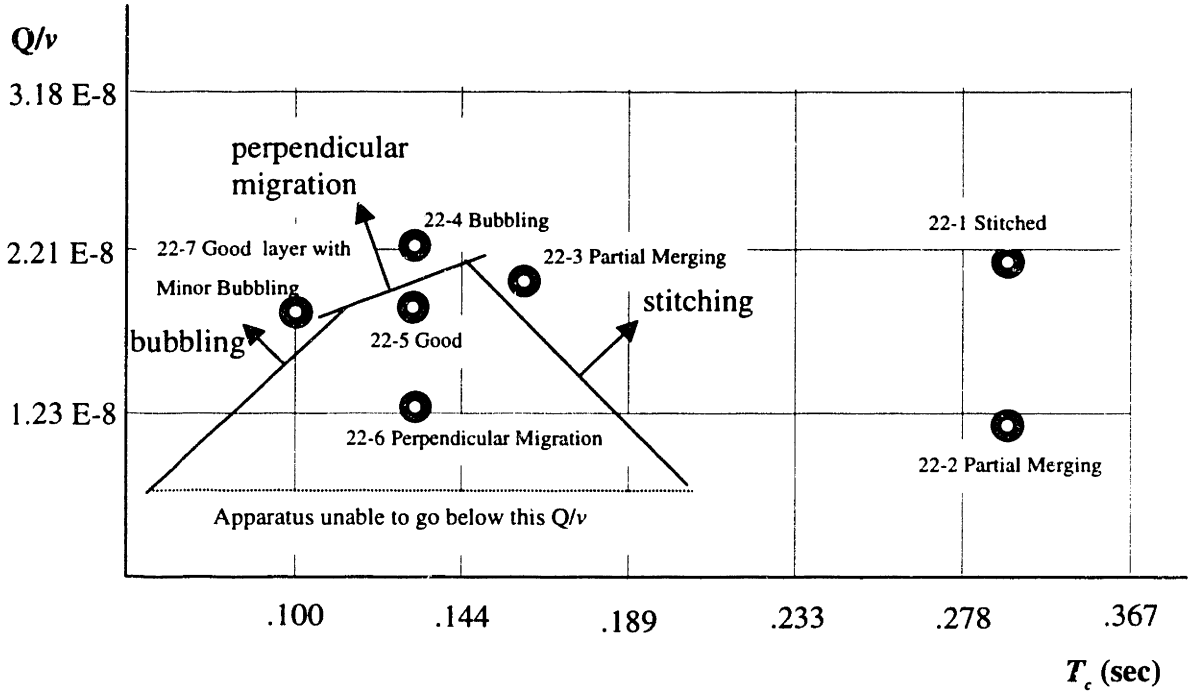

The individual objective functions T_s/T_c and w/l proved useful in determining successful line merging. The objective function based on $1/L_{slurry}$ was not as good. The combined objective function was very useful for identifying ideal operating parameters. The combined model did not clearly distinguish between regions where good layers would be deposited and where perpendicular migration would occur, however. This is in part be due to the inaccuracy of the $1/L_{slurry}$ model which was used to predict the occurrence of slurry migration.

Once the ideal parameters were identified by the 22 vol% trials, they were applied to both 18 vol% and 15 vol% slurries. Extremely good individual layers were deposited with the 18 vol% slurry. The 15 vol% slurry encountered bubbling in all regions near the "ideal" operating parameters. A 20 layer powder bed was deposited with the 18 vol% slurry at the ideal parameters. Overall the bed looked good but some perpendicular migration developed midway through. Another 20 layer powder bed was constructed where alternate layers were deposited at 90 degree angles to each other. This approach demonstrated that it could contain the onset of perpendicular migration and prevent it from propagating through multiple layers.

A large 60 layer powder bed was constructed with an 18 vol% slurry using a 90 degree powder bed rotation scheme to control perpendicular migration. The resulting surface finish was very good with a maximum peak to valley variation of 11 microns in the top layer. SEM analysis of cross-sections of this bed revealed micro-bubbles along inter-layer interfaces. These bubbles nucleated at the bottom of deposited layers and were subsequently frozen by slip casting before they could escape to the layer surface. SEM analysis of a cross-section of a different 5 layer powder bed constructed with 22 vol% did not display any evidence of micro-bubbles. Therefore, it can be concluded that powder beds can be constructed from merged layers without the presence of inter-layer micro-bubbles. The model suggests that the speed at which the wet front advances across the porous substrate will influence the occurrence of bubbling. The results of the experiments suggest that the actual relationship may be more complicated. The wet front advanced at 1.10 mm/s in the 5 layer 22 vol% build when no micro-bubbling occurred. The wet front advanced at 0.86 mm/s in the 60 layer 18 vol% build when micro-bubbling did occur. These results suggest that the likelihood of bubbling may also be related to the slurry solids loading.

A four inch long five layer powder bed was constructed to verify that perpendicular migration was not sensitive to the length of the powder bed being produced. The nozzle traversed the narrow width of the powder bed while the slide pulled the length of the substrate underneath the nozzle. The subsequent layers appeared very smooth and there was no indication that the length of the powder bed would cause the onset of perpendicular migration.

9. CONCLUSIONS

9.1 Summary of Achievements

Slurry-based three dimensional printing is being used to create ceramic parts directly from CAD files. In 3DP, slurry layers have traditionally been deposited by nozzle rastering. In this approach, a nozzle mounted to an x-y linear positioning system deposits closely spaced slurry lines on a powder bed. Powder beds produced in this manner contain many defects: inter-line porosity within a layer, inter-layer porosity between discrete layers, and an inherent surface roughness due to the peaks and valleys between slip cast lines.

Alternate methods of slurry layer deposition were investigated in an effort to produce defect-free powder beds. Tape casting of slurry layers was studied, in an effort to make entire layers quickly in one pass. However, the focus of the project was shifted to single nozzle deposition methods because of problems with scraping and bubbling and because of the desire to enable the formation of vias, which tape casting would not. It is hypothesized that the bubbling problems were caused by air that was displaced during slip casting. Air is forced from a porous substrate when solvent from a deposited slurry layer is drawn into the pore space by capillary action. When slurry is deposited on large regions of a substrate, this displaced air bubbles back up through the slip casting slurry layer. It is possible that tape casting may be used to deposit slurry layers if the speed of the traverse is slowed down significantly. This would make it possible for air to escape out in front of the tape casting unit, as it is forced out by infiltrating solvent. For 30 volume percent alumina slurry, the speed of the traverse would most likely have to be around 1mm/second.

A new approach to layer formation was developed, referred to as "line merging." Line merging differs from nozzle rastering in two ways: lines are deposited in only one direction (during the return pass the nozzle is put into a catch position), and the cycle time between depositing lines is reduced to as little as 0.1 second. The reduced cycle time causes successively deposited slurry lines to merge prior to slip casting. Complete

slip casting requires on the order of 0.5 seconds, so as many as five lines can merge depending on the actual cycle time, slip casting rate, and line spacing.

Line merging has the potential to rapidly deposit a slurry layer while simultaneously avoiding bubbling. When an individual line of slurry is deposited it begins slip casting immediately. The solvent from this line fills the pore space immediately below the line and begins advancing ahead of it. This advancing solvent front can displace air from the substrates pore space prior to the next slurry line being deposited. Thus, when the next adjacent slurry line is deposited bubbling does not occur, because the air has already been displaced from the pore space immediately below the line.

Line merging was initially explored with a rotary deposition apparatus. A 127 micron nozzle was attached to the end of a rotating arm. The revolving nozzle (typically at 600 RPM) deposited arcs of slurry on a substrate moving outward radially from the center of rotation. This set-up confirmed that line merging was capable of producing smooth, uniform slurry layers free of inter-line defects under optimum conditions. When conditions were not ideal, various defects arose. These defects included bubbling, incomplete line merging, over-saturation of the powder bed pore space, and radial lines caused by slurry migration. Slurry migration is a phenomenon in which differential slip casting rates and slurry surface tension cause the slurry to pool in localized regions of the powder bed, resulting in uneven surface finish once slip casting is complete. The cylindrical system also introduced defects that would not be present in a rectilinear system, so a new machine was designed.

A new slurry deposition machine was constructed from a bicycle wheel. Blocks were attached to the rim of the wheel, 180 degrees apart. The wheel was supported by two large plates. Large blocks with springs were located around the circumference of the rim, so that the wheel would oscillate as the wheel blocks bounced back and forth between the springs. A nozzle was mounted to the bottom of the wheel's rim. A substrate was positioned on a ball-screw slide so that it could be pulled under the nozzle when the wheel was oscillating. Nozzle on-off control was added so that slurry lines were only deposited in one-direction. A motor was also added to compensate for energy lost in spring collisions.

A model was developed to predict the optimum parameters for line merging. Presumably the optimum conditions would avoid the defects observed during the initial rotary experiments: bubbling, incomplete line merging, over-saturation of the powder bed pore space, and slurry migration. This model used slurry solids loading, cycle time, and slurry flow rate divided by nozzle speed as independent variables. Optimum conditions could then be predicted for a target dry layer thickness. Optimum conditions were determined by maximizing an objective function comprised of several ratios: time for slip casting over cycle time, slurry line width over line spacing, and one over the width of the slurry wet front (mm^{-1}). A large ratio of slip casting time to cycle time was expected to promote complete line merging since lines would have more time to merge before slip casting. The ratio of line width to line spacing determined the line overlap; presumably a large overlap would promote line merging. The width of the slurry wet front was expected to influence slurry migration. A large wet front would mean that a large amount of wet slurry was present on the surface of the substrate and capable of migrating. Since minimizing the size wet zone should decrease the likelihood of slurry migration occurring, the inverse of the width of the wet zone was maximized.

Experiments conducted with the bicycle wheel apparatus confirmed that the model was useful for designing experiments. Certain portions of the model were more accurate than others. The ratio of slip casting time to cycle time was of critical importance. If this ratio was too low, complete line merging did not occur. The ratio of line width to line spacing was also observed to be useful in determining regions where successful line merging could occur. Typically the higher the ratio the better. The relationship between the inverse of the width of the slurry wet front and the occurrence of perpendicular migration was questionable. Where the model predicted the least likelihood of perpendicular migration none occurred, so in this sense the model was accurate. Unfortunately at these conditions lines were merely stitching together, not merging into a uniform front. In the regions where line merging actually occurred, good layers and layers that contained perpendicular migration were produced at very similar conditions.

Experiments indicated that an 18 vol% alumina slurry (all slurries had 1:1 water/IPA solvent) produced the best merged layers under the optimum conditions. A

five layer powder bed was constructed from 50 micron layers at these conditions. Subtle signs of perpendicular slurry migration appeared in the top layer of the build, but for the most part, SEM analysis of a cross-section of the powder bed revealed that almost all internal defects had been eliminated through line merging. There was no sign of inter-line or inter-layer defects. Additionally there was no sign of significant internal voids.

A new technique of rotating the powder bed 90 degrees between layers during multi-layer builds proved capable of stemming the propagation of perpendicular migration. Using this technique, a 60 layer powder bed was successfully deposited. Surface profilometry indicated that the maximum peak to valley variation in the top layer was 11 microns. SEM analysis of cross-sections confirmed that inter-line defects had been totally eliminated. SEM analysis also revealed the presence of bubbles along the interfaces of deposited layers. These bubbles appeared to nucleate at the bottom of a layer when it was first deposited. Either rapid slip casting or capillary forces trapped the bubbles at the bottom of the layer, so that they were not visible at the layer surfaces and hence were not detected during experimentation.

Additional experiments demonstrated that the onset of perpendicular migration was not sensitive to the length of the powder bed layer being deposited (where the nozzle is depositing lines across the width of the substrate).

The technique of slurry layer formation by line merging demonstrated that it could produce uniform, nearly defect-free layers. The inter-line and inter-layer defects that occurred during layer formation by nozzle rastering were eliminated with the line merging approach. Additionally, top layer surface finish was typical smoother for beds created by line merging than by nozzle rastering. The reduced cycle times between line deposition offer the possibility of ultimately increasing powder bed throughput while simultaneously producing better layers. For these reasons line merging should be further developed.

9.2 Future Work

In order to reliably produce good beds with line merging, the model presented in Chapter 8 needs to be further refined. Experiments clearly demonstrate the importance of

the T_s/T_c ratio and w/l ratio, but maximizing these ratios was not sufficient to produce good layers. Neither ratio seemed to reliably account for the onset of perpendicular migration. The l/L_{slurry} ratio did not appear to correlate with the occurrence of perpendicular migration at all. An effort needs to be made to further understand what triggers the onset of perpendicular migration. There might be a set of parameters for which perpendicular migration does not propagate even in the presence of disturbances.

The model could be further refined if more complete slip casting rate experiments were performed for slurries with 1:1 water/IPA solvent and different solids loadings. Additionally, line merging experiments could be performed with slurries containing different ratios of solvents. In the experiments conducted on the bicycle wheel apparatus only 1:1 water/IPA slurry was used. All water solvents may not be the best approach, because the higher solvent surface tension will significantly reduce the critical saturation thickness.

The design of the bicycle wheel apparatus places some limitations on the width of the powder bed layer that can be deposited. Because the nozzle follows the path of the bicycle wheel's rim, the print distance varies across a substrate. In order to maintain a somewhat uniform print distance, powder beds no wider than 1" – 1.5" can be used. A linear version of the bicycle wheel apparatus would maintain a constant print distance and allow a wider powder beds to be produced. Cycle times, nozzle velocities, and turn around times would still impose limits on the maximum powder bed width that could be produced. A future linear version could incorporated a linear slide, linear motor, and springs and look something like Figure 9.1.

Figure 9.1 Schematic of possible linear machine that would produce layers through line merging

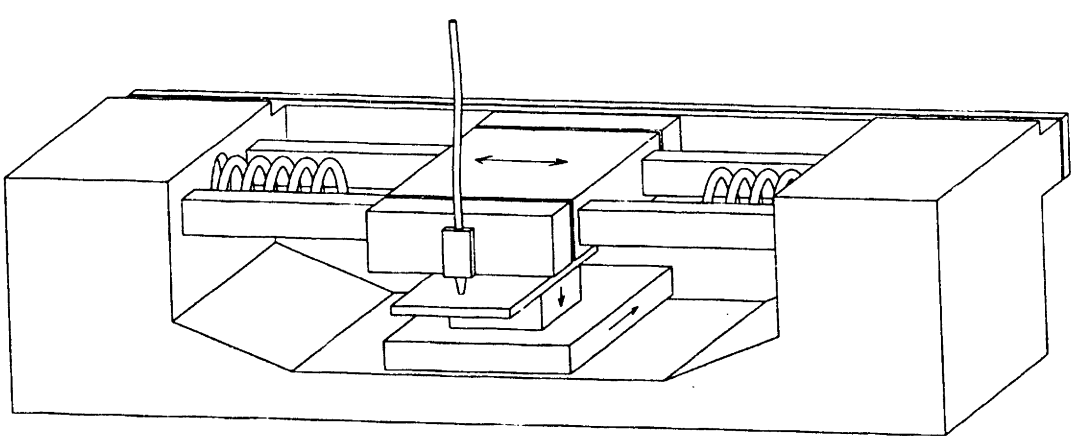

References

Caradonna, Anthony, M.S. Thesis, Massachusetts Institute of Technology, 1997

Myklegard, Brett, "From Concept to Production," Prototyping Technology International '97, pp69-70

Grau, Jason, Ph.D. Thesis, Massachusetts Institute of Technology, 1998

Saxton, Patrick, M.S. Thesis, Massachusetts Institute of Technology, 1999

Middleman, Stanley, Fundamentals of Polymer Processing, McGraw-Hill, Inc, 1977

Richard Holman, personal communication

Kelley, Andrew, M.S. Thesis, Massachusetts Institute of Technology, 1998

Appendix A Slurry Formulation

Required Materials:

1 micron Al_2O_3	Ceralox Aluminum Oxide HPA-1.0 w/ MgO Condea Vista Company – Ceralox Division 7800 South Kolb Rd. Tucson, AZ 85706
Polyethelyne glycol 400M	Carbowax Polyethylene Glycol 400 Union Carbide Corporation 39 Old Ridgebury Rd. Danbury, CT 06817

1.0 M Nitric acid
Isopropyl alcohol
Deionized water
Alumina milling media (~ 1cm diameter balls)
1 Liter Nalgene bottle (or any other appropriate bottle)

Notation:

Vol% Al2O3 - Slurry loading desired, typically between 15% - 40%

Vol Slurry - Total volume of slurry desired, 500 mL is sufficient for most experiments

Wt% - The amount of PEG required is specified as a percentage of the mass of alumina in the slurry, typically 2 wt% is used

Slurry M - The desired molarity for the slurry. The alumina particles in the slurry are acid stabilized, so the slurry M is critical to prevent the slurry from flocculating. The required M is based on alumina solids loading. These are recommended values based merely on what has been used to produce good slurries in the past:

Slurry Loading (Vol%)	Recommended Slurry Molarity
≤ 20	0.3 M
30	0.4 M
45	0.5 M

Parts Solvent - The solvent is composed of some volume ratio of water and isopropyl alcohol. This ratio is specified as 1 part water to 2 parts IPA, etc. The total parts solvent in this case would be 3.

Amounts Required:

Al2O3 Power:

$$\text{Mass } Al_2O_3\ [g] = \left(\frac{\text{Vol\% } Al_2O_3}{100}\right)(\text{Vol Slurry [mL]})(3.96\ [g/cc])$$

PEG 400M:

$$\text{Mass PEG } [g] = \left(\frac{\text{Wt\% PEG (based on alumina)}}{100}\right)(\text{Mass } Al_2O_3\ [g])$$

1.0 M Nitric acid:

$$\text{Vol acid [mL]} = \left(\frac{\text{Desired Slurry Molarity [M]}}{1\,M}\right)(\text{Vol Slurry [mL]})$$

Isopropyl Alcohol:

$$\text{Vol IPA [mL]} = \left(\frac{\text{Parts IPA}}{\text{Tot Parts Solvent}}\right)\left((\text{Vol Slurry [mL]})\left(\frac{100\% - \text{Vol\% } Al_2O_3}{100\%}\right) - \left(\frac{\text{Mass PEG } [g]}{1.100\ [g/cc]}\right)\right)$$

Deionized water:

$$\text{Vol water [mL]} = (\text{Vol Slurry [mL]}) - \left(\left(\frac{\text{Mass } Al_2O_3\ [g]}{3.96\ [g/cc]}\right) + \left(\frac{\text{Mass PEG } [g]}{1.100\ [g/cc]}\right) + (\text{Vol acid [mL]}) + (\text{Vol IPA [mL]})\right)$$

Sample Formulation:

Desired Slurry:	500mL of 30 vol% Alumina slurry 1:1 Water/IPA Solvent	
Amounts Required:	Water	149.6 mL
	IPA	169.6 mL
	PEG	11.88 g
	1.0 M Nitric acid	20 mL
	Alumina powder	594.0 g

Mixing Procedure:

1. Obtain a Nalgene bottle with approximately twice the volume of the slurry to be made.
2. Fill the bottle approximately 1/3 to 1/2 full of milling media
3. Add the de-ionized water
4. Add the isopropyl alcohol if required (not an all water solvent)
5. Add the PEG
6. Add the 1 M Nitric acid
7. Close and shake the bottle to mix the solvent thoroughly
8. If the required solids loading is 20% or less, add all of the required alumina powder
   If the required solids loading is greater than 20%, add approximately half of the required alumina powder
9. Seal the bottle and place it on a ball mill
   - If not all the powder was added in one dose (> 20% solids loading), remove the bottle from the mill after one hour and add the remaining alumina powder. Return to the ball mill for approximately 17 hours.
   - If all of the powder was added (≤ 20% solids loading), leave the bottle on the ball mill for approximately 18 hours
10. After 18 hours total milling time, remove the slurry from the mill. Remove the milling media by pouring the slurry/media mixture through a 45 micron stainless steel seive/filter. If the slurry is not to be used immediately, return it to the bottle and place it back on the ball mill (without milling media) until it is required.

11. The life of alumina slurry is approximately 1 week. After one week flocculation degrades the slurry.

Note:

1. Each time the slurry is used it should be filtered (45 micron filter)

2. Slurries should typically be used with in-line filters

3. The IPA that makes up a portion of the solvent will evaporate if the slurry is exposed to open air for long periods of time, which will increase the effective solids loading of the slurry.

Appendix B-1 Bicycle Wheel Motor Logic

The circuit below shows how the motor attached to the bicycle wheel is controlled. When the upper switch is depressed, the relay is activated, and the motor switches direction. When the lower switch is depressed, power to the relay coil is cut, and the relay deactivates, switching the motor's direction back again. The momentary off switch was added when the circuit was wired to power the motor in only one direction, to prevent the motor from pushing the wheel opposite to its direction of rotation during turn-arounds. It is not necessary for the function of the device, even when the circuit is wired to power the motor in only one direction.

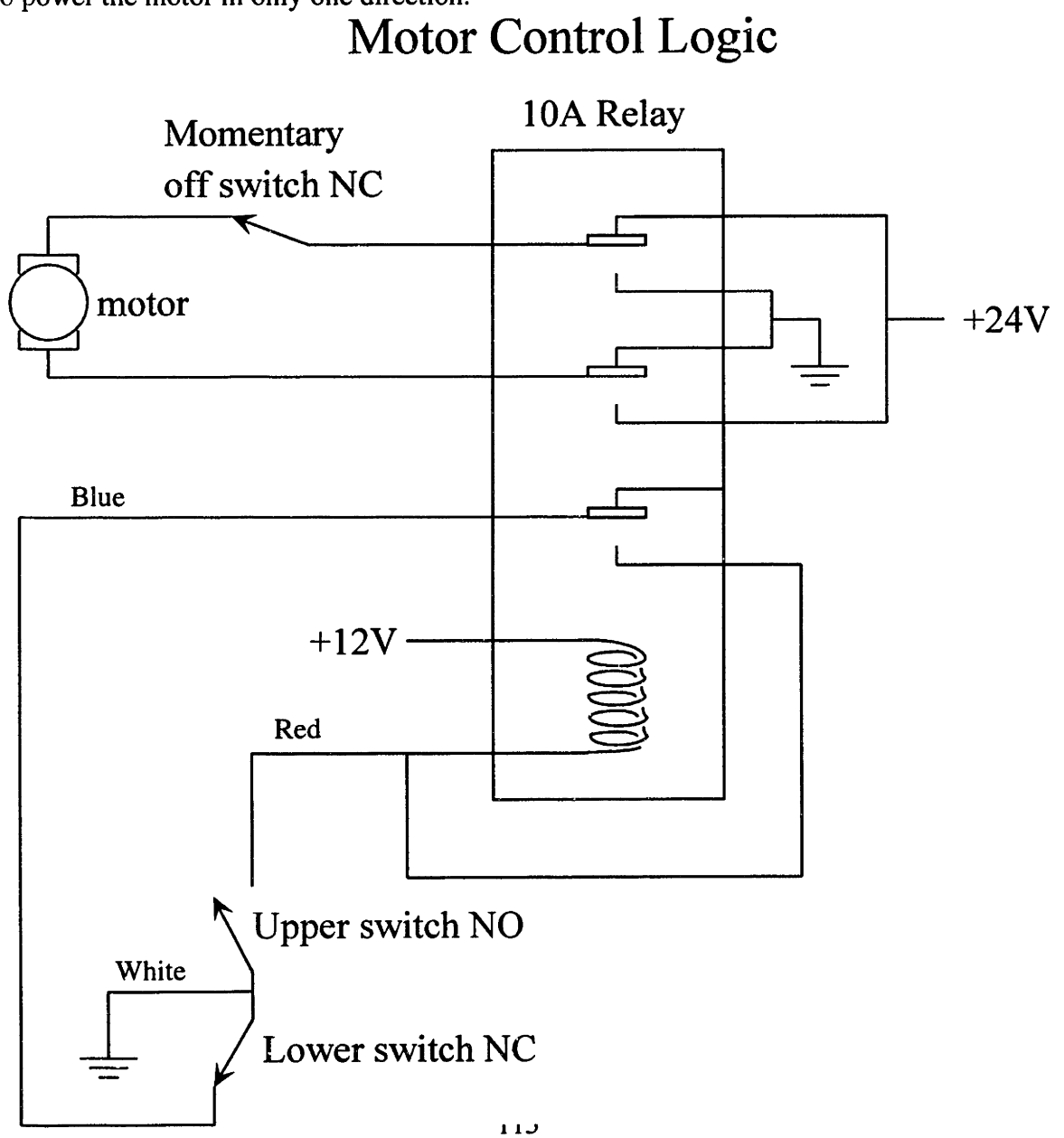

Appendix B-2 Bicycle Wheel Nozzle Logic

The circuit below causes the nozzle (mounted on the read-write head) to switch back and forth from deposition to catch position, as switch #1 and switch #2 are depressed alternately. The design is slightly more complicated than necessary, since the two-relay implementation could easily be replaced by the one-relay implementation used for the motor control (see previous page). The RC networks leading to the read-write head serve to deliver a (roughly) 10V spike which decays to 3V with a time constant of 7 milliseconds. This serves to move the nozzle into its new position quickly, and then hold it in place without overheating the read-write head coils.

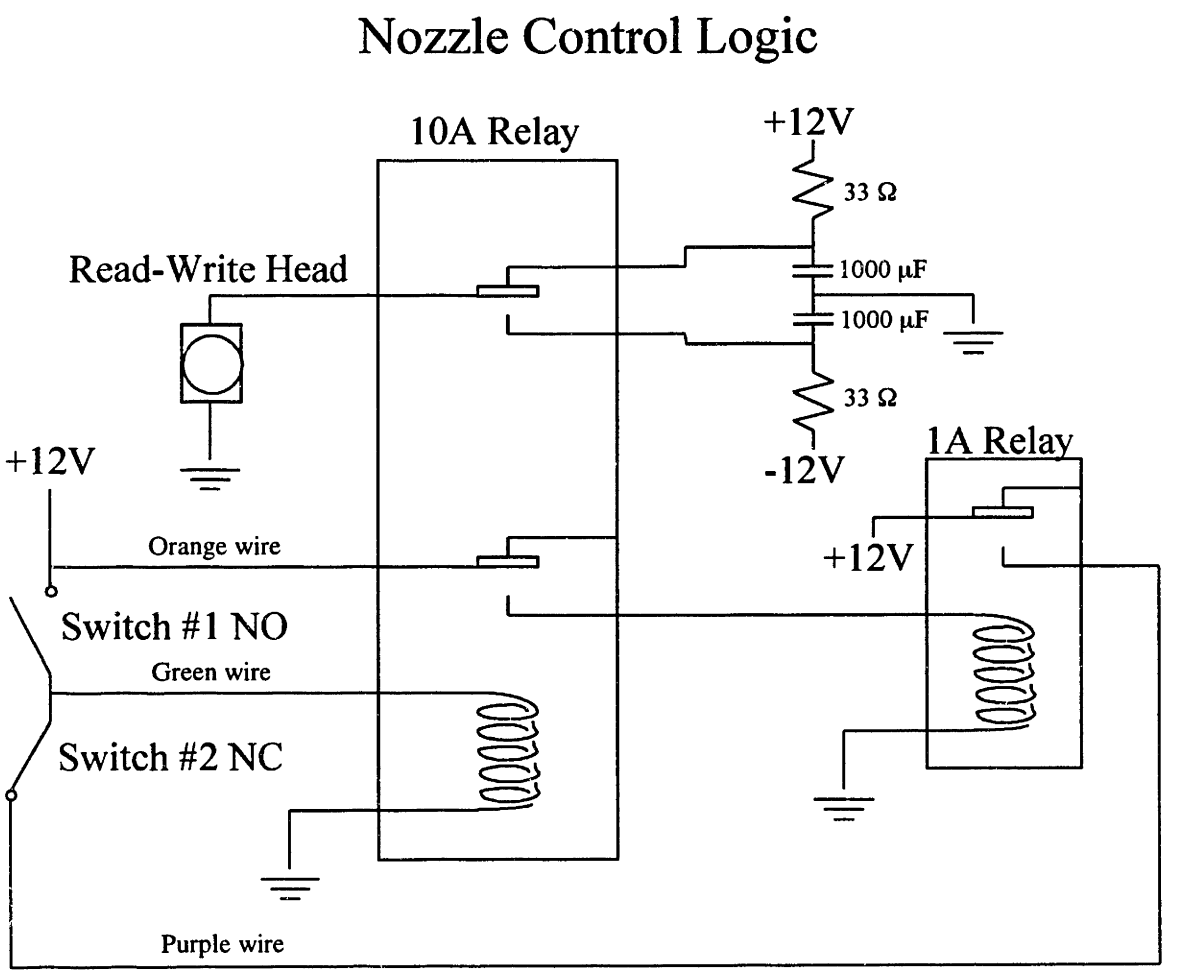

Appendix C Operating the Bicycle Wheel Apparatus

The purpose of this appendix is to provide step-by-step instructions for operating the bicycle wheel apparatus. Some steps may change if the set-up is changed (i.e. if the servo motor that operates the slide is replaced with a stepper motor)

1. Select springs and position the spring blocks to achieve the desired cycle time and print speed. First select a desired T_c. The equations below give an estimated v for the chosen springs and spring block placement. Adjust the springs and block placement until the desired v is reached. The voltage that is applied to the motor can later be used to fine tune the v and T_c.

For a given spring, the turn around time is as follows:

$$t_{TA} = \pi \sqrt{\frac{m}{2\frac{k_{spring}}{0.00571}}} \tag{C-3.1}$$

The m for the bicycle wheel and attachments is approximately 1.3 kg. It is important to note that k_{spring} is in lbf/in, the 0.00571 factor converts the spring constant to metric units. The bicycle wheel's free traverse time (when it is not contacting the springs) is thus:

$$t_{FT} = \frac{(T - 2t_{TA})}{2} \tag{C-3.2}$$

The numbers of degrees traveled by the wheel during free traverse can be found using:

$$\alpha_{FT} = (\#_{LS} - \#_{US})\left(\frac{5°}{\#}\right) - 2(\alpha_{spring}) \tag{C-3.3}$$

The spring position numbers are counted from the top of the base plate down, with a total of 21 positions available at 5 degree increments. The number of degrees occupied by each spring can be found in Table C-3.1 The angular velocity of the wheel during traverse is thus:

$$\omega = \left(\frac{\alpha_{FT}}{t_{FT}}\right)\left(\frac{\pi}{180°}\right) \tag{C-3.4}$$

The resulting nozzle velocity is:

$$v = \omega r \tag{C-3.5}$$

Where $r = 0.34$m from the axle of the bicycle wheel to the nozzle.

Table C-3.1 Degrees occupied by the length of each spring

Spring (identified by k_{spring})	α_{spring}
89.6 lbf/in	11
88.0 lbf/in	16
15.5 lbf/in	16
4.4 lbf/in	19

Note:

There is a maximum v for each spring based on how far the spring is able to compress:

$$I_{wheel} \approx 0.62 m r^2 \tag{C-3.6}$$

$$x_{spring} = \sqrt{\frac{I_{wheel}}{k_{spring}}}\left(\frac{v}{r}\right) \leq x_{\max} \tag{C-3.7}$$

The maximum compression for each spring can be determined experimentally.

2. Align the springs by rotating the spring blocks to ensure that the wheel blocks are flush with the top of the springs when they are in contact. If the wheel block contacts one edge of the spring before it contacts the other, it can produce a torque that ultimately causes wavy slurry lines.

3. Move the motor and nozzle switches so that they are depressed at the wheel's end of travel (when it is in contact with the springs).

4. Turn on the power supplies. These include the 36V 20A motor power supply (keep in mind the motor is rated to 24 V), the Power One power supply that powers the logic, and the encoder switch on the front of the machine (3 1.5V AA batteries).

5. Make sure that all obstacles are removed from the path of the bicycle wheel. Tape the short nozzle feed line down to the rim of the wheel if it is disconnected from the main feed line. Make sure that the nozzle will not hit the trough.

6. Turn on the motor power switch (wall outlet switch) located on the 80-20 brace at the back of the bicycle wheel apparatus. The bicycle wheel may need to be hand pumped to get started (especially when long springs are used).

7. With the oscilloscope, watch the power to the motor on one channel and the encoder signal on the other. The motor signal can be used to determine period of the bicycle wheel's motion, since it will have a rising edge at the beginning of each cycle. The encoder signal can be used to determine the approximate print speed using the following equation:

$$v = \left(\frac{\#\ peaks}{time}\right)\left(\frac{1\,shaft\,rev}{1000\,peaks}\right)\left(\frac{2\pi\,rad}{rev}\right)(r) \qquad \text{(C-3.8)}$$

8. Adjust the motor voltage as necessary to arrive at the approximate cycle time and print speed desired. If the desired cycle time and print speed can not be achieved for a motor voltage between 0-24 V, the springs or spring block locations must be adjusted.

9. Set the desired slide speed by adjusting the voltage to the motor controller. The plot below will help in determining the required controller setting:

Figure C-3.1 Calibration plot for slide motor

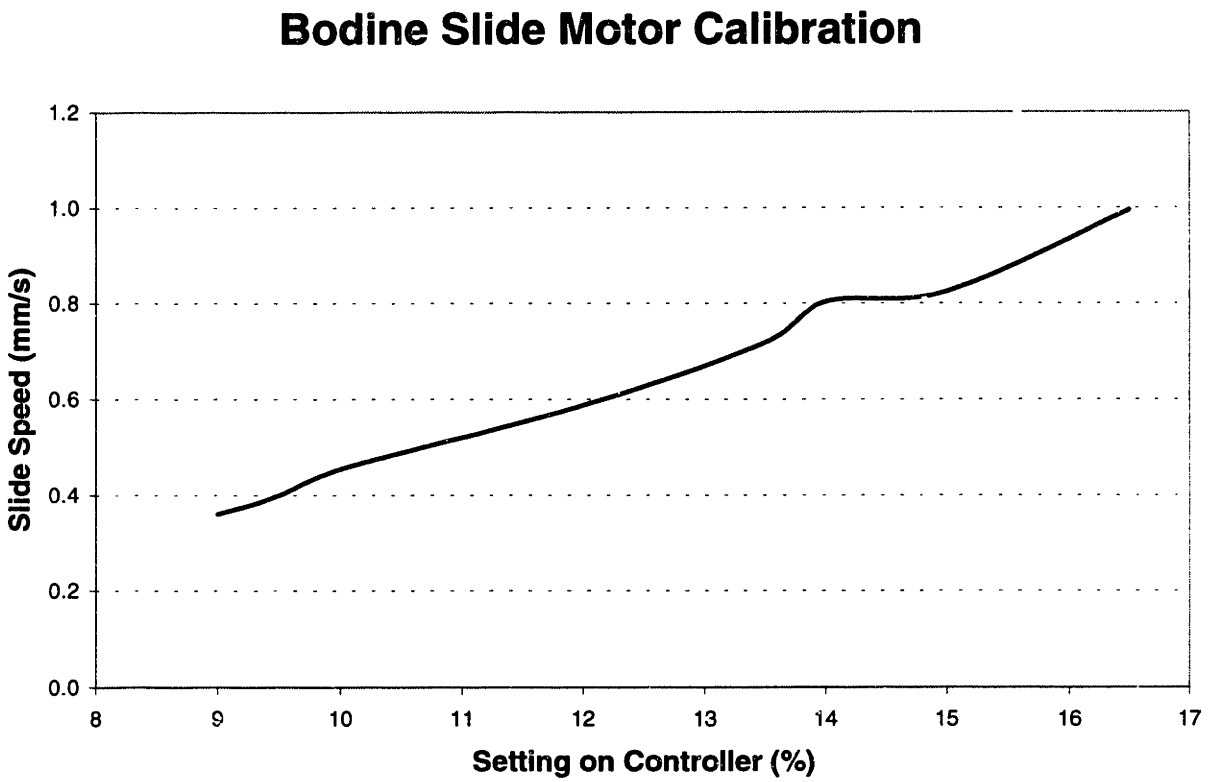

10. Once the target cycle time and print speed is achieved, turn the trough water on by opening the pinch valve on the water feed line. Turn the peri-pump on to suck the water from the other side of the trough. This will establish a uniform flow. The speed of the pump must be adjusted to approximately setting "3" so that the appropriate amount of water flows through the trough without any overflow.

11. Put the slurry in a separate 500 mL Nalgene bottle and place this bottle in the large pressure vessel. Seal the pressure vessel and connect the air line to the Nitrogen tank located against the wall.

12. Clean the in-line 45 micron nylon filter.

13. Use a syringe to purge the slurry nozzle with water.

14. Attach the slurry line from the pressure vessel to the in-line filter. Connect the other side of the filter to the slurry feed line that goes to the bicycle wheel. Squirt some slurry out of the feed line in order to get rid of any dried agglomerates that may be in the line. Connect the other end of this line to the narrow nozzle feed line near the rim of the bicycle wheel. Secure the slurry lines near the rim in such a way that the narrow Teflon tube still has some slack when the nozzle is in the deposition position. Do not restrict the movement of the slurry lines near the axle of the wheel.

15. Pressurize the slurry vessel. Make sure that the regulator is fully closed prior to opening the valve of the nitrogen tank. Open the regulator to the desired pressure and then open the in-line valve.

16. Open the pinch valves along the slurry feed line to the bicycle wheel.

17. Take slurry mass flow readings and adjust the pressure until the desired flow rate is achieved.

18. Position the bicycle wheel such that the slurry jet is angled away from the substrate. Place a small catch vessel in position to catch the slurry. If this slurry is not left exposed to open air for extended periods it can be recycled.

19. Place a steel-backed substrate on the slide magnet. Make sure the trough is positioned correctly. A correctly positioned trough will not only catch slurry on the deposition pass, it will also act as a guide to assist the user in bringing the substrate to the correct height. Adjust the height of the substrate by turning the z-axis knob. If the trough

is positioned correctly, bringing the top surface of the substrate up to the bottom surface of the trough (leaving a small air gap) will result in a distance of approximately 1mm between the surface of the substrate and the nozzle at its lowest point.

20. Move the slide forward so that the substrate is tucked part way under the trough assembly. Ensure that the nozzle will be off the substrate when the bicycle wheel is first started up. Note the position of the indicator dial when substrate is correctly positioned.

21. Turn the wheel motor switch on, hand pump the bicycle wheel, and wait for it to come up to speed. The oscilloscope can be used to determine when it has reached steady-state.

22. Turn the slide motor dial from the brake position to the reverse position to move the substrate underneath the path of the nozzle.

23. When the entire substrate has passed under the nozzle, turn the motors off and wait for the bicycle wheel to stop. Position the bicycle wheel so that the slurry jet is once again angled away from the substrate and into the catch vessel.

24. For single layers, the substrate can be removed and examined. If multiple layers are required, back the slide away from the bicycle wheel, such that there is room for the halogen lamp to be positioned over it. Turn the halogen lamp on and dry for 30-45 seconds (time depends on amount of liquid deposited). Cool substrate with fan if necessary.

25. For multiple layers, run the slide all the way forward such that the substrate is once again underneath the trough assembly. Use the indicator attached to the slide to return to the correct starting location. Repeat steps 20-23.

Note: Before making entire layers, it is important to make individual lines to be inspected for waves and nodes. Waves tend to be created by poor spring alignment; nodes tend to be created by pressure pulses in the fluid lines. These pressure pulses can appear if the fluid lines are being yanked or are flopping about.

Appendix D Troubleshooting

Problem	Solution
Bicycle wheel apparatus makes loud banging noises when it gets up to speed	Reduce voltage to the wheel motor. Either the springs are bottoming out, or, if the spring blocks are as far apart as possible, the nozzle assembly gusset plate is banging into a spring block.
Individual lines contain nodes	Adjust fluid lines; ensure there is slack in the thin Teflon fluid line when nozzle is in deposition position; ensure nozzle is contacting end of travel when in deposition position.
Individual lines are wavy	Adjust springs: ensure springs are straight; ensure springs are flush with spring blocks during initial contact; ensure blocks are contacting springs in center (if they are not, see below).
Blocks on one side are too far forwards and blocks on the other side are too far backwards	Plates of bicycle wheel apparatus are misaligned so that axle of bicycle wheel is no longer perpendicular to plates. Realign plates.
Powder beds have black marks on top surfaces	Lower powder bed so that bottom of trough does not touch it when vibrating.
Powder bed wanders when the bicycle wheel oscillates	Lower powder bed so that bottom of trough does not touch it when vibrating.
Slurry drips down on powderbed from trough when bicycle wheel oscillates	Check to make sure the slurry jet points into the trough throughout the duration of the return pass. Confirm that the peri pump is turned on and set to the correct setting.
Line placement is erratic	Check nozzle for clog.
Slide motor stops working after a crash	Replace fuse inside of controller.
Slide gets stuck on end of travel	Replace diode across end of travel switch.

Appendix E Making Substrates

The purpose of this appendix is to inform readers how substrates may be created from slurry.

1. Obtain a clean plaster block with a flat, level surface.

2. Obtain molds with smooth walls, containing no sharp corners, and having openings at the top and bottom.

3. Place the molds on the plaster block. If there is a draft angle to the mold, orient the mold so that it can be pulled away from the substrate and the plaster block.

4. Dispense equal volumes of slurry into each of the molds and cover with plastic cling wrap.

5. Wait 2 to 3 days, then check to see if slurry has fully slip cast. If it has, lift up the molds from the plaster block. If newly created substrates are dry, their edges will have pulled away from the edges of the mold. Allow substrates to dry if they are still damp.

6. Burn the organics out of the substrates in an oven located under a fume hood. Use following firing schedule: Ramp up at 5 degrees C per minute to 600 degrees C. Hold at 600 C for two hours. Ramp down to room temp at 5 degrees C per minute.

7. Bisque fire the substrates using the following firing schedule: Ramp up to 1100 degrees C in 1 hour 50 minutes. Hold at 1100 C for one hour. Ramp back down to room temperature in 1 hour 50 minutes.

8. If delamination occurs on surface, sand off with course sand paper, then smooth using increasingly finer grit sand paper.

9. Affix a carbon steel sheet metal backing to the substrate with a gel or paste epoxy (less viscous epoxies may penetrate the pore space of the substrate). Take care to ensure that the steel backing and top of the substrate are parallel.

Appendix F: Further Details Concerning Tape Casting Experiments

Plaster blocks were made to be used as substrates. 50 micron layers of alumina slurry were tape cast on the substrates, and after each layer was deposited, it was dried for thirty seconds using a halogen lamp set to 90V (past experience had shown that most of the solvent in a 50 micron layer could be evaporated with this amount of drying). The layers produced by this technique were optically smooth, and also very dense (a sintered powder bed made by this technique was 99.6% dense as compared with a sintered powder bed made by nozzle rastering, which was 97.8% dense). Thus initial tape casting experiments appeared to be a great success.

At a certain point in the project, bubbles started popping up in tape cast layers, despite the fact that the tape casting was being done under conditions that were nearly identical to those of the initial successful builds. First it was thought that additional vibration had been introduced, and that the new vibration was responsible for the bubbling. Steps were undertaken to reduce vibration, but the tape cast layers still bubbled. Then it was thought that the geometry of the new tape casting unit was different enough from the original tape casting unit to introduce bubbles into the system. The tape casting unit's blades were modified and relocated several times, and still there was bubbling. Then it was thought that the slurry was not being prepared in exactly the same way as the initial slurry, so the slurry chemistry was tweaked several times, but the bubbling still persisted. Then it was thought that the temperature of the drying step of the tape casting cycle had changed, so this was modified carefully, but the bubbling still persisted. Finally, it was discovered that the reason the slurry did not bubble at first was because the plaster substrates were so moist when they were freshly made that they kept the powder beds made on top of them damp, and subsequently prevented bubbling. As the plaster substrates dried out over time, they lost their ability to keep powder beds damp, and layers made on top of them bubbled.

Although it was very informative to learn the reason for the sudden change in behavior of the system, it was determined that keeping powder beds damp was not an acceptable solution to the bubbling problem, primarily because this approach guaranteed

the occurrence of binder bleeding. Attempts were made to pre-wet the top surface of powderbeds prior to adding new layers, but this approach was determined to be very problematic, primarily because the top surface would become partly redispersed, or cracked, or both.

For these reasons, tape casting was abandoned in favor of approaches employing the deposition of slurry from a single nozzle. During the course of experimenting with these approaches, it became apparent that line merging at a given substrate traverse speed should be no different physically than tape casting at the same traverse speed (assuming the layer thicknesses were matched). By that time line merging had successfully produced high-quality powder beds with a substrate traverse speed of 1mm/sec. This was **250 times** slower than the substrate traverse speeds employed during tape casting. It was hypothesized at that point that if line merging were done with a fast enough substrate traverse speed, bubbling would arise just as it had in the tape casting experiments. This hypothesis was confirmed with the bicycle wheel apparatus, when slide speeds exceeding 1.8 mm/sec were employed to make layers of 30 volume percent slurry. As lower and lower solids loadings were used, the critical slide speed to produce bubbling decreased steadily, possibly because of slower slip casting and lower slurry viscosities. For 15 volume percent slurry, bubbling occurred for slide speeds as low as 0.5mm/sec. Since the hypothesis had been supported very convincingly, it became very tempting to revisit tape casting, slowing down the traverse speed to 1mm/sec (for 30 v/o slurry). However, this was not undertaken, partly because of concerns about scraping, partly because of the desire to be able to make vias.

Appendix G Slurry Thickening

One of the approaches used when attempting to eliminate bubbling was to thicken the slurry. This approach was not successful, but the method of thickening the slurry may be of interest to the reader, and is presented below.

The slurry was thickened by substituting in higher molecular weight PEG for the standard 400MW PEG. Enough PEG was added to fill 10% of the powder bed pore space.

Three different slurries were compared to each other. All were 30v/o with a water to methanol ratio of 3:2. The PEG in the first slurry was 400 molecular weight (standard), the PEG in the second was 8000, and the PEG in the third was 20M (meaning 20,000 for some reason). The viscosity of each slurry was measured. Then the slurries were poured into sample dishes and allowed to settle and dry. Pieces of the dried samples were then placed in a wire basket hanging from a gantry sitting on a scale. A beaker of water was supported above the scale below the gantry, and the wire basket was lowered into the water. As the powder bed redispersed, a data acquisition system took periodic readings of the weight measured by the scale. In this way, it was possible to accurately measure the progress of the redispersion. The water surrounding the redispersing samples was **not** agitated in this experiment. The results are given below in Figure G. A summary of the data gathered in the experiment is given in the table below.

Molecular weight	Slurry Viscosity	Amount remaining after 1645 seconds
400	13cp	37.5%
8000	25cp	85%
20M (20,000)	48cp	97%

Figure G: Redispersion Experiment

Redispersion of Powder Beds Made With Slurries Containing Different Molecular Weight PEG

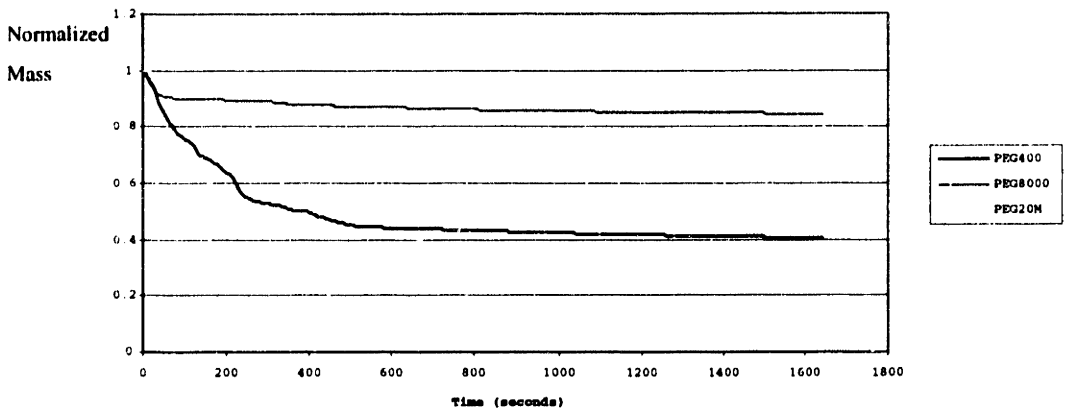

An experiment was done to get a rough idea as to how much slower water would wick into a powderbed if it contained PEG 8000. Ten alumina powder beds were placed flat on a table. A drop of water was placed on each one and the infiltration time for each one was recorded. Then, ten grams of PEG 8000 were dissolved in 100mL of water. This produced a solution that was twice the viscosity of water. Ten more alumina powder beds were placed flat on a table. A drop of the PEG solution was placed on each one and the infiltration time for each one was recorded. For both the pure water and the PEG solution droplets, the droplet volume was roughly 1/42cc. The results of this experiment are tabulated below.

Infiltration Times (seconds):

	Mean	Standard Deviation
Pure water	2.5	1
PEG solution	18	3
Difference	15	3
Ratio	9	5

Methyl cellulose was also tried as a thickener, but it did not appear to dissolve in the methanol-water very well, so it was not used in any experiments.

Appendix H Explanation of Figure 3.3 and Information on Predicting Layer Height.

The location of the bottom of the doctor blade was calculated:

$$location\ of\ blade\ bottom = layer\ number * layer\ thickness + extra\ height\ at\ start$$

Using this information the thickness of the wet layer was calculated:

$$thickness\ of\ wet layer = location\ of\ blade\ bottom - location\ of\ top\ surface\ of\ powder\ bed$$

Using this information the thickness of the dry layer is computed:

$$thickness\ of\ dry\ layer = \frac{thickness\ of\ wet\ layer * solids\ loading}{packing\ fraction}$$

This is what is graphed in figure 3.3. Using this information the location of the top surface resulting from the addition of the new layer is computed:

$$location\ of\ new\ top\ surface = location\ of\ old\ top\ surface + thickness\ of\ dry\ layer$$

Appendix I Line Merging Experiments

Trial 22 –1

The first trial was for T_c = 0.29 sec and Q/v = 2.07 E-8 m^2. This layer showed no signs of line merging. Instead, the lines appeared to overlap and stitch together just as lines do in traditional nozzle rastering.

Trial 22 – 2

The second trial was also conducted for T_c = 0.29, but the Q/v was reduced to 1.19 E-8 m^2. Lowering Q/v effectively reduces the cross-sectional area of the line that is deposited. In order to maintain the target layer thickness, lines must be overlapped even more. Increasing the w/l ratio by reducing l reduces the chances of line stitching. The layer deposited with these settings showed signs of partial line merging. According to the model, in order to achieve complete line merging Q/v could be reduced further or T_c could be reduced. Since Q/v was approaching its lower bound, T_c was reduced.

Trial 22-3

The third trial was conducted for Tc = 0.16 sec and Q/v = 1.99 E-8 m^2. This trial was similar to trial 22 – 1 except that the cycle time was now halved. These conditions yielded a bed that demonstrated partial merging. The layer was significantly better than previous two layers, but it was not optimum.

Trial 22-4

The T_c was further reduced to approximately 0.13 sec for approximately the same Q/v = 1.83 E-8 m^2. This set of conditions produced a very good layer. There were some slight ridges and valleys visible indicating that the lines had not entirely merged into one uniform front, but the surface roughness was much better than that of a rastered layer.

Trial 22 –5

The previous trial established the set of parameters at which a good 50 micron layer could be produced. The fifth trial explored what happens if Q/v is increased; the parameters for this layer were T_c= 0.13 sec and Q/v = 2.24 E-8 m^2. This layer showed evidence of bubbling. Raising the Q/v meant that the cross-sectional area of a deposited line was increased. In order to maintain 50 micron layer height, the line spacing was increased. For the same T_c, this meant a faster slide speed (x mm/s). The end result was that bubbling occurred because the wet slurry front advanced across the substrate more rapidly than the solvent could infiltrate the pore space.

Trial 22-6

The sixth trial explored reducing Q/v (relative to trial 4). The parameters for this layer were T_c = 0.13 sec and Q/v = 1.29 E-8 m^2. Perpendicular migration was observed in the deposited layer (Figure 9.6). The perpendicular migration was most likely due to how quickly the lines were slip casting. At very low Q/v each individual deposited line has very little cross-sectional area and therefore slip casts very quickly. If the line is so small that it slip casts before the next line can be deposited than the slip casting model that the overall line merging model relies on is no longer valid. This model assumes that each individual line remains wet long enough for the equilibrium wet layer thickness to build up on top of it. It is then this total wet layer thickness that is used to predict layer slip casting times. Apparently Q/v has an additional lower bound that is not accounted for in the model. This lower bound established by this trial is a useful tool for predicting perpendicular migration.

Trial 22-7

The seventh trial explored further reducing T_c to 0.1 sec. Q/v was returned to its value in trial 22-4 (1.79 E-8 m^2). At these conditions the layer exhibited both minor bubbling and slight perpendicular migration. A lower T_c forced the slurry wet front to move more rapidly across the substrate in order to maintain the same line spacing. The slurry front advanced more rapidly than the solvent in the pore space and bubbling resulted. The presence of slight perpendicular migration indicated that Q/v could not be

lowered any further to avoid bubbling. Additionally Q/v could not be raised or bubbling would get worse. For a 22 vol% slurry it appeared that quality layers could not be produced if T_c or Q/v were further reduced.

22 vol% Trials

Trial		22-1	22-2	22-3	22-4	22-5	22-6	22-7	22-8
Number of Layers		1	1	1	1	1	1	1	10
Settings									
Solids Load	%	22	22	22	22	22	22	22	22
Speed	m/s	2.8	2.8	2.8	2.65	2.65	2.65	2.6	2.7
Cycle Time	msec	290	290	160	130	130	135	100	100
Mass Flow	g/30sec	2.73	1.57	2.63	2.79	2.28	1.61	2.27	2.28
Slide	mm/s	0.63	0.35	1.08	1.33	1.1	0.74	1.54	1.48
Q/V	mm^2	2.07E-08	1.19E-08	1.99E-08	2.24E-08	1.83E-08	1.29E-08	1.85E-08	1.79E-08
Ratios									
T_s/T_c		2.41	2.41	4.37	5.37	5.37	5.18	6.99	6.99
w/l		2.84	3.75	2.90	2.73	3.02	3.60	3.01	3.06
$1/L_{slurry}$		2.51	4.36	1.44	1.04	1.27	1.87	0.97	1.00

18 vol% Trials

Trial		18-1	18-2	18-3	18-4	18-5	18-6	18-7
Number of Layers		1	1	1	20	20	60	Long Build
Settings								
Solids Load	%	18	18	18	18	18	18	18
Slurry Denisty	g/cc	1.45	1.45	1.45	1.45	1.45	1.45	1.45
Speed	m/s	2.8	2.8	2.8	2.8	2.8	2.8	2.8
Cycle Time	msec	100	100	100	100	100	100	100
Mass Flow	g/30sec	2.21	1.71	1.44	1.71	1.71	1.62	1.66
Slide	mm/s	1.2	0.95	0.95	0.95	0.97	0.86	0.91
Q/V	mm^2	1.81E-08	1.40E-08	1.18E-08	1.40E-08	1.40E-08	1.33E-08	1.36E-08
Ratios								
T_s/T_c		11.54	11.54	11.54	11.54	11.54	11.54	11.54
w/l		4.01	4.56	4.96	4.56	4.56	4.68	4.62
$1/L_{slurry}$		0.73	0.95	1.12	0.95	0.95	1.00	0.97

15 vol% Trials

Trial		15-1	15-2	15-3	15-4
Number of Layers		1	1	1	1
Settings					
Solids Load	%	15	15	15	15
Slurry Denisty	g/cc	1.35	1.35	1.35	1.35
Speed	m/s	2.65	2.65	2.65	2.70
Cycle Time	msec	100	100	100	200
Mass Flow	g/30sec	1.48	1.30	1.75	1.77
Slide	mm/s	0.78	0.59	0.82	0.41
Q/V	mm^2	1.38E-08	1.21E-08	1.63E-08	1.62E-08
Ratios					
T_s/T_c		17.85	17.85	17.85	17.85
w/l		5.81	6.21	5.35	5.37
$1/L_{slurry}$		0.74	0.85	0.63	0.63

THESIS PROCESSING SLIP

FIXED FIELD: ill. _____ name _____

index _____ biblio _____

▶ COPIES: (Archives) Aero Dewey (Eng) Hum

Lindgren Music Rotch Science

TITLE VARIES: ▶ ☐ _____

NAME VARIES: ▶ ☒ N Ørskov

IMPRINT: (COPYRIGHT) _____

▶ COLLATION: 133 l

▶ ADD: DEGREE: _____ ▶ DEPT.: _____

SUPERVISORS: _____

NOTES:

cat'r: date:

page: 5137

▶ DEPT: M.E.

▶ YEAR: 1999 ▶ DEGREE: S.M.

▶ NAME: DEBEAR, Bjørn N.